DE TTK

1949

Theoretical Study of Charge Transfer in Ion-Molecule Collisions

Ph.D. Thesis
Egyetemi doktori (Ph.D.) értekezés

Emese Tünde Rozsályi

Supervisors/Témavezetők
Dr. Ágnes Vibók
Dr. Gábor Halász
Dr. Marie-Christine Bacchus-Montabonel

University of Debrecen
Ph.D. School in Physics
Debreceni Egyetem
Természettudományi Doktori Tanács
Fizikai Tudományok Doktori Iskolája
Université Claude Bernard Lyon 1
École Doctorale de Physique

Debrecen
2012

Ezen értekezést a Debreceni Egyetem Természettudományi Doktori Tanács Fizikai Tudományok Doktori Iskola Atom- és molekulafizika programja keretében készítettem a Debreceni Egyetem természettudományi doktori (PhD) fokozatának elnyerése céljából.

Debrecen, 2012. .....

Rozsályi Emese Tünde

Tanúsítom, hogy Rozsályi Emese Tünde doktorjelölt 2008-2011 között a fent megnevezett Doktori Iskola Atom- és molekulafizika programjának keretében irányításommal végezte munkáját. Az értekezésben foglalt eredményekhez a jelölt önálló alkotó tevékenységével meghatározóan hozzájárult. Az értekezés elfogadását javaslom.

Debrecen, 2012. .....

Dr. Vibók Ágnes

témavezető

Tanúsítom, hogy Rozsályi Emese Tünde doktorjelölt 2008-2011 között a fent megnevezett Doktori Iskola Atom- és molekulafizika programjának keretében irányításommal végezte munkáját. Az értekezésben foglalt eredményekhez a jelölt önálló alkotó tevékenységével meghatározóan hozzájárult. Az értekezés elfogadását javaslom.

Debrecen, 2012. .....

Dr. Halász Gábor

témavezető

Theoretical Study of Charge Transfer in Ion-Molecule Collisions

Értekezés a doktori (Ph.D.) fokozat megszerzése érdekében
a fizika tudományágban

írta: Rozsályi Emese Tünde okleveles fizikus

Készült a Debreceni Egyetem Fizikai Tudományok doktori iskolája
(Atom- és molekulafizika programja) keretében

Témavezetők: Dr. Vibók Ágnes
Dr. Halász Gábor

A doktori szigorlati bizottság:
elnök: Dr. .....
tagok: Dr. .....
Dr. .....
A doktori szigorlat időpontja: 20... . ...

Az értekezés bírálói:
Dr. .....
Dr. .....
A bírálóbizottság:
elnök: Dr. .....
tagok: Dr. .....
Dr. .....
Dr. .....
Dr. .....

Az értekezés védésének időpontja: 20... . ...

Contents

1 Chapter

Foundations and Purpose of this Research

1.1 Introduction

Investigations of charge exchange reactions are of fundamental interest to physicists studying a wide range of phenomena in astrophysics, where the displacement of electrons effects the behavior of all interstellar gases [1], and to plasma physics where edge effects, in part due to electron transfer, have detrimental consequences on the process of thermonuclear fusion [2]. These reactions are also determinant in understanding the complex mechanisms involved in ion beam therapy of cancer disease.

A detailed theoretical description of charge transfer is so challenging that several approximative techniques have been developed, from the simpler methods such as the Landau-Zener approximation, or the classical trajectory Monte Carlo model, to very accurate quantum mechanical methods, such as the quantum mechanical close-coupling approximation. Quantal calculations, in which both the projectile and electronic motions are described quantum mechanically, are necessary for low collision energies (E $\leq$ 50 eV/a.m.u.). Collisions of ions with atoms and molecules at impact energies above 50 eV/a.m.u. are usually described by semiclassical methods. In these methods, the relative ion-atom (molecule) motion is treated by means of a classical trajectory and the remaining degrees of freedom are described quantally. For E$>$20 keV/a.m.u., purely classical calculations can

be performed in the framework of the model potential approximation.

Detection methods, like photon emission spectroscopy, translational energy spectroscopy, energy gain spectroscopy, Auger electron spectroscopy or recoil ion momentum spectroscopy has allowed charge transfer to be studied leading to a wealth of experimental data being available.

This chapter attempts to provide a succinct outline of the historical background of the charge-transfer process and reviews on aspects of ion beam therapy. Near the end of this chapter the motivation and objectives behind this research are formulated. The organization of this document is presented at the end of the chapter.

1.2 Historical Review

Charge exchange was discovered by G. H. Henderson (1923) during course of experiments in which α-particles were passed through absorbing screens of mica [3]. Numbers of singly charged He^+ ions and also He atoms were observed to emerge from the far side of the screens, and these were attributed to the capture of electrons by the α-particles. This interpretation of the experiments was confirmed, and the measurements extended to electron capture by α-particles from air and hydrogen, by E. Rutherford [4], G. H. Henderson [5], and J. C. Jacobsen [6].

Shortly after the discovery of charge exchange in ion-atom collisions by Henderson, a theoretical model of such reactions was constructed by Thomas in 1927 [7], based on classical mechanics. It was assumed that the electrons in the target were at rest and were uniformly distributed over the surface of a sphere. Kinematically the reaction requires twos successive collisions to take place. In the first the incident ion of velocity v_0 strikes an electron in the target. Since the ion is much heavier than the electron it is essentially undeflected. On the other hand it is possible for the electron to acquire the speed v_0 and to make a collision with the target nucleus in such a way that it is deflected to move in the same direction as the incident ion. Those electrons which emerge moving with the same velocity as the incident ion and in the same direction are considered to be captured. This mechanism produced a capture cross section decreasing with velocity like v_0^{-11}, which is, in fact found from quantum theory to be the correct asymptotic velocity variation of the non-relativistic cross section.

At the same time other theories have emerged. The first applications of quantum mechanics to charge exchange were perturbation treatments by Oppenheimer in 1928 [8] and by Brinkman and Kramers in 1930 [9]. The latter authors were the first to make use of the fact that, at all except the very lowest energies, the wavelength associated with the relative motion of the heavy particle is very small compared with the distance over which interaction takes place, with the consequence that the heavy-particle motion follows a classical Newtonian trajectory; only the electronic motion needs to be treated by quantum mechanics. At low energies the charge exchange cross section is large and a perturbation treatment is not adequate. When the relative velocity of the heavy particles is small, the interaction time is long compared with the characteristic times of electrons in bound state orbits. Under these circumstances the electron to be captured is shared between the two ions during the collision, forming quasimolecule. The electrons are fast enough to adjust their motion to the relative position of nuclei at each instant of time. The first theoretical description of this mechanism was given by Massey and Smith (1933) who developed a theory based on the expansion of the electronic wave function in a series of molecular orbitals [10]. In the original form this model contained some serious difficulties, and it was not until some twenty-five years later that Bates and his collaborators [11–15] corrected these and presented the theory in its modern form [16]. The title of the first paper of the series entitled 'Inelastic heavy particle collisions involving the crossing of potential energy curves' is 'Charge transfer from H atoms to Be^{2+}, Si^{2+} and Mg^{2+} ions' [11].

The development and application of the models for a more accurate understanding of the charge-transfer processes of increasingly complex systems continue till today.

1.3 Reviews on Aspects of Ion-Beam Therapy

The interaction of ionizing radiation with biological tissue can induce important damage to DNA. The cell has a very efficient repair system for single and isolated lesions like single strand breaks that occurs very frequently and is not only caused by ionising radiation. Even simultaneous damage at both DNA strands, i.e. double strand breaks, can be repaired

by the cell rather quickly with a reduced but still high fidelity. But if the local damage is enhanced by higher local doses more complex DNA damage (cluster damage) is produced which is less reparable [17]. Important damage has been shown to be due not only to the primary radiation itself, but to the secondary particles, low energy electrons, radicals, and also ions which are generated along the track after interaction of the ionizing radiation with the biological medium [18].

1.3.1 Physical Advantage

The most prominent advantage of ion beams compared to conventional photon radiation (X-rays, gamma rays, high energy photons) is their favourable depth-dose profile. A comparison of depth-dose profiles for photon and particle beams is displayed in Fig. 1.1. Low energy X-rays show a

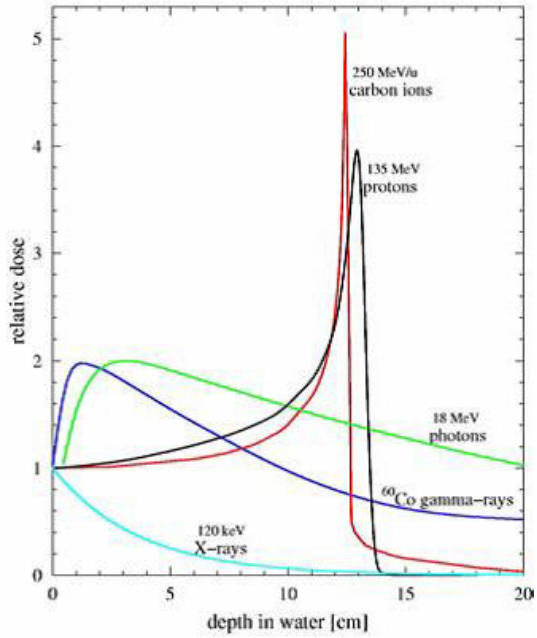

1.1. Figure: Depth-dose distribution of photon and particle beams. [19]

steep exponential decrease of dose with depth. For high-energy photons (mostly used in conventional therapy nowadays) the initial buildup, mainly caused by forward scattered Compton electrons, shifts the peak dose by a few

centimeters away from the surface of the patient's body, thereby improving the target-to-entrance dose and sparing the radiosensitive skin. In contrast to photons, the dose profiles of protons and heavier ions are characterized by a distinct narrow peak at the end of their path [20]. Because of their charge, the ions interact mainly with the electrons of the penetrated tissue. At the high initial speed, this interaction is short and only little energy is transferred to the tissue. With increasing depth, the ions are slowed down and the local interaction becomes longer, transferring a higher dose to the tissue. Therefore, the dose increases at the end of the ion range to very high values, the so called Bragg maximum. This yields an ideal depth-dose distribution for therapy: a low dose at the entrance channel in the normal tissue and a large dose at the end of the penetration in the tumour volume [21].

The increased energy deposition with penetration depth up to a sharp maximum at the end of the particle range was first measured by Sir William Henri Bragg wit alpha particles in air [22], and therefore this maximum is known as the Bragg peak. Many years later R. Wilson has recognized the potential for using the Bragg-peak feature of protons or heavier ions for radiation therapy. In his paper Wilson mainly discusses protons but also mentions alpha particles and carbon ions [23]. It took almost 10 years from his first publication until the first patient was treated with protons at Lawrence Berkeley National Laboratory in 1954. Ions heavier than protons, such as helium and later on argon, first came into use at Lawrence Berkeley Laboratory in 1957 and 1975, respectively. Argon ions were tried in order to increase the effectiveness against radioresistant tumours, but problems arose owing to non-tolerable side effects in the normal tissues. Trials with silicon and neon ions did not give good results and only toward the end of the program was found that the neon charge is too large and undesirable effects were produced in the traversed and downstream healthy tissues [24]. Until its closure in 1993 the Bevalac radiotherapy facility was the only facility worldwide using heavy ions for radiotherapy of localized deep-seated tumours. Over time it became evident that carbon ion beams were the most effective at treating certain types of cancers that were not responsive to conventional therapies or involved greater radiation doses to surrounding normal tissues.

For ions heavier than protons, like the carbon beams, the nuclear fragmentation as a second process beside the energy loss determines the depth-

dose distribution. In these nuclear reactions, lighter ions are created that continue their path with approximately the same velocity. However, because they are lighter, they have a larger penetration and create a dose tail at the distal side of the Bragg peak [25]. A frequent process is the stripping of one or two neutrons, converting the stable ^{12}C to ^{11}C and ^{10}C. Both isotopes are radioactive and decay with a half life of 20 minutes and 19 seconds, respectively under the emission of a positron [26]. The positron annihilates with a target electron and emits two 511 keV gamma rays coincidently under 180°. A large fraction of these coincident quanta can be detected by two gamma cameras on opposite sites of the patient and their origin i.e. the region of the stopping carbon ions can be reconstructed after each treatment session. Using this technique of positron emission tomography (PET) it is possible to verify with a precision of two millimeters whether the target volume was irradiated correctly [27]. For protons, there is no dose tail and also no projectile isotopes that can be used for a PET analysis.

1.3.2 Biological Advantage

Besides the physical differences discussed in the previous section there can be biological differences in terms of dose response dependent on the irradiation type. For a given survival fraction less dose is needed for carbons compared to photons. Thus, for the same dose the biological effect of carbon is higher than for photons.

Furthermore, the choice of carbon ions as the optimum ion is mainly determined by the gain in radiobiological efficiency between entrance channel and tumour. For light ions like protons, only at the very end of the track i.e. at the last few micrometers, a clustering of DNA damage can be realized. This seems not to be of major importance for therapy. Heavier ions like Argon are extremely efficient in cell killing but unfortunately the efficient region also extends into the normal tissue in front of the tumour, causing heavy severe late effects. For ions between proton and argon, in the region of carbon, the energy loss and consequently the lesion density is distributed in a very favourable manner. At high energies, the local ionization is low. Therefore, individual DNA lesions are produced with a large repair potential and the damage produced in the normal tissue in front of the target is reparable. At the end of the carbon ions' range, in the last centimetres, the local ionisation density reaches a level where a majority of irreparable DNA

damage is produced in a single particle track yielding high radiobiological efficiency values and efficient tumor inactivation [17].

Carbon ions are best in the balance of the production of lethal lesion in the tumour on one hand and reduced damage to the normal tissue on the other. Measurements of DNA double strand breaks as well as of cell survival have confirmed the high repair rate in the healthy tissue and the very effective cell killing in the tumor region [28].

1.3.3 Carbon Therapy Facilities in the World

Encouraged by the prospective results of heavy-ion radiotherapy at Lawrence Berkeley National Laboratory and the recent progresses in the accelerator and beam-delivery technologies [29], in 1994 the NIRS (National Institute of Radiological Sciences) in Chiba, Japan decided to carry out heavy-ion radiotherapy using the HIMAC (Heavy-Ion Medical Accelerator in Chiba) synchrotron, and clinical trials with carbon at the GSI (Helmholtzzentrum für Schwerionengorschung GmbH) in Darmstadt, Germany followed. The heavy-ion therapy at NIRS began treatment with carbon ions right from the start, although it would have been possible to accelerate heavier ions up to Argon at the HIMAC. The therapy unit at Chiba is the first heavy-ion accelerator that is dedicated solely to therapy. On the base of the excellent clinical results obtained on about 4500 patients in Chiba and on 400 patients at GSI, several hospital-based ion therapy centers have been proposed worldwide.

The Hyogo Ion Beam Medical Center was constructed in 2001 as the world's first charged particle radiotherapy center where both proton and carbon-ion radiotherapy can be performed. Superficially-placed tumours have been treated with carbon ions at the Institute of Modern Physics (IMP), Chinese Academy of Sciences (CAS), since November 2006. The Heidelberg Ion Therapy Center (HIT) started clinical operation in November 2009. The third carbon ion therapy facility in Japan was commissioned at the Gunma University Heavy Ion Medical Center (GHMC) at Maebashi, where its first patient was treated in March 2010. The Saga Heavy Ion Medical Accelerator project (Saga-HIMAT) in Tosu started construction of a carbon-ion radiotherapy facility in February 2010. This is based on the design of the GHMC facility and will be opened in 2013. In France, the ETOILE (Espace de Traitement Oncologique par Ions Légers dans le cadre Européen) cen-

ter in Lyon will be chiefly dedicated to clinical practice while ARCHADE (Advanced Resource Centre for Hadrontherapy in Europe) in Caen will be the first center in the world devoted to hadron therapy research, helping both clinicians and their patients. The ETOILE Center will receive its first patients in 2015. Besides, three other facilities are in advanced phase of construction: the Italian Hadron Therapy (CNAO) at Pavia, the Kooperativen Ionen Therapie Zentrum at Marburg (KITZ) and the North European Radiooncological Center (NRoCK) at Kiel.

Following its successful clinical operation, new ion beam particle centers will be soon constructed in: Wiener Neustadt (2015), Austria; Shanghai (2015) and Lanzhou, China; and Busan (2016), Korea. Kanagawa Cancer Center (KCC) is also pursuing plans to introduce a carbon ion radiotherapy system and start its operation in 2015.

Clinical research are carried out at these institutions to enhance beam delivery accuracy, such as beam scanning that compensates for organ movements, which will further improve the clinical efficacy of the ion-beam therapy in the future.

1.4 Purpose of this Work

Owing to high dose localization and high biological effect of the carbon-ion beam used in cancer radiotherapy, the carbon-ion beam is considered to be useful against intractable, photon-resistant cancers, and to greatly reduce the treatment period compared with photon or proton radiotherapy.

The analysis of such mechanisms at the molecular level is important to provide detailed information on the different processes occurring during the collision, as charge transfer between the projectile ion and the molecule. This may involve direct processes where collisions of ions with biomolecular targets have to be considered, but also indirect processes corresponding to reactions of ions with the environment, in particular the solvent, generally water. Such reactions have indeed been shown to drive important damage [30] and charge transfer with water or OH targets are of fundamental interest.

We have been interested in particular in charge-transfer processes involving diatomic targets, as the OH radical which may be formed in the biological system. Besides, we have extended our research taking account of the characteristics of the molecular target (electronic structure, electronega-

tivity of its elements) to have a better understanding of the charge-transfer mechanism for different diatomics and, if possible, establish a number of general rules for these reactions.

Motivated particularly by ion beam therapy studies, this thesis describes in detail charge-transfer process in collisions of C^{2+} ions with hydrogen halide molecules (HF, HCl) for which experimental measurements have been proposed by the Institute of Nuclear Research of the Hungarian Academy of Sciences. The comparison between theoretical and experimental results is of great importance from both sides, i.e. with the intention of either checking the theory or interpreting the experiments.

A comparative analysis is presented involving quite similar molecular targets in order to investigate the efficiency of the charge-transfer process with regard to nonadiabatic interactions, influenced by the proposed experimental results.

The structure of this thesis is as follows.

CHAPTER 1 gives a general introduction on the particle radiation therapy with some special emphasis on the physical and biological rationale for the use of ions (especially carbon ions) compared to conventional photon radiation, together with a glance at the world carbon therapy facilities.

CHAPTER 2 describes the theoretical background for the *ab initio* calculations and reviews the theoretical concepts of semiclassical dynamical treatment of ion-molecule collisions.

CHAPTER 3 presents numerical methods used to solve the Schrödinger equation. Quantum chemical approaches are introduced to calculate the potential energy surfaces and related nonadiabatic coupling terms. The objectives of using effective core potentials and translation factors are discussed.

CHAPTER 4 presents our detailed analysis of the charge-transfer process in collisions of C^{2+} ions with hydrogen halide molecules in the keV collision energy range. The mechanism is investigated in detail in connection with avoided crossings between states involved in the reaction. The orientation of the projectile towards the molecular target is developed for the $C^{2+} + HF$ collision system. The vibration of the molecular target is also analyzed and cross sections on different vibrational levels of HF^{+} are

estimated in the Franck-Condon approximation. The theoretical treatment of charge-transfer processes induced by collision of the C^{2+} projectile on hydrogen chloride is also presented. A comparative analysis is performed for hydrogen halide targets.

CHAPTER 5 includes the summary of the results, reports the conclusions and also presents the future developments and perspectives.

2 Chapter

Theory of Ion-Molecule Collisions

2.1 The Adiabatic and Born-Oppenheimer Approximations

The starting point of all that follows is non-relativistic quantum mechanics. Thus, one starts from the time-dependent Schrödinger equation

$$i\hbar\frac{\partial}{\partial t}\Psi(\vec{r_i},\vec{R_I};t) = \hat{H}\Psi(\vec{r_i},\vec{R_I};t). \tag{2.1}$$

The standard form of the non-relativistic molecular Hamiltonian in an arbitrary coordinate system takes into account five contributions to the total energy of the system: the kinetic energies of the electrons and nuclei, the attraction of the electrons to the nuclei, and the interelectronic and internuclear repulsions. Casting the Hamiltonian into mathematical notation, we have

$$\begin{aligned}\hat{H} &= \hat{T}_{nuc} + \hat{T}_{el} + \hat{V}_{nuc,el} + \hat{V}_{el,el} + \hat{V}_{nuc,nuc} \\ &= -\sum_I \frac{\hbar^2}{2M_I}\nabla_I^2 - \sum_i \frac{\hbar^2}{2m_e}\nabla_i^2 \\ &\quad - \frac{1}{4\pi\varepsilon_0}\sum_{I,i}\frac{e^2 Z_I}{\mid \vec{R}_I - \vec{r}_i \mid} + \frac{1}{4\pi\varepsilon_0}\sum_{i<j}\frac{e^2}{\mid \vec{r}_i - \vec{r}_j \mid} + \frac{1}{4\pi\varepsilon_0}\sum_{I<J}\frac{e^2 Z_I Z_J}{\mid \vec{R}_I - \vec{R}_J \mid} \\ &= -\sum_I \frac{\hbar^2}{2M_I}\nabla_I^2 + \hat{H}_{el},\end{aligned} \tag{2.2}$$

for the $\vec{R}_I$ nuclear positions and $\vec{r}_i$ electronic coordinates. I and J run over nuclei, i and j run over electrons. M_I and Z_I are mass and atomic number of the Ith nucleus, the electron mass and charge are denoted by m_e and $-e$, and ε_0 is the vacuum permittivity. In order to keep the current derivation as transparent as possible, the more convenient atomic units (a.u.) will be introduced only at a later stage.

Accurate wave functions for many-particle molecular systems are extremely difficult to express because of the correlated motions of particles. That is, the Hamiltonian in Eq. 2.2 contains pairwise attraction and repulsion terms, implying that no particle is moving independently of all of the others. It is convenient to compute electronic energies for fixed nuclear positions. This allows the electronic part to be solved with the nuclear positions as parameters.

Assume for the moment that the exact solution of the corresponding time-independent electronic Schrödinger equation,

$$\hat{H}_{el}(\vec{r}_i;\vec{R}_I)\Phi_k(\vec{r}_i;\vec{R}_I) = E_k(\vec{R}_I)\Phi_k(\vec{r}_i;\vec{R}_I) \tag{2.3}$$

is known for clamped nuclei at positions R_I. The spectrum of $\hat{H}_{el}$ is assumed to be discrete and the eigenfunctions to be orthonormalized

$$\int \Phi_k^*(\vec{r}_i;\vec{R}_I)\Phi_l(\vec{r}_i;\vec{R}_I)d\vec{r} = \delta_{kl} \tag{2.4}$$

at all possible positions of the nuclei. Knowing all these adiabatic eigenfunctions at all possible nuclear configurations, the total wave function in

Eq. 2.1 can be expanded

$$\Psi(\vec{r}_i, \vec{R}_I; t) = \sum_{l=0}^{\infty} \Phi_l(\vec{r}_i; \vec{R}_I)\chi_l(\vec{R}_I; t) \tag{2.5}$$

in terms of the complete set of eigenfunctions $\{\Phi_l\}$ of H_{el} where the nuclear wave functions $\{\chi_l\}$ can be viewed to be time-dependent expansion coefficients.

Applying the ∇_I operator to the wavefunction on the right hand side of Eq. 2.5 gives

$$\begin{aligned}\nabla_I^2[\Phi_l(\vec{r}_i; \vec{R}_I)\chi_l(\vec{R}_I; t)] &= \nabla_I[\nabla_I\Phi_l(\vec{r}_i; \vec{R}_I)\chi_l(\vec{R}_I; t)] \\ &= \Phi_l(\vec{r}_i; \vec{R}_I)\nabla_I^2\chi_l(\vec{R}_I; t) + \chi_l(\vec{R}_I; t)\nabla_I^2\Phi_l(\vec{r}_i; \vec{R}_I) \\ &\quad + 2(\nabla_I\chi_l(\vec{R}_I; t))(\nabla_I\Phi_l(\vec{r}_i; \vec{R}_I)).\end{aligned} \tag{2.6}$$

Insertion of Eq. 2.5 into the time-dependent Schrödinger equation Eq. 2.1 followed by multiplication from the left by $\Phi_k^*(\vec{r}_i; \vec{R}_I)$ and integration over all electronic coordinates $\vec{r}$ leads to a set of coupled differential equations

$$\left[-\sum_I \frac{\hbar^2}{2M_I}\nabla_I^2 + E_k(\vec{R}_I)\right]\chi_k(\vec{R}_I; t) + \sum_l c_{kl}\chi_l(\vec{R}_I; t) = i\hbar\frac{\partial}{\partial t}\chi_k(\vec{R}_I; t), \tag{2.7}$$

where

$$\begin{aligned}c_{kl} = &\int \Phi_k^*(\vec{R}_I)\left[-\sum_I \frac{\hbar^2}{2M_I}\nabla_I^2\right]\Phi_l(\vec{R}_I)d\vec{r} \\ &+ \sum_I \frac{1}{M_I}\left\{\int \Phi_k^*(\vec{R}_I)\left[-i\hbar\nabla_I\right]\Phi_l(\vec{R}_I)d\vec{r}\right\}\left[-i\hbar\nabla_I\right]\end{aligned} \tag{2.8}$$

is the exact nonadiabatic coupling operator. The first term is a matrix element of the kinetic energy operator of the nuclei, whereas the second term depends on their momenta.

The diagonal contribution c_{kk} depends only on a single adiabatic wave function Φ_k and as such represents a correction to the adiabatic eigenvalue E_k of the electronic Schrödinger equation Eq. 2.3 in this kth state. As a result, the adiabatic approximation to the fully nonadiabatic problem Eq.

2.7 is obtained by considering only these diagonal terms,

$$c_{kk} = -\sum_I \frac{\hbar^2}{2M_I} \int \Phi_k^* \nabla_I^2 \Phi_k d\vec{r}, \tag{2.9}$$

the second term of Eq. 2.8 being zero when the electronic wave function is real, which leads to complete decoupling

$$\left[-\sum_I \frac{\hbar^2}{2M_I} \nabla_I^2 + E_k(\vec{R}_I) + c_{kk}(\vec{R}_I) \right] \chi_k = i\hbar \frac{\partial}{\partial t} \chi_k \tag{2.10}$$

of the fully coupled original set of differential equations Eq. 2.7. This, in turn, implies that the motion of the nuclei proceeds without changing the quantum state, k, of the electronic subsystem during time evolution [31].

The next simplification consists in neglecting also the diagonal coupling terms

$$\left[-\sum_I \frac{\hbar^2}{2M_I} \nabla_I^2 + E_k(\vec{R}_I) \right] \chi_k = i\hbar \frac{\partial}{\partial t} \chi_k, \tag{2.11}$$

which defines the Born-Oppenheimer approximation [32].

The term $\langle \Phi_k | \nabla_I | \Phi_l \rangle \nabla_I \chi_l$ in Eq. 2.7 corresponds to the dynamical coupling. With the choice of molecular frame in spherical coordinates, it is decomposed in nonadiabatic coupling elements. The radial coupling $\langle \Phi_k | \frac{\partial}{\partial R} | \Phi_l \rangle$ couples states of same symmetry and same spin multiplicity, while the rotational coupling $\langle \Phi_k | iL_y | \Phi_l \rangle$ couples states of same spin multiplicity but different symmetry. The nonadiabatic coupling matrix elements are important as they generate transitions between the different molecular states involved in the process.

The Born-Oppenheimer separation of the electronic and nuclear motions is a cornerstone in molecular physics and chemistry. The physical picture of Born-Oppenheimer approximation is one where the fast moving electrons are able to readapt instantaneously to new nuclear geometry, as a result of the light electron mass with respect to the nuclear one. Once the electronic Schrödinger equation has been solved for a large number of nuclear geometries, the potential energy (hyper)surface (PES) is known. The motion of the nuclei on a given predetermined electronic potential energy surface can then be solved. The major computational effort is in solving the electronic

Schrödinger equation for a given set of nuclear coordinates. The solution of the electronic time-independent Schrödinger equation with given nuclear geometry represent one point of the PES. Methods aimed at solving the electronic Schrödinger equation are broadly referred to as 'electronic structure calculations'.

The nonadiabatic coupling terms are responsible for the coupling between the adiabatic states, and since for a long time most studies were related to the ground state, it was believed that the Born-Oppenheimer approximation always holds due to the weakness of the nonadiabatic coupling terms. This belief persisted although it was quite early recognized, due to the Hellmann-Feynman theorem, that nonadiabatic coupling terms are not necessarily weak, on the contrary, they may be large and eventually become singular. They become singular at those instances when two successive adiabatic states turn out to be degenerate.

Introducing the electronic Hamiltonian defined by Eq. 2.2 one obtains

$$\langle \Phi_k | \hat{H}_{el} \left(\frac{\partial}{\partial R} \right) | \Phi_l \rangle - \langle \Phi_k | \left(\frac{\partial}{\partial R} \right) \hat{H}_{el} | \Phi_l \rangle = - \langle \Phi_k | \frac{\partial \hat{H}_{el}}{\partial R} | \Phi_l \rangle . \quad (2.12)$$

Using Eq. 2.3 the left-hand side of 2.12 becomes equal to $(E_k(\vec{R}) - E_l(\vec{R}))$ $\langle \Phi_k | \frac{\partial}{\partial R} | \Phi_l \rangle$, thus the matrix element of the operator $\partial/\partial R$ can be expressed as

$$\langle \Phi_k | \frac{\partial}{\partial R} | \Phi_l \rangle = \frac{\langle \Phi_k | \frac{\partial \hat{H}_{el}}{\partial R} | \Phi_l \rangle}{E_l(\vec{R}) - E_k(\vec{R})} \qquad (k \neq l). \quad (2.13)$$

By the Wigner and von Neumann non-crossing rule [33], the difference of the adiabatic potential energies $(E_l(\vec{R}) - E_k(\vec{R}))$ can never vanish at any value of R, if the adiabatic states Φ_k and Φ_l have the same symmetry. However potential energy curves for states of the same symmetry can approach each other in a narrow region about some value of R and this is called an avoided crossing. In the region of the avoided crossing we see from Eq. 2.13 that the matrix element $\langle \Phi_k | \frac{\partial}{\partial R} | \Phi_l \rangle$ is large. At low energies in many systems charge exchange only takes place with a significant probability in the region of one, or a few, avoided crossings of this type, and this fact in turn implies that accurate cross sections can be obtained from limited sets which contain these crossings [34].

The non-crossing rule is strictly valid only for diatomic molecules. For polyatomic system involving N atoms, where $N \geq 3$ (i.e. for not diatomic molecules), any two adjacent adiabatic electronic states can be degenerate for a set of nuclear geometries even if those electronic states have the same symmetry [35]. Such intersections, also called conical intersections because of the topology of the surfaces at the crossing point, occur more frequently in such polyatomic systems [36] than it was previously believed. The reason is that these systems possess three or more internal nuclear motion degrees of freedom, and only two independent relations between three electronic Hamiltonian matrix elements (in a simple two electronic state picture) are sufficient for the existence of doubly degenerate energy eigenvalues. As a result, these relations can be easily satisfied explaining thereby the frequent occurrence of intersections [37–40]. The question whether a true conical intersection or avoided crossing is observed for a particular system of interest can be answered only with quantum mechanical calculations of high accuracy.

2.2 Adiabatic-to-Diabatic Transformation

If two surfaces become degenerate, the coupling $\langle \Phi_k | \dfrac{\partial}{\partial R} | \Phi_l \rangle$ exhibits a singular behaviour. As a result, the electronic wave function becomes discontinuous and the energy has a cusp like behavior at such points, making the uniquely defined adiabatic representation unsuitable for the numerical simulation of the dynamics. In order to deal with this situation, one resorts to a diabatic electronic representation, where these diverging kinetic energy coupling elements are transformed into smooth potential energy couplings and thereby the discontinuity of the adiabatic representation is avoided. This representation is not unique and different approaches are proposed. The diabatic molecular states are constructed by a unitary transformation of the corresponding adiabatic electronic states. The Hamiltonian in the diabatic representation $\hat{H}^{dia}$ can be obtained from that in the adiabatic representation $\hat{H}^{adia}$ through the following unitary transformation

$$\hat{H}^{dia} = \boldsymbol{A}\hat{H}^{adia}\boldsymbol{A}^{+} = \hat{T}_{nuc}\mathbf{1} + \boldsymbol{W}. \tag{2.14}$$

Here $\boldsymbol{A}$ defines the orthogonal transformation matrix. For a 2×2 Hamiltonian $\boldsymbol{A}$ is given by

$$\begin{pmatrix} cos\alpha & sin\alpha \\ -sin\alpha & cos\alpha \end{pmatrix},$$

where α represents the adiabatic-to-diabatic transformation angle and $\Psi^{dia} = \boldsymbol{S}\Psi^{adia}$. In doing so, the diverging kinetic couplings of Eq. 2.13 are transformed into the smooth potential coupling (off-diagonal elements of $\boldsymbol{W}$ in Eq. 2.14) and thereby the discontinuity of the adiabatic representation is avoided. In the diabatic representation the electronic wave functions are no longer eigenfunctions of the electronic Hamiltonian. The transition between two adiabatic states corresponds to remaining in the same diabatic state. Such diabatic electronic states can be constructed in several ways.

Baer suggested the derivation of the adiabatic-to-diabatic matrix for a tri-atom system by involving an integral equation along a two-dimensional contour, and analyzed the validity of the transformation in regions where the nonadiabatic coupling becomes singular [41,42]. Pascher et al. developed the block diagonalization method to obtain the transformation matrix directly [43].

Mead and Truhlar emphasized that strictly diabatic electronic states do not exist in general [44]. Exceptions are the case of a single nuclear degree of freedom as for atomic collision processes, and the case where the complete manifold of interacting states is considered in the diabatization procedure.

The two approaches are expected to yield similar results because the two frameworks are connected by an unitary transformation. However, it was shown that the two frameworks cannot always be connected through an unitary transformation [45, 46].

Despite the limitations, difficulties in obtaining the nonadiabatic coupling elements for polyatomic molecules have lead to the development of alternative approaches to provide the diabatic or quasidiabatic representation. A basis is called strictly diabatic if in that basis the derivative couplings vanish and quasidiabatic, if in that basis these couplings still exist but do not display the singular behavior of the adiabatic representation.

2.3 Basic Scattering Theory

In the following outline the general formulation of the typical collision process involving the N-electron diatomic molecule problem is presented. It is convenient to work in the atomic unit system, which is defined by setting $m_e = e = \hbar = 1$. The total Hamiltonian which describes the motion of the system formed by two colliding atoms, A and B, may be written as

$$\begin{aligned}\hat{H} = &-\frac{1}{2M_A}\nabla^2_{\vec{R}_A} - \frac{1}{2M_B}\nabla^2_{\vec{R}_B} - \frac{1}{2}\sum_{i=1}^{N}\nabla^2_{\vec{r}_i} \\ &- \sum_{i=1}^{N}\left(\frac{Z_A}{|\vec{r}_{iA}|} + \frac{Z_B}{|\vec{r}_{iB}|}\right) + \sum_{i<j}^{N}\frac{1}{|\vec{r}_{ij}|} + \frac{Z_A Z_B}{\left|\vec{R}\right|},\end{aligned} \tag{2.15}$$

where N is the number of electrons, and $\left|\vec{R}\right|$ is the internuclear distance.

Sometimes spin-orbit coupling terms must be introduced in the definition of the total potential energy operator.

The Hamiltonian takes the form in the center of mass frame

$$\hat{H} = -\frac{1}{2M}\nabla^2_{\vec{R}_C} - \frac{1}{2\mu}\nabla^2_{\vec{R}} - \frac{1}{2}\sum_{i=1}^{N}\nabla^2_{\vec{r}_{iO}} - \frac{1}{2\left(M_A + M_B\right)}\left(\sum_{i=1}^{N}\nabla_{\vec{r}_{iO}}\right)^2 + \hat{V}, \tag{2.16}$$

where $M = M_A + M_B + \sum_{i=1}^{N} m_e$ is the total mass of the system, $\mu = \frac{M_A \cdot M_B}{M_A + M_B}$ is the reduced mass, $\vec{R}_C$, $\vec{R}_O$, $\vec{R} = \vec{R}_B - \vec{R}_A$ and $\vec{r}_{iO} = \vec{r}_i - \vec{R}_O$ are the total center of mass, the nuclear center of mass and the internuclear vectors, respectively, as shown in Fig. 2.1. The origin of electronic coordinates is taken to be the nuclear center of mass.

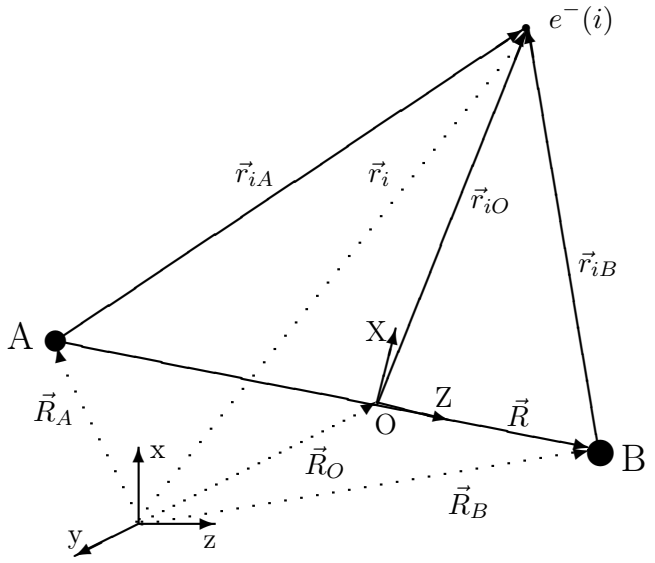

2.1. Figure: Schematic figure of a system formed by two colliding atoms.

The fourth term $\frac{1}{2\left(M_A+M_B\right)}\left(\sum_{i=1}^{N}\nabla_{\vec{r}_{iO}}\right)^2$ represents a mass polarization contribution; owing to the electron-to-mass ration, this term is negligible with respect to the second term and is usually dropped. Separation of the total center of mass yields a new Hamiltonian

$$\hat{H}=-\frac{1}{2\mu}\nabla^2_{\vec{R}}\Big|_{\vec{r}_{iO}}+\hat{H}_{el}\left(\vec{r},\vec{R}\right), \tag{2.17}$$

where $\hat{H}_{el}$ is the Born-Oppenheimer electronic Hamiltonian

$$\hat{H}_{el}=-\frac{1}{2}\sum_{i=1}^{N}\nabla^2_{\vec{r}_{iO}}\Big|_{\vec{R}}+\hat{V}. \tag{2.18}$$

The time-independent Schrödinger equation corresponding to the Hamiltonian of Eq. 2.17 is

$$\left(\hat{H}-E\right)\Psi=0. \tag{2.19}$$

To solve Eq. 2.19 for a collision $A + B \rightarrow A' + B'$ one must specify the boundary conditions.

The scattering angle θ is given by the expression $cos\theta = \hat{k}_I \cdot \hat{k}_F$, where $\hat{k}_I$ denote the direction of the incident beam and $\hat{k}_F$ is the direction of observation.

When the initial and final states of internal energy E_I and E_F can be presented by $\Phi_I^A \Phi_I^B$ and $\Phi_F^A \Phi_F^B$ (elastic and inelastic scattering) the linear momenta of the atoms for $R \rightarrow \infty$ are defined by $E = \frac{k_I^2}{2\nu} + E_I = \frac{k_F^2}{2\nu} + E_F$.

For charge-exchange processes the final state, with an internal energy E'_F, corresponds to $\Phi_F^{A'} \Phi_F^{B'}$, and we define $E = \frac{k_F'^2}{2\nu'} + E'_F$.

$\nu = \frac{\left(M_A + \sum_{i=1}^{N_A} m_e\right)\left(M_B + \sum_{j=1}^{N_B} m_e\right)}{M}$ and

$\nu' = \frac{\left(M_A + \sum_{i=1}^{N'_A} m_e\right)\left(M_B + \sum_{j=1}^{N'_B} m_e\right)}{M}$ are the reduced mass of atoms (A, B), (A', B'), while $\vec{s}_A$, $\vec{s}_B$, $\vec{s_B}'$ and $\vec{s_B}'$ denote the center of mass of atoms A, B, A', B', respectively. We define $\vec{s} = \vec{s}_B - \vec{s}_A$ and $\vec{s}\,' = \vec{s_B}' - \vec{s_A}'$.

The boundary condition for elastic and inelastic processes is

$$\lim_{s\rightarrow\infty} \Psi = e^{i\vec{k}_I \vec{s}} \Phi_I^A \Phi_I^B + \sum_F \frac{e^{ik_F s}}{s} f_F(\theta, \varphi) \Phi_F^A \Phi_F^B, \tag{2.20}$$

where the first term represents the incident plane wave corresponding to the relative motion of the centers of mass of A and B, times the initial atomic wavefunctions; the second term represents outgoing spherical waves, with scattering amplitude $f_F(\theta, \varphi)$ for each possible final atomic state; for charge-transfer processes [47]

$$\lim_{s'\rightarrow\infty} \Psi = \sum_F \frac{e^{ik'_F s'}}{s'} f'_F(\theta, \varphi) \Phi_F^{A'} \Phi_F^{B'}. \tag{2.21}$$

2.4 Cross Sections

For a flux of projectile particles (i.e. the number of particles crossing per unit time a unit surface placed perpendicular to the direction of propa-

gation), the differential cross section is defined to be the number of particles in the state F scattered in the direction (θ, φ) into an element of solid angle $d\Omega$, per unit time divided by the incident flux of projectile particles

$$\frac{d\sigma_F}{d\Omega}(\theta,\varphi) = \frac{\text{Number of particles scattered in direction}(\theta,\varphi)/td\Omega}{\text{Incident flux}}. \quad (2.22)$$

The differential cross section for scattering from an initial state to a final state is given in terms of the scattering amplitude $f_F(\theta, \phi)$ by

$$\frac{d\sigma_F}{d\Omega}(\theta,\varphi) = \frac{\nu}{\nu'}|f_F(\theta,\varphi)|^2, \quad (2.23)$$

where $\frac{\nu}{\nu'}$ is the ratio of reduced masses between subsystems in the entry and exit channels. The total cross section σ_F is obtained by integrating the differential cross section over all angles

$$\sigma_F = \int d\Omega \frac{d\sigma_F}{d\Omega}(\theta,\varphi). \quad (2.24)$$

2.5 Description of Ion-Molecule Collisions

In our work we study collisions between atomic ions and diatomic molecules. The basic idea of a slow heavy-particle collision is to view as a process of temporary formation and then breakup of a sort quasimolecular system built from all the nuclei and electrons of the colliding partners. One may thereby effect the well-known separation of electronic and nuclear motions, which fundamental step rests on the electronic to nuclear mass ratio. Electrons in a molecule are likely to move so fast compared to nuclei that they may be assumed to readjust instantaneously and continuously to the slowly varying nuclear field. The different Born-Oppenheimer electronic wavefunctions are obtained for different arrangements of the clamped nuclei and depend not only on the electronic coordinates but also on those of the nuclei, even if parametrically so. Likewise, the corresponding eigenvalues of the electronic Hamiltonian depend on the nuclear coordinates; these electronic energies are intended to represent the potentials that govern the nuclear motions. A collision problem henceforth splits into two parts: (1) determination of electronic wavefunctions and energies for fixed nuclei and

(2) treatment of the nuclear motion.

Neglecting the mass polarization term, we may write the non-relativistic Hamiltonian of the ion-molecule system containing N electrons

$$\hat{H} = -\frac{1}{2\mu}\nabla^2_{\vec{R}} - \frac{1}{2\mu_{12}}\nabla^2_{\vec{\rho}} - \frac{1}{2}\sum_{i=1}^{N}\nabla^2_{\vec{r}_i} + \frac{Z_A Z_1}{\left|\vec{R} - u\vec{\rho}\,\right|} + \frac{Z_A Z_2}{\left|\vec{R} + v\vec{\rho}\,\right|} + \frac{Z_1 Z_2}{|\vec{\rho}|} - \sum_{i=1}^{N}\frac{Z_A}{|\vec{r}_{iA}|} - \sum_{i=1}^{N}\frac{Z_1}{|\vec{r}_{iB} - u\vec{\rho}\,|} - \sum_{i=1}^{N}\frac{Z_2}{|\vec{r}_{iB} + v\vec{\rho}\,|} + \sum_{i=1}^{N}\sum_{j=i+1}^{N}\frac{1}{|\vec{r}_{ij}|}, \tag{2.25}$$

where the target is formed now by two nuclei of mass M_1 and M_2 as illustrated in Fig. 2.2 by '1' and '2', respectively. Besides, $\vec{\rho}$ is the vector joining the two nuclei of the diatomic molecule. The distance of the diatomic center of mass from each of these nuclei is $u_\rho = \dfrac{M_2}{M_1 + M_2}\,|\vec{\rho}|$ and $v_\rho = \dfrac{M_1}{M_1 + M_2}\,|\vec{\rho}|$. $\mu = \dfrac{M_A(M_1 + M_2)}{M_A + M_1 + M_2}$ is the reduced mass of the projectile nucleus with charge Z_A and the two molecular nuclei. $\mu_{12} = \dfrac{M_1 M_2}{M_1 + M_2}$ is the reduced mass of the two nuclei and Z_1, Z_2 their charge numbers. $\vec{R}$, $\vec{r}_{iA}$, $\vec{r}_{iB}$ and $\vec{r}_{ij}$ connect the nuclear center of mass of the molecule and the projectile nucleus, the ith electron and the projectile nucleus, the ith electron and the nuclear center of mass of the molecule, and two electrons, respectively. $\vec{r} = \vec{r}_1, \vec{r}_2, ..., \vec{r}_N$ denotes all electronic coordinates with respect to origin.

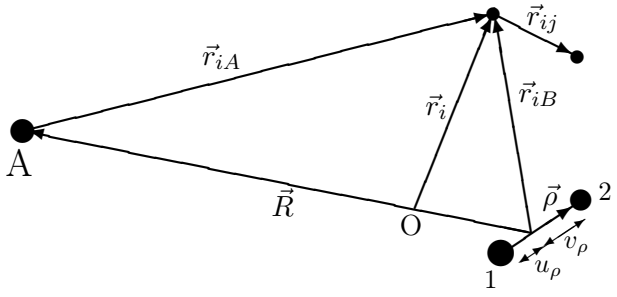

2.2. Figure: Schematic figure of an ion-molecule collision system. 'A' represents the projectile nucleus, while '1' and '2' the two nuclei of the diatomic molecule.

Indicating the Born-Oppenheimer electronic Hamiltonian by $\hat{H}_{el}$, the Hamiltonian of the presented ion-molecule system takes the form

$$\hat{H}(\vec{r},\vec{\rho},\vec{R}) = -\frac{1}{2\mu}\nabla^2_{\vec{R}} - \frac{1}{2\mu_{12}}\nabla^2_{\vec{\rho}} + \hat{H}_{el}(\vec{r};\vec{\rho},\vec{R}). \tag{2.26}$$

The wave function $\Psi(\vec{r},\vec{\rho},\vec{R})$ of the system in the center of mass frame may be written as a development of electronic functions $\{\Phi_l\}$

$$\Psi(\vec{r},\vec{\rho},\vec{R}) = \sum_l \chi_l(\vec{\rho},\vec{R})\Phi_l(\vec{r};\vec{\rho},\vec{R}), \tag{2.27}$$

where $\Phi_l(\vec{r};\vec{\rho},\vec{R})$ depend parametrically on $\vec{R}$ and $\chi_l(\vec{\rho},\vec{R})$ are the nuclear functions. The electronic wave functions $\{\Phi_l\}$ involved in the development Eq. 2.27 of $\Psi(\vec{r},\vec{\rho},\vec{R})$ are the eigenfunctions of the electronic Hamiltonian

$$\hat{H}_{el}\Phi_l(\vec{r};\vec{\rho},\vec{R}) = E_l(\vec{\rho},\vec{R})\Phi_l(\vec{r};\vec{\rho},\vec{R}). \tag{2.28}$$

Insertion of Eq. 2.27 in the time-independent Schrödinger equation

$$\hat{H}\Psi = E\Psi, \tag{2.29}$$

we obtain

$$\left(-\frac{1}{2\mu}\nabla^2_{\vec{R}} - \frac{1}{2\mu_{12}}\nabla^2_{\vec{\rho}} + \hat{H}_{el} - E\right)\sum_l \chi_l(\vec{\rho},\vec{R})\Phi_l(\vec{r};\vec{\rho},\vec{R}) = 0. \tag{2.30}$$

Multiplying Eq. 2.30 from the left side by Φ^*_k, and integrating over the electronic coordinates $\vec{r}$ with the orthonormality condition between the electronic wave functions, we obtain the coupled equations for the expansion coefficients in Eq. 2.27

$$\sum_l c_{kl}\chi_l = \left(E - E_k(\vec{\rho},\vec{R}) + \frac{1}{2\mu}\nabla^2_{\vec{R}} + \frac{1}{2\mu_{12}}\nabla^2_{\vec{\rho}}\right)\chi_k, \tag{2.31}$$

where

$$\begin{aligned} c_{kl} = &- \frac{1}{2\mu} \langle \Phi_k | \nabla^2_{\vec{R}} | \Phi_l \rangle - \frac{1}{2\mu_{12}} \langle \Phi_k | \nabla^2_{\vec{\rho}} | \Phi_l \rangle \\ &- \frac{1}{\mu} \langle \Phi_k | \nabla_{\vec{R}} | \Phi_l \rangle \nabla_{\vec{R}} - \frac{1}{\mu_{12}} \langle \Phi_k | \nabla_{\vec{\rho}} | \Phi_l \rangle \nabla_{\vec{\rho}}. \end{aligned} \tag{2.32}$$

In the present work the dynamics of the ion-molecule charge-transfer process is investigated in the semiclassical framework, known to be well suited to the intermediate energy region we are interested in. Therefore the eikonal approximation is presented in the following.

2.6 Eikonal Approximation

Originally introduced in quantum scattering theory by Moliére [48], the eikonal approximation has been considerably developed by Glauber [49] who proposed a very fruitful many-body generalization of the method. Basically, this approximation coming from optics, where we assume that light travels in a straight line. This assumption is valid as long as the size of the obstacle is large compared to the wavelength of light.

Semiclassical methods are useful when the de Broglie wavelength $\lambda = 2\pi/k$ of the projectile is sufficiently short with respect to the distance in which the potential varies by an appreciable amount. If the potential varies smoothly and has a range a, this short wavelength condition is equivalent to the requirement that $ka \gg 1$ [50]. However, the eikonal approximation also requires high scattering energies, such that $E \gg |V_0|$, where $|V_0|$ is a typical strength of the potential [51].

The eikonal approximation can be derived starting from either the Schrödinger equation, or the Lippmann-Schwinger equation by a linearization of the Green's function in momentum space. Here we follow the first approach.

In order to introduce the eikonal approximation in the context of ion-molecule collisions, we must subtract from the total Hamiltonian the nuclear kinetic energy term associated with the coordinate $\vec{R}$

$$\hat{H}(\vec{r}, \vec{\rho}, \vec{R}) = -\frac{1}{2\mu}\nabla^2_{\vec{R}} + \hat{H}_{int}(\vec{r}, \vec{\rho}, \vec{R}). \tag{2.33}$$

Since the potential varies slowly on the length scale of the incident wavelength, it is reasonable to extract the free incident plane wave from the

scattering wave function as a factor [52]. Developing formally the solutions of Eq. 2.29 in a power of series of μ^{-1},

$$\Psi(\vec{r},\vec{\rho},\vec{R}) = e^{i\vec{K}\vec{R}}\left[\psi(\vec{r},\vec{\rho},\vec{R}) + \frac{1}{\mu}\psi^{(1)}(\vec{r},\vec{\rho},\vec{R}) + \left(\frac{1}{\mu}\right)^2\psi^{(2)}(\vec{r},\vec{\rho},\vec{R}) + ...\right] \tag{2.34}$$

substituting in Eq. 2.29, and setting the coefficient of each power of μ equal to zero, and defining a vector $\vec{K}$ such that $|\vec{K}|^2 = 2\mu E$ we obtain,

$$i\vec{K}\cdot\nabla_{\vec{R}}\psi = \mu\hat{H}_{int}\psi. \tag{2.35}$$

In the semiclassical eikonal approximation the projectile-target relative motion is treated classically by means of a rectilinear trajectory

$$\vec{R} = \vec{b} + \vec{v}t, \qquad \vec{v}\perp\vec{b} \tag{2.36}$$

with $\vec{R}$, internuclear distance, $\vec{v}$, relative constant velocity and impact parameter $\vec{b}$. Replacing $\nabla_{\vec{R}}$ by a time derivative using the relation

$$\nabla_{\vec{R}} = \frac{\vec{v}}{v^2}\frac{\partial}{\partial t}, \tag{2.37}$$

Eq. 2.35 can be written as

$$\left(\hat{H}_{int} - i\frac{\partial}{\partial t}\Big|_{\vec{r},\vec{\rho}}\right)\psi(\vec{r},\vec{\rho},\vec{R}) = 0. \tag{2.38}$$

The semiclassical equation (Eq. 2.38) must be solved with the appropriate initial condition; this can be obtained by looking for the solutions of Eq. 2.38 in the limit when $t\to-\infty$. In particular, the semiclassical wavefunction fulfills

$$\lim_{t\to-\infty}\psi = \rho^{-1}Y_{JM}(\hat{\rho})\chi_\nu(\rho)\,\Phi_i(\vec{r};\vec{\rho})e^{-iE_it}, \tag{2.39}$$

where Y_{JM} is a spherical harmonic, χ_ν denotes the vibrational wavefunction of the molecule, Φ_i is the initial electronic wavefunction and E_i is the initial asymptotic internal energy of the system.

2.7 Sudden Approximation

At nuclear velocities that are sufficiently large, the collision time is short compared to the nuclear vibration and rotation periods. In the sudden approximation one therefore assumes that no appreciable change in the ro-vibrational wavefunction is effected whilst electronic transitions take place. Therefore the collision can be divided into two independent steps: the collision itself, where capture processes occur, and the ro-vibration of the molecule.

In this approach, the eikonal wavefunction describing the collision system is expressed as

$$\psi = \rho^{-1} Y_{JM}(\hat{\rho}) \chi_\nu(\rho)\, \Psi(\vec{r};\vec{\rho},t), \tag{2.40}$$

with $\Psi(\vec{r};\vec{\rho},t)$ describing the electronic structure. Furthermore, the electronic wavefunction $\Psi(\vec{r};\vec{\rho},t)$ of Eq. 2.40 is expanded in terms of the molecular wavefunctions $\Phi_l(\vec{r};\vec{\rho},\vec{R})$, eigenfunctions of $\hat{H}_{el}$ for the quasimolecular system

$$\hat{H}_{el}\Phi_l(\vec{r};\vec{\rho},\vec{R}) = \varepsilon_l(\vec{\rho},\vec{R})\Phi_l(\vec{r};\vec{\rho},\vec{R}). \tag{2.41}$$

For each value of $\vec{\rho}$, this expansion takes the form:

$$\Psi = \sum_l a_l(t;\vec{\rho})\Phi_l(\vec{r};\vec{\rho},\vec{R}) e^{-i\int_0^t \varepsilon_l dt'}, \tag{2.42}$$

where from Eq. 2.39 for the entrance channel may be written

$$\lim_{R\to\infty} \Phi_i(\vec{r};\vec{\rho},\vec{R}) = \Phi_i(\vec{r};\vec{\rho}). \tag{2.43}$$

The expansion coefficients $a_l(t;\vec{\rho})$ are then obtained by substituting 2.40 and 2.42 in 2.38. For a given nuclear trajectory and fixed $\vec{\rho}$, one obtains [53]:

$$i\frac{da_l}{dt} = \sum_k a_k \left\langle \Phi_l \right| \hat{H}_{el} - i\frac{\partial}{\partial t} \left| \Phi_k \right\rangle e^{-i\int_0^t (\varepsilon_k - \varepsilon_l)dt'}. \tag{2.44}$$

2.8 Dynamical Couplings

The dynamical couplings $\langle \Phi_l | - i\dfrac{\partial}{\partial t} | \Phi_k \rangle$ cause transitions between the molecular states Φ_l.

While Eqs. 2.38 and 2.39 are expressed in a laboratory reference frame XYZ, with the Z-axis pointing along the direction of $\vec{v}$ and the X-axis along the direction $\vec{b}$, the MOs are calculated in a molecular frame X'Y'Z', with the Z'-axis along the internuclear direction $\vec{R}$ as displayed in Fig. 2.3.

Considering the molecular system represented in Fig. 2.3, within the semiclassical impact parameter treatment, the coupling operator may be expressed as

$$\begin{aligned} -i\frac{\partial}{\partial t} &= -i\vec{v}\nabla_{\vec{R}} = -iv\frac{\partial}{\partial Z} \\ &= -iv\left[\frac{\partial Z'}{\partial Z}\frac{\partial}{\partial Z'} + \frac{\partial X'}{\partial Z}\frac{\partial}{\partial X'}\right] = -i\frac{vZ}{R}\frac{\partial}{\partial Z'} + i\frac{bv}{R}\frac{\partial}{\partial X'}, \end{aligned} \tag{2.45}$$

where the plane ZX coincides with the so-called collision plane $Z'X'$, defined by the projectile, the nuclear center of mass of the target molecule and the velocity vector $\vec{v}$. Therefore the Y-axis coincides with the Y'-axis, both perpendicular to the collision plane. The vector $\vec{\rho}$ is generally not placed in the previously mentioned plane.

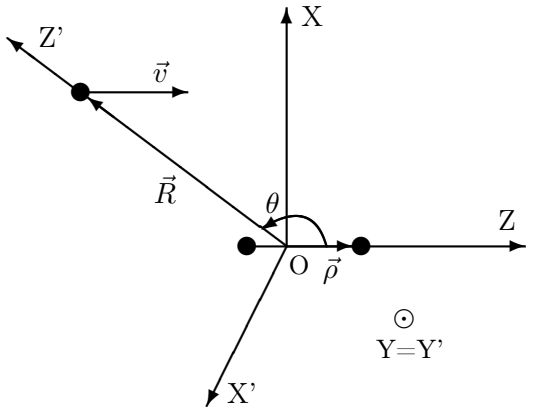

2.3. Figure: The relationship between the laboratory reference frame XYZ and the molecular frame X'Y'Z' with $\vec{R}$ directed along OZ'.

Changing into spherical coordinates, and by considering the coincidence of the unit vectors of the molecular frame $(\hat{X}, \hat{Y}, \hat{Z})$ and newly defined system $(\hat{\theta}, \hat{\phi}, \hat{R})$, we may write

$$\begin{aligned} \frac{\partial}{\partial X'} &= \frac{1}{R}\frac{\partial}{\partial \theta}, \\ \frac{\partial}{\partial Y'} &= \frac{1}{Rsin\theta}\frac{\partial}{\partial \phi}, \\ \frac{\partial}{\partial Z'} &= \frac{\partial}{\partial R}. \end{aligned} \tag{2.46}$$

The matrix element of the operator $\dfrac{\partial}{\partial Z'}$ corresponds to the radial coupling, whereas $\dfrac{\partial}{\partial X'}$ denotes the rotational coupling. The last mentioned operator is related to the total electronic angular momentum operator $\hat{\vec{L}}$.

Developing the derivatives defined in the laboratory-fixed frame with respect to the molecular-fixed frame, we may write

$$\frac{\partial}{\partial \theta}\Big|_{R,\phi,\vec{\rho},\vec{r}} = \frac{\partial}{\partial \theta}\Big|_{R,\phi,\vec{\rho}',\vec{r}'} + \sum_{i=1}^{N} \sum_{r_i'=x_i',y_i',z_i'} \frac{\partial r_i'}{\partial \theta}\Big|_{R,\phi,\vec{\rho},\vec{r}} \frac{\partial}{\partial r_i'}\Big|_{R,\phi,\vec{\rho}',\vec{r}'}, \tag{2.47}$$

and

$$\frac{\partial}{\partial \phi}\Big|_{R,\theta,\vec{\rho},\vec{r}} = \frac{\partial}{\partial \phi}\Big|_{R,\theta,\vec{\rho}',\vec{r}'} + \sum_{i=1}^{N} \sum_{r_i'=x_i',y_i',z_i'} \frac{\partial r_i'}{\partial \phi}\Big|_{R,\theta,\vec{\rho},\vec{r}} \frac{\partial}{\partial r_i'}\Big|_{R,\theta,\vec{\rho}',\vec{r}'}. \tag{2.48}$$

The components of the position vector of the ith electron in the laboratory system $(x_i,\ y_i,\ z_i)$ are related to those in the molecular system $(x_i',\ y_i',\ z_i')$ by

$$\begin{aligned} x_i' &= x_i cos\theta cos\phi + y_i cos\theta sin\phi - z_i sin\theta, \\ y_i' &= -x_i sin\phi + y_i cos\phi, \\ z_i' &= x_i sin\theta cos\phi + y_i sin\theta sin\phi + z_i cos\theta. \end{aligned} \tag{2.49}$$

Using the relations Eq. 2.49, we find

$$\begin{aligned} &\frac{\partial x'_i}{\partial\theta} = -z'_i, \qquad &&\frac{\partial y'_i}{\partial\theta} = 0, \qquad &&\frac{\partial z'_i}{\partial\theta} = x'_i, \\ &\frac{\partial x'_i}{\partial\phi} = y'_i cos\theta, \qquad &&\frac{\partial y'_i}{\partial\phi} = -x'_i cos\theta - z'_i sin\theta, \qquad &&\frac{\partial z'_i}{\partial\phi} = y'_i sin\theta, \end{aligned} \tag{2.50}$$

then using these relations with Eq. 2.47 and Eq. 2.48, it is seen that

$$\frac{\partial}{\partial\theta}\Big|_{\phi,R,\vec{\rho},\vec{r}} = \sum_{i=1}^{N}\left[-z'_i\frac{\partial}{\partial x'_i} + x'_i\frac{\partial}{\partial z'_i}\right], \tag{2.51}$$

$$\frac{\partial}{\partial\phi}\Big|_{R,\theta,\vec{\rho},\vec{r}} = sin\theta\sum_{i=1}^{N}\left[y'_i\frac{\partial}{\partial z'_i} - z'_i\frac{\partial}{\partial y'_i}\right] + cos\theta\sum_{i=1}^{N}\left[y'_i\frac{\partial}{\partial x'_i} - x'_i\frac{\partial}{\partial y'_i}\right]. \tag{2.52}$$

Using the expressions below

$$\begin{aligned} \hat{L}_{x'} &= -i\sum_j\left[y'_j\frac{\partial}{\partial z'_j} - z'_j\frac{\partial}{\partial y'_j}\right], \\ \hat{L}_{y'} &= -i\sum_j\left[z'_j\frac{\partial}{\partial x'_j} - x'_j\frac{\partial}{\partial z'_j}\right], \\ \hat{L}_{z'} &= -i\sum_j\left[x'_j\frac{\partial}{\partial y'_j} - y'_j\frac{\partial}{\partial x'_j}\right], \end{aligned} \tag{2.53}$$

we obtain

$$\frac{\partial}{\partial\theta}\Big|_{\phi,R,\vec{\rho},\vec{r}} = -i\hat{L}_{y'}, \tag{2.54}$$

$$\frac{\partial}{\partial\phi}\Big|_{R,\theta,\vec{\rho},\vec{r}} = i(sin\theta\hat{L}_{x'} - cos\theta\hat{L}_{z'}), \tag{2.55}$$

where $\hat{L}_{x'}$, $\hat{L}_{y'}$ and $\hat{L}_{z'}$ are the components of the electronic angular momentum in the molecular frame. Since the collision is considered in the XZ plane, the term of the derivative $\dfrac{\partial}{\partial\phi}$ is zero, as follows the electronic angular momentum vector has only a Y-direction component.

Eq. 2.45 may be expressed as

$$-i\frac{\partial}{\partial t} = -i\frac{vZ}{R}\frac{\partial}{\partial R}\Big|_{\theta,\phi,\vec{\rho}',\vec{r}'} + \frac{bv}{R^2}\hat{L}_{y'}, \tag{2.56}$$

where $\hat{L}_{y'}$ is the Y' component of the electronic angular momentum. Therefore, dynamical couplings have two components:
(i) Radial couplings: $\langle\Phi_l|\,\frac{\partial}{\partial R}\,|\Phi_k\rangle$, which are due to the change of the wavefunctions with the internuclear distance $\vec{R}$.
(ii) Rotational couplings: $\langle\Phi_l|\,i\hat{L}_{y'}\,|\Phi_k\rangle$, which are due to the rotation of the internuclear axis during the collision.

The first step in the application of the molecular expansion is the solution of Eq. 2.41 in order to obtain the wavefunctions and their energies. Efficient techniques have been developed to solve Eq. 2.41 and also to evaluate the dynamical couplings. Electronic energies and couplings are then substituted in the system Eq. 2.44, which is solved to obtain coefficients $a_l(t;\vec{\rho})$ of Eq. 2.42.

2.9 Calculation of the Cross Sections

When molecular vibration can be ignored, the probability P_{if} for transition to the final state Φ_f is calculated from the coefficient a_f of expansion Eq. 2.42 obtained by solving Eq. 2.44

$$P_{if}(b,v,\vec{\rho}) = \lim_{t\to\infty}|a_f(t;\vec{\rho})|^2. \tag{2.57}$$

The partial cross section for the electron capture to the final state is obtained by integrating the corresponding transition probability over all possible values of the impact parameter

$$\sigma_{if}(v,\vec{\rho}) = 2\pi\int_0^\infty bP_{if}(b,v,\vec{\rho})db, \tag{2.58}$$

or

$$\sigma_{if}(v,\vec{\rho}) = 2\pi \int_0^{b_{max}} bP_{if}(b,v,\vec{\rho})db. \tag{2.59}$$

where b_{max} is the maximum value of parameter b beyond which the particle is no longer subject to the influence of the potential.
The total cross section is a sum of the partial cross sections

$$\sigma(v,\vec{\rho}) = \sum_f \sigma_{if}(v,\vec{\rho}). \tag{2.60}$$

All along this work, the cross sections have been calculated by means of EIKONX program of Allan [54–57], which is a development from the previous program PAMPA [55].

2.10 Centroid Approximation

An estimate of the vibrational motion of the diatomic molecule, neglecting the rotational modes, may be obtained by introducing Franck-Condon factors in the framework of the centroid approximation.

The centroid method is basically a peaking approximation in which one takes into account that the product of the initial and final vibrational wavefunctions $\chi_0\chi'_\nu$ exhibits especially as ν increases, a sharply peaked structure. One may then approximate the amplitude $a_j(\infty;\vec{\rho})$ by its value at $\rho = \bar{\rho}$, where $\bar{\rho}$ is usually the distance for which the product $\chi_0\chi'_\nu$ takes its first (and largest) extremum

$$P^C_{0\nu}(b,v,\hat{\rho}) = P^{el}(b,v,\bar{\rho})F_{0\nu}, \tag{2.61}$$

where the capture probabilities are given by

$$P^{el}(b,v,\bar{\rho}) = \sum_j |a_j(\infty;\bar{\rho})|^2, \tag{2.62}$$

with the summation extending over all charge-exchange channels, and $F_{0\nu}$

is the Franck-Condon factor

$$F_{0\nu} = \left(\int \chi_0(\rho) \chi'_\nu(\rho) d\rho \right)^2 . \tag{2.63}$$

By integration over impact parameter we find the expression for the capture cross sections

$$\sigma^C_{0\nu}(v) = \sigma^{el}(v, \bar{\rho}) F_{0\nu}. \tag{2.64}$$

Finally the roughest approximation draws from the Franck-Condon method of vertical transitions in molecular spectroscopy. It is generally assumed that at high collision energies the population of the vibrational states of the diatomic molecule subsequent to electronic transitions obeys the Franck-Condon principle. In Franck-Condon approximation, the centroid is approximated by the equilibrium distance ρ_{eq} of the target molecule

$$\sigma^{FC}_{0\nu}(v) = \sigma^{el}(v, \rho_{eq}) F_{0\nu}. \tag{2.65}$$

An obvious advantage of this approach is that since ρ_{eq} is independent of ν, summation of the cross sections over all values of ν yields by closure ($\sum_\nu F_{0\nu} = 1$) the corresponding electronic cross section σ^{el}. Therefore when vibrationally-resolved cross sections are not required, one could just ignore vibration, and treat the electronic dynamics with the target internuclear distance fixed at the equilibrium value [58].

3 Chapter

Electronic Structure Calculation

3.1 Electronic Structure Methods

Ab initio quantum chemistry has become an essential tool in the study of atoms and molecules. Firstly, the Born-Oppenheimer approximation [32] is applied. The *ab initio* program like Molpro [59] computes the electronic energy by solving the electronic Scrödinger equation for fixed nuclear configuration. The electronic energy as a function of the 3N-6 internal nuclear degrees of freedom defines the potential energy surface.

The electronic Schödinger equation cannot be solved exactly, except for very simple systems like the hydrogen atom. Therefore, the electronic wavefunction is represented in certain finite basis sets, and the Schrödinger equation is transformed into an algebraic equation which can be solved using numerical methods.

The simplest type of *ab initio* electronic structure calculation is the Hartree-Fock (HF) method [60, 61], in which each electron moves in an average potential of the remaining electrons, but has no knowledge of the positions of these. Thus, even though the Coulomb interaction between the electrons is taken into account in an averaged way, the electrons with opposite spin are unable to avoid each other when they come close, and therefore the electron repulsion is overestimated in Hartree-Fock method. Many types of calculations begin with a Hartree-Fock calculation and sub-

sequently introduce electron-electron repulsion correction, referred to as electronic correlation. If we want to describe a molecular system accurately, we have thus to take into account the electron correlation by going beyond the Hartree-Fock approximation. Møller-Plesset (MP) perturbation theory [62], Configuration Interaction (CI) [63,64], Coupled Cluster (CC) theory [65–67], Multiconfiguration Self-Consistent Field (MCSCF) [68,69], Complete Active Space Self-Consistent Field (CASSCF) [68–73] and Multireference Configuration Interaction (MRCI) [74–76] are examples of these post-Hartree-Fock methods. Today, by far the most popular post-HF method is the Configuration Interaction (CI). The standard CI method relies on partitioning the exact wavefunction into a selected collection of smaller functions and their corresponding coefficients. Using the method of undetermined multipliers, the contribution of these other determinants can be determined utilizing the constraint of the already known Hartree-Fock wavefunction. If this set is complete, it is a full CI (FCI) calculation.

Many of the most interesting research directions in quantum chemistry have involved the solution of multireference problems. Chemically speaking, a multireference system is a molecule or reaction in which the one-electron approximation is not only quantitatively but also qualitatively wrong. Practically all reactions that involve bond-breaking are of this type, as are some low-lying excited electronic states of many molecules. In such situation, the typical HF wavefunction is not a good description of the system, and something more complex is necessary to reproduce the chemistry. The simplest idea is the MCSCF technique, which performs an HF/SCF calculation upon a set of configurations chosen for their chemical importance. More general techniques mainly differ as to how the various determinants are included in the wavefunction; perhaps the most popular method is the CASSCF method. Using CASSCF, the references are selected by choosing an active space of several chemically important orbitals and performing a FCI in the span of the active space. If it appears necessary to include excitations into the higher orbitals, a perturbational calculation is performed on each reference to improve the correlation description. Such a calculation is referred to as CASSCF plus second-order perturbation theory, or (CASPT2). If a completely variational method is desired, then a multireference version of the CI method (MRCI) is the method of choice.

Density functional theory (DFT) [77, 78] represents somewhat of a departure from conventional *ab initio* quantum chemical methods in that it

does not formally deal with wavefunctions, but rather with the electron density. In some revolutionary work done the early 1960s, Kohn and coworkers discovered that all ground-state properties of a molecular system could be completely described using only the electron density and the (fixed) nuclear positions. The first Hohenberg-Kohn theorem [77] proved the existence of a unique functional relationship between the electron density and the electronic Hamiltonian. Thus, if the exact relationship were known we could compute all of the molecular properties using only the electron density (which depends on only three coordinates) and avoid the building of a wavefunction (which depends on 3N coordinates). From a practical perspective, the most important advance was made in 1965 by Kohn and Sham. Utilizing the well-developed iterative techniques of the HF/SCF method, a computationally feasible approach to DFT was found which avoided the explicit construction of the electronic kinetic energy portion of the energy functional. This formalism is called Kohn-Sham Density Functional Theory (KS-DFT) [78] and it can be fairly easily implemented with computation times comparable to conventional SCF procedures. The chief difference between the SCF and KS-DFT approaches lies in the exchange-correlation density functional, which accounts for both electron correlation and nonclassical exchange effects on the energy. If the exact form for the exchange-correlation functional were known, the KS-DFT approach would give the exact energy. KS-DFT therefore requires the construction of accurate exchange-correlation functionals [79].

The choice of the method is always a compromise between several factors. The level of accuracy is the first and foremost criterion, and then the computational cost has to be taken into account. The computational cost grows with the size of the system and the level of the method and accuracy required. Each methods has its advantages and its limits. Some care is needed to decide which method is the best compromise and in that sense, this method cannot be used as a black box method and the results have to be analyzed carefully.

The *ab initio* methods used in this work are introduced in this chapter.

In the Hartree-Fock approach, it is assumed, in accordance with the independent particle approximation and the Pauli exclusion principle, that the N-electron wave function is a Slater determinant Φ, or in other words an antisymmetric product of individual electron spin-orbitals. Choosing the single determinant as a trial function, the variational principle can be used

to derive the Hartree-Fock equations, by minimizing the energy subject to the boundary condition, that the Φ_i are orthonormal.

$$\Phi(1,...,N) = \frac{1}{\sqrt{N!}} \begin{vmatrix} \Phi_1(1) & \Phi_2(1) & \dots & \Phi_N(1) \\ \Phi_1(2) & \Phi_2(2) & \dots & \Phi_N(2) \\ \vdots & \vdots & \ddots & \vdots \\ \Phi_1(N) & \Phi_2(N) & \dots & \Phi_N(N) \end{vmatrix}; \quad \langle \Phi_i | \, \Phi_j \rangle = \delta_{ij} \tag{3.1}$$

The columns in a Slater determinant are single-electron wave functions, orbitals, while the electron coordinates are along the rows. We are interested in solving the electronic Schrödinger equation for a molecule. The one-electron functions are thus molecular orbitals, which are given as the product of a spatial orbital and a spin function, also known as spin-orbitals, which may be taken as orthonormal. Since a determinant vanishes when two columns (or rows) are equal, the Slater determinant will vanish if two electrons have the same values of the four quantum numbers.

If we denote by $\hat{P}$ a permutation of the electron coordinates, we may rewrite the Slater determinant as

$$\begin{aligned} \Phi(1,...,N) &= \frac{1}{\sqrt{N!}} \sum_{P=0}^{N-1} (-1)^P \hat{P} \Phi_1(1) ... \Phi_N(N) \\ &= \hat{A} \Phi_H. \end{aligned} \tag{3.2}$$

Φ_H is the simple product of spin-orbitals

$$\Phi_H = \Phi_1(1) ... \Phi_N(N), \tag{3.3}$$

which is referred as a Hartree wave function. The operator which appears in Eq. 3.2 is the antisymmetrisation operator

$$\hat{A} = \frac{1}{\sqrt{N!}} \sum_{P=0}^{N-1} (-1)^P \hat{P} = \frac{1}{\sqrt{N!}} \left[\hat{1} - \sum_{ij} \hat{P}_{ij} + \sum_{ijk} \hat{P}_{ijk} - \dots \right]. \tag{3.4}$$

Using Eq. 3.2 the energy may be written in terms of the permutation

operator as

$$\begin{aligned} E &= \langle\Phi|\,\hat{H}_{el}\,|\Phi\rangle = \langle\hat{A}\Phi_H|\,\hat{H}_{el}\,|\hat{A}\Phi_H\rangle = \sqrt{N!}\,\langle\Phi_H|\,\hat{H}_{el}\,|\hat{A}\Phi_H\rangle \\ &= \sum_P (-1)^P\,\langle\Phi_H|\,\hat{H}_{el}\,|\hat{P}\Phi_H\rangle\,. \end{aligned} \tag{3.5}$$

The nuclear-nuclear repulsion term of the electronic Hamiltonian operator does not depend on electron coordinates and is a constant for a given nuclear geometry. The nuclear-electron attraction is a sum of terms, each depending only on one electron coordinate. The electron-electron repulsion, however, depends on two electron coordinates. The operators may be collected according to the number of electron indices.

$$\begin{aligned} \hat{h}_i &= -\frac{1}{2}\nabla_i^2 - \sum_I \frac{Z_I}{\mid \vec{R}_I - \vec{r}_i \mid} \\ \hat{g}_{ij} &= \frac{1}{\mid \vec{r}_i - \vec{r}_j \mid} \\ \hat{H}_{el} &= \sum_i \hat{h}_i + \sum_{i<j} \hat{g}_{ij} + \hat{V}_{nuc,nuc} \end{aligned} \tag{3.6}$$

The one-electron operator $\hat{h}_i$ describes the motion of electron i in the field of all the nuclei, and $\hat{g}_{ij}$ is a two-electron operator giving the electron-electron repulsion.

The Hartree-Fock approximation is obtained from the variational minimum of the energy expectation value $\langle\Phi|\,\hat{H}_{el}\,|\Phi\rangle$ using a single Slater determinant $\Phi = 1/\sqrt{N!}\,\det\{\Phi_i\}$ to represent the exact electronic wave function subject to the constraint that the one-electron particle wave functions (namely the orbitals) Φ_i are orthonormal. The standard Hartree-Fock differential equations are given by

$$\hat{F}_i\,\Phi_i = \varepsilon_i\,\Phi_i, \tag{3.7}$$

where the $\hat{F}$ is the Fock operator, which can be given in the following form

$$\hat{F}_i = \hat{h}_i + \sum_j \left(\hat{J}_j - \hat{K}_j\right). \tag{3.8}$$

The Fock operator is an effective one-electron energy operator, describing the kinetic energy of an electron and the attraction to all the nuclei ($\hat{h}_i$), as well as the repulsion to all the other electrons through the $\hat{J}$ and $\hat{K}$ operators

$$\begin{aligned} \hat{J}_j(1)\,|\Phi_i(1)\rangle &= \langle \Phi_j(2)|\,\hat{g}_{12}\,|\Phi_j(2)\rangle\,|\Phi_i(1)\rangle\,, \\ \hat{K}_j(1)\,|\Phi_i(1)\rangle &= \langle \Phi_j(2)|\,\hat{g}_{12}\,|\Phi_i(2)\rangle\,|\Phi_j(1).\rangle \end{aligned} \tag{3.9}$$

The orbital energies can be considered as matrix elements of the Fock operator with the molecular orbitals. The total energy can be written in terms of molecular orbital energies

$$\begin{aligned} E &= \sum_i \varepsilon_i - \frac{1}{2}\sum_{i,j}(J_{ij} - K_{ij}) + V_{nuc,nuc}, \\ \varepsilon_i &= \langle \Phi_i|\,\hat{F}_i\,|\Phi_i\rangle = h_i + \sum_i (J_{ij} - K_{ij})\,. \end{aligned} \tag{3.10}$$

The total energy is not simply a sum of molecular orbital energies. The Fock operator contains terms describing the repulsion to all other electrons ($\hat{J}$ and $\hat{K}$ operators), and the sum over molecular orbital energies therefore counts the electron-electron repulsion twice, which must be corrected for. The total energy cannot be exact, as it describes the repulsion between an electron and all other electrons, assuming that the spatial distribution is described by a set of orbitals. The electron-electron repulsion is only accounted for in an average fashion, and the Hartree-Fock method is therefore also referred to as a mean-field approximation [80].

3.2 Electron Correlation

The exact wave function for a system of many interacting electrons is never a single determinant or a simple combination of a few determinants. Hartree-Fock method replaces the instantaneous electron-electron repulsion with the repulsion of each electron with an average electron charge cloud. These instantaneous interactions are keeping out the electrons of each other's way and, as a result, the inter-electronic repulsion is reduced. The motion of these electrons is said to be correlated as they avoid each other. That is referred to as electron correlation. When electrons come close together there

is a very strong repulsive effect inducing an error of the Hartree-Fock energy due to a positive contribution resulting from lack of proper electron correlation. The correlation energy E_{corr}, is defined as the difference between the exact non-relativistic energy of the system E and the Hartree-Fock energy E_{HF} obtained in the limit in a given basis set

$$E_{corr} = E - E_{HF}. \tag{3.11}$$

The inclusion of electron correlation is at least necessary to obtain reliable order of magnitude of the energies of excited and transition states. There are three main methods for calculating electron correlation: Configuration Interaction (CI), Many-Body Perturbation Theory (MBPT) and Coupled Cluster (CC) theory.

3.3 Basis Sets

Each molecular orbital (one electron function) Φ_i is expressed as a linear combination of n basis functions φ_μ

$$\Phi_i = \sum_{\mu=1}^{N} c_{\mu i}\varphi_\mu. \tag{3.12}$$

The coefficients $c_{\mu i}$ are called molecular orbital expansion coefficients. The basis functions $\varphi_{1\ldots N}$ are assumed to be normalized. Usually these basis functions are located at the center of atoms and are therefore often called atomic basis functions, although they in general are not solutions to an atomic Schrödinger equation.

There are two commonly used types of functions to built the atomic orbitals: Slater type orbitals (STO) and Gaussian type orbitals (GTO).

Slater type orbitals have the functional form shown in Eq. 3.13

$$\varphi(r,\theta,\phi;\zeta,n,l,m) = NY_{l,m}(\theta,\phi)r^{n-1}e^{-\zeta r}, \tag{3.13}$$

The radial part $r^{n-1}e^{-\zeta r}$ depends on the distance r from the origin of the basis function (usually the location of the nucleus), the orbital exponent ζ, and the principal quantum number n. The spherical part $Y_{l,m}$ depends on the angular quantum number l and the magnetic quantum number m. The

normalization constant N is chosen such that the integral over the square of the basis function yields unity.

Gaussian type orbitals can be written in terms of polar or Cartesian coordinates as shown in Eq. 3.14

$$\begin{aligned}\varphi(r,\theta,\phi;\alpha,n,l,m) &= NY_{l,m}(\theta,\phi)r^{2n-2-l}e^{-\alpha r^2},\\ \varphi(x,y,z;\alpha,a,b,c) &= Nx^a y^b z^c e^{-\alpha(x^2+y^2+z^2)}.\end{aligned} \tag{3.14}$$

The radial extend is proportional to $e^{-\alpha r^2}$, α being the exponent. The normalization constant N serves a similar purpose as for STOs. The spherical part may be expressed through the cartesian x, y and z in powers of a, b, and c, respectively. The sum of these exponents $l = a + b + c$ is used to define the angular momentum of the basis functions: s-type ($l = 0$), p-type ($l = 1$), d-type ($l = 2$), f-type ($l = 3$), g-type orbital ($l = 4$), etc. Although a GTO appears similar in the two set of coordinates, there is a subtle difference. A d-type GTO written in terms of the spherical functions has five components ($Y_{2,2}$, $Y_{2,1}$, $Y_{2,0}$ $Y_{2,-1}$, $Y_{2,-2}$), but there appear to be six components in the Cartesian coordinates (x^2, y^2, z^2, xy, xz, yz). The latter six functions, however, may be transformed to the five spherical d-functions and one additional s-function ($x^2+y^2+z^2$). Modern programs for evaluating two-electron integrals are geared to Cartesian coordinates and they generate pure spherical d-functions by transforming the six Cartesian components to the five spherical functions.

Slater-type orbitals are similar to Hydrogenic orbitals in the regions close to the nuclei. Specifically, they have a non-zero slope near the nucleus on which they are located

$$\frac{d}{dr}\left(e^{-\zeta r}\right)_{r=0} = -\zeta, \tag{3.15}$$

therefore they can have proper electron-nucleus cusps. In contrast, GTOs have zero slope near $r = 0$ because

$$\frac{d}{dr}\left(e^{-\alpha r^2}\right)_{r=0} = 0. \tag{3.16}$$

The other problem is that the GTO falls off too rapidly far from the nucleus compared with an STO. Nevertheless, the great advantage of GTOs is that all the integrals can be calculated either analytically, or with a limited com-

putational effort (one-dimensional integrals), thus saving precious computer time.

In order to combine the best feature of GTOs (computational efficiency) with that of STOs (proper radial shape), most of the first basis sets developed with GTOs used them as building blocks to approximate STOs. That is, the basis functions used for SCF calculations were not individual GTOs, but instead a linear combination of GTOs fit to reproduce as accurately as possible a STO, i. e.,

$$\varphi(x, y, z; \{\alpha\}, a, b, c) = \sum_{j=1}^{M} c_j \varphi(x, y, z; \alpha_j, a, b, c), \tag{3.17}$$

where M is the number of Gaussians used in the linear combination, and the coefficients c are chosen to optimize the shape of the basis function sum and ensure normalization. When a basis function is defined as a linear combination of Gaussians, it is referred to as a contracted basis function, and the individual Gaussians from which it is formed are called primitive Gaussians, and could be s, p, d, f, etc. type Gaussian functions. Thus, in a basis set of GTOs, each basis function is defined by the contraction coefficients c and exponents α of each of its primitives. The contraction coefficients are fixed for the basis set, and do not vary in any calculation. The degree of contraction M refers to the total number of primitives used to make all of the contracted functions. However, contracted GTO does not really correctly produce a cusp because every Gaussian has a zero slope at $r = 0$, thus any combination will have zero slope.

Hehre, Stewart, and People (1969) were the first to systematically determine optimal contraction coefficients and exponents for mimicking STOs with contracted GTOs for a large number of atoms in the periodic table. They constructed a series of different basis sets for different choices of M in Eq. 3.17. In particular, they considered $M = 2$ to 6, and they called these different basis sets STO-MG, for 'Slater-Type Orbital approximated by M Gaussians'. The optimum combination of speed an accuracy (when comparing to calculations using STOs) was achieved for $M = 3$ [81].

The STO-3G basis set is what is known as a single-ζ basis set or a minimal basis set. One way to increase the flexibility of a basis set is to decontract it. Taking the STO-3G basis set, and instead of constructing each basis function as a sum of three Gaussians, one could construct two

basis functions for each AO, the first being a contraction of the first two primitive Gaussians, while the second would simply be the normalized third primitive. A basis set with two functions for each AO is called a double-ζ basis. The next step up is a triple-ζ basis, which contains three times as many functions as the minimum basis.

Core orbitals are only weakly affected by chemical bonding. Valence orbitals, on the other hand, can vary widely as a function of chemical bonding. Atoms bonded to significantly more electronegative elements take on partial positive charge from loss of valence electrons, and thus their remaining density is distributed more compactly. The reverse is true when the bonding is to a more electropositive element. From a chemical standpoint, then, there is more to be gained by having flexibility in the valence basis functions than in the core, and recognition of this phenomena let to the development of so-called split-valence or valence-multiple-ζ basis sets. In such basis sets, core orbitals continue to be represented by a single (contracted) basis function, while valence orbitals are split into arbitrarily many functions.

One very economical, small split valence basis set is the 3-21G basis set [82–84]. The nonvalence electrons are described by single basis functions composed of a contraction of three Gaussians. This is a valence double-ζ basis set as there are 2 digits after the hyphen. Each valence electron is described by two basis functions. The first of these basis function is composed of two Gaussian primitives while the second consists of a single uncontracted Gaussian primitive.

Dunnings D95 basis set has been derived from an already existing large atomic basis set of nine uncontracted Gaussians primitives of s- and five uncontracted Gaussian primitives of p-type [85]. Six of the nine s-type functions have been grouped into a single contraction, while the other three s-type functions have been left alone. Similarly, four of the five p-type functions have been contracted into a single function, while one function was left uncontracted. Overall, this yields a basis set of four s-type and two p-type basis functions. The D95 basis set is a full double-ζ basis set in that it allocates two basis functions for each atomic orbital of the core as well as the valence region occupied in the electronic ground state. The standard nomenclature used specifies the uncontracted basis set in brackets and the resulting contracted version in square brackets. Using the D95 basis set as an example, the contraction can be described as (9s,5p)$\rightarrow$[4s,2p]. This notation does not specify, how many primitives are contained in each contraction. This

can be specified in more detail as (6111,41), listing first the s-type functions (here distributed over four contractions) and the p-type functions.

The so-called segmented contraction implies that the primitives used for one basis function are not used for another of the same angular momentum. One method to carrying out a segmented contraction is to use a general contraction. In a general contraction, there is a single set of primitives that are used in all contracted basis functions, but they appear with different coefficients in each. Example of split-valence basis set using general contraction is the cc-pVTZ, set of Dunning and co-workers [86], where the acronym stands for 'correlation-consistent polarized Valence Triple Zeta'. The 'correlation-consistent' part of the name implies that the exponents and contraction coefficients were variationally optimized not only for Hartree-Fock calculations, but also for calculations including electron correlation to agree within some tolerance with experimental data. If 'cc' is missing, the AO exponents and contraction coefficients were determined to make the Hartree-Fock atomic state energies agree with experiment to some precision. The 'p' specifies that polarization basis orbitals have been included in the basis. 'VTZ' specifies three contracted or primitive GTOs for each valence orbital. Nothing is said about the core orbitals because each of them is described by a single contracted Gaussian type basis orbital.

The molecular orbitals, which are eigenfunctions of a Schrödinger equation involving multiple nuclei at various positions in space, require more mathematical flexibility than do the atoms. To further increase the flexibility of the orbital description, basis sets are frequently augmented with basis functions of higher angular momentum. This does allow for different preferred directions in space for electrons to wonder around it. A typical first step consists of the addition of a set of d-type functions to the basis set of those atoms, which have occupied s- and p-shells in their electronic ground states. For hydrogen, this corresponds to the addition of a set of p-type functions. In most cases, high angular momentum functions are important. The use of polarized basis sets is especially important for the proper description of bonds of strongly electronegative elements such as oxygen and fluorine and for theoretical studies using correlated methods [87]. For independent-particle wave functions, where electron correlation is not considered, the first set of polarization functions (i.e. *p*-functions for hydrogen and *d*-functions for heavy atoms) is by far the most important, and will in general describe most of the important charge polarization effect.

The theoretical description of negatively charged species is particularly challenging for *ab initio* MO theory. This is due to the fact that the excess negative charge spreads outward to a much larger degree than is typically the case for uncharged or positively charged molecules. The description of such a diffuse charge distribution is not very well possible with the typical split valence basis sets. Addition of very diffuse basis functions (with correspondingly small orbital exponents) cures this problem to a certain extend as it allows the description of electron density relatively far from the nucleus [88, 89]. Diffuse basis functions are typically added as an additional set of uncontracted Gaussian functions of the same angular momentum as the valence electrons. In the Dunning notation 'aug' specifies that (conventional) diffuse basis functions have been added, but the number and kind depend on how the valence basis is described. At the pVDZ level, one s, one p, and one d diffuse function appear; at pVTZ a diffuse f function also is present; at pVQZ a diffuse g set is also added; and at pV5Z a diffuse h set is present.

In methods including electron correlation are used, higher angular momentum functions are essential. Electron correlation describes the energy lowering by the electrons avoiding each other, beyond the average effect taken into account by Hartree-Fock methods. Two types of correlation can be identified, a radial and an angular correlation. The radial correlation refers to the situation where one electron is close to, and the other far from, the nucleus. To describe this, the basis set needs functions of the same type, but with different exponents. The angular correlation refers to the situation where two electrons are on opposite sides of the nucleus. To describe this, the basis set needs functions with the same magnitude exponents, but different angular momentum. The angular correlation is of similar importance as the radial correlation, and higher angular momentum functions are consequently essential for correlated calculations.

3.4 Configuration Interaction

The exact adiabatic wavefunctions which satisfy $\hat{H}_{el}\Psi = E\Psi$ can be expressed as a linear combination of Slater determinants built from a complete set of orbitals. A whole series of determinants may be generated by replacing molecular orbitals that are occupied in the Hartree-Fock determinant by

molecular orbitals that are unoccupied (virtual). This linear combination has infinite terms and its truncation is the foundation of the Configuration Interaction (CI) method. We can write the wave function as

$$\begin{aligned}\Psi =& c_0\Phi_0 + \underbrace{\sum_{i=1}^{N}\sum_{a=N+1}^{K} c_i^a\Phi_i^a}_{\text{single excitations (S)}} + \underbrace{\sum_{i>j=1}^{N}\sum_{a>b=N+1}^{K} c_{ij}^{ab}\Phi_{ij}^{ab}}_{\text{double excitations (D)}} \\ &+ \underbrace{\sum_{i>j>k=1}^{N}\sum_{a>b>c=N+1}^{K} c_{ijk}^{abc}\Phi_{ijk}^{abc}}_{\text{triple excitations (T)}} + \underbrace{\sum_{i>j>k>l=1}^{N}\sum_{a>b>c>d=N+1}^{K} c_{ijkl}^{abcd}\Phi_{ijkl}^{abcd}}_{\text{quadrupole excitations (S)}} + \ldots,\end{aligned} \tag{3.18}$$

where Φ_0 is the ground-state Hartree-Fock wave function, Φ_i^a is a Slater determinant with an electron excited from the ith occupied orbital to the ath unoccupied orbital (which differ from Φ_0 in having the spin-orbital Φ_i replaced by Φ_a), Φ_{ij}^{ab} are the doubly excited Slater determinants, and so on.

The ground and excited states of the appropriate symmetry are constructed from the variationally computed SCF wavefunctions and orbitals.

Because, in practice, one can never compute all the unoccupied Hartree-Fock orbitals, the upper limit in the sum is designed to indicate that there are only K orbitals. When we truncate at zeroth-order, we have the Hartree-Fock determinant. Φ_0 being the determinant formed from the N lowest energy spin-orbitals. At first order, we have configuration interaction with single excitations, at second order we have configuration interaction with single and double excitations, and so on. When we do not truncate the expansion in Eq. 3.18 (so that we include N-electron excitations) we say we are doing a Full Configuration Interaction calculations, which is called full CI.

If we have K spin-orbitals, N will be occupied in $|\Phi_0\rangle$ and $K-N$ will be unoccupied. We can choose n spin orbitals from those occupied in $|\Phi_0\rangle$ in $\binom{N}{n}$ ways. Similarly, we can choose n orbitals from the $K-N$ virtual orbitals in $\binom{K-N}{n}$ ways. Thus the total number of n-tuply excited determinants is $\binom{N}{n}\binom{K-N}{n}$. Even for small molecules and one-electron

basis sets of only moderate size, the number of n-tuply excited determinants is extremely large for all n except 0 and 1 [90].

Given the trial function of Eq. 3.18 we can find the corresponding energies by using the linear variational method. This consists of forming the matrix representation of the Hamiltonian in the basis of the N-electron functions of expansion Eq. 3.18 and then finding the eigenvalues of this matrix. This is called the full CI matrix, and the method is referred to as full CI, as already mentioned. The difference between the lowest eigenvalue and the Hartree-Fock energy obtained within the same one-electron basis is called the basis set correlation energy. As the one-electron basis set approaches completeness, this basis set correlation energy approaches the exact correlation energy.

It is convenient to rewrite the expansion of Eq. 3.18 in a symbolic form

$$\Psi = c_0\Phi_0 + \sum_S c_S\Phi_S + \sum_D c_D\Phi_D + \sum_T c_T\Phi_T + \ldots = \sum_{i=0} c_i\Phi_i. \qquad (3.19)$$

The energy should be minimized under the constraint that the total CI wave function is normalized. Introducing Lagrange multiplier, we may write

$$\begin{aligned} L &= \langle\Psi|\,\hat{H}\,|\Psi\rangle - \lambda\left(\langle\Psi|\,\Psi\rangle - 1\right), \\ \langle\Psi|\,\hat{H}\,|\Psi\rangle &= \sum_{i=0}\sum_{j=0} c_i c_j \langle\Phi_i|\,\hat{H}\,|\Phi_j\rangle = \sum_{i=0} c_i^2 E_i + \sum_{i=0}\sum_{j\neq i} c_i c_j \langle\Phi_i|\,\hat{H}\,|\Phi_j\rangle, \\ \langle\Psi|\,\Psi\rangle &= \sum_{i=0}\sum_{j=0} c_i c_j \langle\Phi_i|\,\Phi_j\rangle = \sum_{i=0} c_i^2 \langle\Phi_i|\,\Phi_j\rangle = \sum_{i=0} c_i^2. \end{aligned} \qquad (3.20)$$

The diagonal elements in the sum involving the Hamiltonian operator are energies of the corresponding determinants. The overlap elements between different determinants are zero as they are built from the orthogonal molecular orbitals (Eq. 3.1). The variational procedure corresponds to setting all the derivatives of the Lagrange function with respect to the c_i expansion

coefficients equal to zero

$$\begin{aligned} \frac{\partial L}{\partial c_i} &= 2\sum_j c_j \langle \Phi_i | \hat{H} | \Phi_j \rangle - 2\lambda c_i = 0, \\ c_i (E_i - \lambda) &+ \sum_{j \neq i} c_j \langle \Phi_i | \hat{H} | \Phi_j \rangle = 0. \end{aligned} \tag{3.21}$$

If there is only one determinant in the expansion ($c_0 = 1,\ c_{i\neq 0} = 0$), the latter equation shows that the Lagrange multiplier λ is the (CI) energy.

As there is one equation 3.21 for each i, the variational problem is transformed into solving a set of CI secular equations, which may be written as a matrix equation

$$\boldsymbol{HC} = \boldsymbol{ESC} \tag{3.22}$$

where $\boldsymbol{C}$ is the coefficient matrix, $\boldsymbol{E}$ is the diagonal matrix of energies E, $\boldsymbol{H}$ is hamiltonian matrix with elements

$$H_{ij} = \langle \Phi_i | \hat{H} | \Phi_j \rangle , \tag{3.23}$$

and $\boldsymbol{S}$ is the overlap matrix

$$S_{ij} = \langle \Phi_i | \Phi_j \rangle. \tag{3.24}$$

The CI energy is obtained as the lowest eigenvalue of the CI matrix. The second lowest eigenvalue corresponds to the first excited state, etc. [80]

The CI matrix elements can be evaluated by the strategy employed for calculating the energy of a single determinant used for deriving the Hartree-Fock equations. This involves expanding the determinants in a sum of products of MOs, thereby making it possible to express the CI matrix elements in terms of MO integrals. There are, however, some general features that make many of the CI matrix elements equal to zero. The full CI matrix is presented below:

$$
\begin{array}{c}
 \\
\langle\Phi_0| \\
\langle\Phi_S| \\
\langle\Phi_D| \\
\langle\Phi_T| \\
\langle\Phi_Q| \\
\vdots
\end{array}
\begin{array}{c}
\begin{array}{ccccccc}
|\Phi_0\rangle & |\Phi_S\rangle & |\Phi_D\rangle & |\Phi_T\rangle & |\Phi_Q\rangle & \cdots
\end{array} \\
\begin{pmatrix}
\langle\Phi_0|\hat{H}|\Phi_0\rangle & 0 & \langle\Phi_0|\hat{H}|\Phi_D\rangle & 0 & 0 & \cdots \\
0 & \langle\Phi_S|\hat{H}|\Phi_S\rangle & \langle\Phi_S|\hat{H}|\Phi_D\rangle & \langle\Phi_S|\hat{H}|\Phi_T\rangle & 0 & \cdots \\
\langle\Phi_D|\hat{H}|\Phi_0\rangle & \langle\Phi_D|\hat{H}|\Phi_S\rangle & \langle\Phi_D|\hat{H}|\Phi_D\rangle & \langle\Phi_D|\hat{H}|\Phi_T\rangle & \langle\Phi_D|\hat{H}|\Phi_Q\rangle & \cdots \\
0 & \langle\Phi_T|\hat{H}|\Phi_S\rangle & \langle\Phi_T|\hat{H}|\Phi_D\rangle & \langle\Phi_T|\hat{H}|\Phi_T\rangle & \langle\Phi_T|\hat{H}|\Phi_Q\rangle & \cdots \\
0 & 0 & \langle\Phi_Q|\hat{H}|\Phi_D\rangle & \langle\Phi_Q|\hat{H}|\Phi_T\rangle & \langle\Phi_Q|\hat{H}|\Phi_Q\rangle & \cdots \\
\vdots & \vdots & \vdots & \vdots & \vdots & \ddots
\end{pmatrix}
\end{array}
$$

The schematic procedure for the CI calculations may be as follows: we choose one-electron basis set, iteratively solve the Hartree-Fock equations to determine one-electron atomic or molecular orbitals Φ_l as a linear combinations of the basis set, form many electron functions Φ_i using the orbitals Φ_l, express the wave function Ψ as a linear combination of these configuration functions, solve Eq. 3.22 and obtain the coefficients in Eq. 3.19.

3.5 Multiconfiguration Self-Consistent Field Method

The Multiconfiguration Self-Consistent Field (MCSCF) method can be considered as a CI where not only the coefficients in front of the determinants (Eq. 3.19) are optimized by the variational principle, but also the molecular orbitals used for constructing the determinants are optimized. Each molecular orbital is defined as a linear combination of atomic orbitals or a linear combination of basis functions which is simply a guess function developed on a basis of orthogonal functions. The MCSCF optimization is iterative like the SCF procedure.

MCSCF methods are rarely used for calculating large fractions of the correlation energy. The orbital relaxation usually does not recover much electron correlation, and it is more efficient to include additional determinants and keep the molecular orbitals fixed (CI) if the interest is just in obtaining a large fraction of the correlation energy.

The advantage of the MCSCF method is that both the expansion coefficients (c_i) and the orthonormal orbitals contained in $|\Phi_i\rangle$ are optimized simultaneously, thus the size of MCSCF wave functions treated is somewhat smaller than in CI calculations.

3.6 Complete Active Space Self-Consistent Field Method

The major problem with MCSCF methods is selecting which configurations are necessary to include for the property of interest. One of the most popular approaches is the Complete Active Space Self-Consistent Field (CASSCF) method. This method is a variant of the MCSCF method and uses the same procedure in its implementation. In this case, the molecular orbitals used in the configuration state functions are divided into inactive and active orbitals. Inactive molecular orbitals are always doubly occupied in the wavefunction. Active molecular orbitals can be doubly, singly or unoccupied. Electrons in the active orbitals are called active electrons. Within the active molecular orbitals a full CI is performed and all the proper symmetry-adapted configurations are included in the optimization. Which molecular orbitals to include in the active space must be decided manually, by considering the problem at hand and the computational expense.

This method is a multiconfigurational variational method which improves the SCF wavefunction and energy by taking into account a part of the electron correlation. The wavefunction is a linear combination

$$\Psi = \Phi_0 + \sum \Phi_i \tag{3.25}$$

where Φ_0 is usually the SCF wavefunction and Φ_i are the wavefunctions obtained from Φ_0 by occupying the active orbitals with active electrons in all possible ways with symmetry restrictions.

The success of this method lies in the concept of active space. All the important configurations that are relevant to describe the processes under consideration must be in the active space.

3.7 Multireference Configuration Interaction

In the CI methods the Hartree-Fock SCF wavefunction Φ_0 is used as a reference configuration and configuration state functions are formed by electron excitation from occupied orbitals into virtual (unoccupied) ones. In multireference configuration interaction (MRCI) approach, a set of reference

configurations is created, from which excited determinants are formed to be used in CI calculation. For example, one procedure would be to perform an MCSCF calculation and select a set of reference configurations from the determinants that have a coefficient c_i larger than some threshold value in the final normalized MCSCF wavefunction. For each reference determinant, electrons are moved from occupied spin-orbitals to unoccupied spin-orbitals to create more determinants included in the CI expansion in Eq. 3.19. Then the configuration interaction calculation is performed, optimizing all the coefficients c_i. The reference determinants will often be singly and doubly excited determinants with respect to Φ_0 and single and double excitations from the reference determinants are often included. As a result, the final MRCI wavefunction will include determinants that are triply and quadruply excited from Φ_0. Generally, a large fraction of the correlation energy can be recovered from MRCI calculations with a much smaller number of determinants.

The CASSCF results are only qualitative values, but we can go beyond this level with the MRCI treatment. Using a selected space of configurations (for instance the most important configurations of a CASSCF wavefunction that contain the relevant information about the studied physical phenomena), a new wavefunction is built, as was mentioned above, by generating single and double excitations within this restricted space. The method introduces mixing between configurations allowing interactions of reference states with each other. If the CASSCF treatment takes into account the static electron correlation of the system, the MRCI built on the CASSCF reference wavefunction handles for the remaining dynamical correlation effects due to the short range instantaneous interactions between electrons.

The validity of this method is strongly dependent on the quality of the zeroth order wavefunction, usually a CASSCF wavefunction. If an important reference configuration is missing or if the active space is too small and not flexible enough, electronic state inversion or convergence problems may occur. The MRCI can give excellent results when the active space is adequate and representative. However, the choice of active space remains in the hands of the user.

3.8 Effective Core Potentials

The theoretical study of electronic structures can be made simplier if the atomic core electrons are considered invariant in the molecular environment. Considerable savings in computer resources ca be obtained removing the core electrons and considering explicitly only the valence electrons. It was Hellmann who first proposed [91] the replacement of electrons with analytical functions that would reasonably accurately, and much more efficiently, represent the combined nuclear-electronic core to the remaining electrons. Such functions are referred to as effective core potentials (ECPs).

The Fock operator in the atomic case may be given in the following form

$$\begin{aligned} \hat{F}_i &= -\frac{1}{2}\nabla^2_{r_i} - \frac{Z}{r_i} + \frac{l(l+1)}{2r_i^2} + \sum_{j=1}^{N}\left(\hat{J}_j - \hat{K}_j\right), \\ \hat{h}_i &= -\frac{1}{2}\nabla^2_i - \frac{Z}{r_i} = -\frac{1}{2}\left(\nabla^2_{r_i} - \frac{l(l+1)}{2r_i^2}\right) - \frac{Z}{r_i}, \end{aligned} \tag{3.26}$$

where r_i is the distance between ith electron and an atomic nucleus, l is the orbital quantum number of ith electron, and $\nabla^2_{r_i} = -\frac{1}{r_i^2}\frac{\partial}{\partial r_i}\left(r_i^2\frac{\partial}{\partial r_i}\right)$ is the radial part of ∇^2_i. The action of operators $\hat{J}_j$ and $\hat{K}_j$ is defined by Eq. 3.9.

The orbitals are divided now into a group of N_c core orbitals and N_v valence orbitals. The Fock operator can be expressed as

$$\hat{F}_i = -\frac{1}{2}\nabla^2_{r_i} - \frac{Z}{r_i} + \frac{l(l+1)}{2r_i^2} + \hat{V}_{val} + \hat{V}_{core}. \tag{3.27}$$

$\hat{V}_{val}$ represents the coulombic and exchange integrals involving only the valence orbitals and $\hat{V}_{core}$ represents all the core coulombic integrals as well as the core-core and core-valence exchange terms.

In order to reduce the computational intensity, it would be useful to replace and develop an equation analogous to the Fock equation. Replacing the core electrons in a calculation with an effective potential simply means eliminating the need for the core basis functions, which usually require a

large set of Gaussians to describe them.

$$\left[-\frac{1}{2}\nabla^2_{r_i} - \frac{Z_{eff}}{r_i} + \frac{l(l+1)}{2r_i^2} + \hat{V}_{val} + \hat{V}^{eff}\right]\Phi_i = \varepsilon_i \Phi_i \tag{3.28}$$

where the potential $\hat{V}_{core}$ has been replaced by an effective core potential (ECP) $\hat{V}^{eff}$, and the nuclear charge Z has been replaced by the effective nuclear charge Z_{eff}. The atomic orbitals and eigenvalues needed in the construction of the effective core potentials are obtained from exact numerical Hartree-Fock calculations in accordance with the frozen core approximation, in which the lowest-lying molecular orbitals (occupied by the inner shell-electrons) are constrained to remain doubly-occupied in all configurations.

The full atomic valence orbitals $\{\Phi_i\}$, may be replaced by approximate pseudo-orbitals $\{\chi_i\}$, which are nodeless. The use of approximate valence orbitals brings a new definition of $\hat{V}^{eff}$, since the valence orbitals now satisfy the equation

$$\left[-\frac{1}{2}\nabla^2_{r_i} - \frac{Z_{eff}}{r_i} + \frac{l(l+1)}{2r_i^2} + \hat{V}'_{val} + \hat{V}_l^{eff}\right]\chi_i = \varepsilon_i \chi_i. \tag{3.29}$$

The prime on $\hat{V}'_{val}$ indicates that the valence potential is evaluated over valence pseudo-orbitals. Because $\hat{V}'_{val}$ will differ from $\hat{V}_{val}$, the ECP must represent not only the core-core and core-valence interactions, but also the parts of the valence-valence interaction which were lost in the switch from Φ_i to χ_i. By solving Eq. 3.29 for $\hat{V}_l^{eff}$ we obtain

$$\hat{V}_l^{eff} = \varepsilon_i + \frac{Z_{eff}}{r_i} - \frac{l(l+1)}{2r_i^2} + \frac{\frac{1}{2}\nabla^2_{r_i} - \hat{V}'_{val}\chi i}{\chi_i}. \tag{3.30}$$

The total $\hat{V}^{eff}$ for an atom may be written as a development in spherical harmonics $|lm\rangle$

$$\hat{V}_{eff} = \sum_l \hat{V}_l^{eff} \sum_{m=-l}^{l} |lm\rangle \langle lm| . \tag{3.31}$$

The radial wavefunction of the valence orbitals is required to be orthogonal to the core orbitals of the same angular momentum as that valence orbital.

Equation 3.31 may be written analytically

$$V_{eff} = V_{lmax} + \sum_{l}^{l_{max}-1} V_l^{eff} - V_{l_{max}} \sum_{l} V_l^{eff} \sum_{m=-l}^{l} |lm\rangle \langle lm| . \tag{3.32}$$

Once the nodeless pseudo-orbitals have been selected, it is possible to simply solve Eq. 3.30 numerically. Once this has been done, a parametrized analytic form may be fit to the numerical data. When the ECP has been modeled by some set of functions, then Eq. 3.28 is complete and may be implemented for a chosen set of valence orbitals.

3.9 Determination of the Dynamical Couplings

3.9.1 Radial Couplings

The radial couplings take into account the variation of the electronic wave function due to the radial motion of nuclei and connect electronic states of the same symmetry. These radial coupling matrix elements are given by

$$g_{KL}^{rad}(R) = \langle \Psi_K | \frac{\partial}{\partial R} | \Psi_L \rangle , \tag{3.33}$$

where the wave functions Ψ_K and Ψ_l are the eigenvectors of the CI matrix. The operator $\frac{\partial}{\partial R}$ is antisymmetric and only non-diagonal elements are not zero. Expanding the two wavefunctions in a linear combinations of Slater determinants $\Psi_K = \sum_i C_{iK}(R)\Phi_i(R)$, Eq. 3.33 becomes

$$\begin{aligned} g_{KL}^{rad}(R) = & \sum_{i,j} C_{iK}^*(R) C_{iL}(R) \langle \Phi_i(R) | \frac{\partial}{\partial R} | \Phi_j(R) \rangle \\ & + \sum_{i,j} C_{iK}^*(R) \frac{\partial}{\partial R} C_{iL}(R) \langle \Phi_i(R) | \Phi_j(R) \rangle . \end{aligned} \tag{3.34}$$

Taking into account the orthogonality condition of CI functions Φ_i, which are linear combinations of the molecular orbitals φ_m, we have

$$g_{KL}^{rad}(R) = \sum_{n \neq m} \rho_{nm}^{KL} \langle \varphi_n | \frac{\partial}{\partial R} | \varphi_m \rangle + \sum_i C_{iK}^*(R) \frac{\partial}{\partial R} C_{iL}(R), \tag{3.35}$$

$$g_{KL}^{rad}(R) = g_{KL}^{MO}(R) + g_{KL}^{CI}(R), \tag{3.36}$$

where ρ_{nm}^{KL} is the transition density matrix. The term $g_{KL}^{MO}(R)$ represents the variation of molecular orbitals when the internuclear distance varies, and the term $g_{KL}^{CI}(R)$ corresponds to the changing of the coefficients C_{ij} of the wave function.

The determination of nonadiabatic couplings between molecular states is of interest for the theoretical interpretation of variety of phenomena, as collision processes, where adiabatic states are close in energy and then coupled by nonadiabatic couplings. There are several methods to evaluate the radial couplings $\langle \Psi_K | \frac{\partial}{\partial R} | \Psi_L \rangle$, which can be categorized into two major methods, namely analytical methods, and numerical methods.

The analytical ones [92–94] are based on the well known Hellmann-Feynman theorem [95], which assumes electronic wavefunctions Ψ_L to be exact eigenfunctions of the electronic Hamiltonian

$$\hat{H}_{el} | \Psi_L \rangle = E_L | \Psi_L \rangle . \tag{3.37}$$

Derivating this relation with respect to the internuclear distance R, multiplying from left side by function $\langle \Psi_k |$ and using the orthonormality condition between the electronic wave functions, we obtain the radial coupling matrix element

$$g_{KL}^{rad}(R) = \langle \Psi_K | \frac{\partial}{\partial R} | \Psi_L \rangle = (E_L - E_K)^{-1} \langle \Psi_K | \frac{\partial \hat{H}_{el}}{\partial R} | \Psi_L \rangle . \tag{3.38}$$

Since the wavefunctions Ψ_K and Ψ_L are presented by their corresponding

column vectors $\vec{C}_K$ and $\vec{C}_L$, we obtain

$$\begin{aligned}\vec{C}_K^* \frac{\partial \vec{C}_L}{\partial R} &= \frac{1}{E_L - E_K} \vec{C}_K^*(R) \frac{\partial \boldsymbol{H}}{\partial R} \vec{C}_L(R) \\ &= \lim_{\Delta \to 0} \frac{1}{\Delta} \frac{1}{E_L - E_K} \vec{C}_K^*(R) \left[\boldsymbol{H}(R+\Delta) - \boldsymbol{H}(R) \right] \vec{C}_L(R),\end{aligned} \tag{3.39}$$

where the matrix $\boldsymbol{H}$ contains the electronic Hamiltonian matrix elements.

Analytical methods are not limited by Hellmann-Feynman assumption [96, 97], and are appropriate for wavefunctions built from GTOs.

Numerical methods are usually employed [98–100]. These techniques are based on the finite difference technique, where the eigenvectors are calculated by diagonalization of CI matrix for two nearby internuclear distances, R and $R+\Delta$, Δ being very small. The radial coupling matrix element is thus defined as

$$\begin{aligned}g_{KL}^{rad}(R) &= \lim_{\Delta \to 0} \frac{1}{\Delta} \left\langle \Psi_K(R) \right| \left. \Psi_L(R+\Delta) - \Psi_L(R) \right\rangle \\ &= \lim_{\Delta \to 0} \frac{1}{\Delta} \left[\left\langle \Psi_K(R) \right| \left. \Psi_L(R+\Delta) \right\rangle - \left\langle \Psi_K(R) \right| \left. \Psi_L(R) \right\rangle \right].\end{aligned} \tag{3.40}$$

The $\dfrac{\partial}{\partial R}$ operator is antisymmetric and Ψ_K and Ψ_L are orthogonal, finally we obtain

$$g_{KL}^{rad}(R) = \lim_{\Delta \to 0} \frac{1}{\Delta} \left\langle \Psi_K(R) \right| \left. \Psi_L(R+\Delta) \right\rangle. \tag{3.41}$$

As the last expression may be divided in $g_{KL}^{MO}(R)$ and $g_{KL}^{CI}(R)$ contributions, we have

$$g_{KL}^{MO}(R) = \lim_{\Delta \to 0} \frac{1}{\Delta} \left\{ \sum_{i,j \neq 1} C_{iK}^*(R) C_{jL}(R) \left\langle \Phi_i(R) \right| \left. \Phi_j(R+\Delta) \right\rangle \right\} \tag{3.42}$$

and

$$g_{KL}^{CI}(R) = \lim_{\Delta \to 0} \frac{1}{\Delta} \left\{ \sum_i C_{iK}^*(R) C_{iL}(R+\Delta) \right\}, \tag{3.43}$$

where the j index describes all of the determinants of Φ_j, which differs from Φ_i, only by one spin-orbital.

The use of these numerical methods requires checking the stability with

respect to the differentiation step Δ. A disadvantage is the need of evaluating the wave functions in two nearby points R and $R + \Delta$, and it is necessary to ensure that the sign of the wave functions is the same in both points. In order to obtain better numerical accuracy one can use the three-point numerical differentiation technique with calculations at $R - \Delta$, R and $R + \Delta$ [101]. This method can be relatively expensive computationally but gives reliable results and is very widely used.

3.9.2 Rotational Couplings

The evaluation of rotational couplings is carried out analytically and it does not involve a special difficulty from the computational level [102]. It couples electronic states of different symmetries and the same spin multiplicity. The rotational coupling matrix elements are given by

$$g_{KL}^{rot}(R) = \langle \Psi_K | \, iL_y \, | \Psi_L \rangle \,, \tag{3.44}$$

where iL_y is the y component of the electronic angular momentum, as it has been shown previously.

In numerical calculations, the rotational matrix elements $\langle \Psi_K | \, iL_y \, | \Psi_L \rangle$ between states of angular momentum $\Delta\Lambda = \pm 1$ are calculated directly at the CI level of theory from the quadrupole moment tensor.

It may also be evaluated analytically by means of L_+ and L_- operators from the following relations [103]

$$iL_y = \frac{L_+ - L_-}{2} \tag{3.45}$$

and

$$L_\pm \langle n, l, m| = \sqrt{l(l+1) - m(m \pm 1)} \, \langle n, l, m \pm 1| \,. \tag{3.46}$$

This calculation neglects the contributions corresponding to Gaussian functions centred on different atoms.

3.10 Translation Factors

In finite basis set the dynamical couplings not satisfy the asymptotic conditions and can thus have a nonvanishing asymptotic limit. The quan-

tity $\langle\Phi_k|\,\dfrac{\partial}{\partial R}\,|\Phi_l\rangle$, corresponding to the radial coupling, tends towards some constant when $R \to \infty$, and quantity $\langle\Phi_k|\,iL_y\partial R\,|\Phi_l\rangle$, corresponding to rotational coupling, decreases slowly in $\dfrac{1}{R}$ when $R \to \infty$. In addition the couplings depend on the origin of coordinates and the Galilean invariance is not guaranteed.

According to the Born Oppenheimer approach, nonzero couplings provide transitions between molecular states even at $R \to \infty$. The nonvanishing asymptotic couplings are a consequence of a fundamental shortcoming. The coordinates used in the standard adiabatic approach to describe molecular states of the collision complex at small and intermediate distances are not suited for the description of the free atoms in the asymptotic region and a single term of the total wave function expansion does not give the correct asymptotic incoming or outgoing wave functions [104]. The use of electronic molecular states leads to dependence of both radial and rotational nonadiabatic couplings on the origin of the electronic coordinates.

The reason for the spurious couplings was first recognized by Bates and McCarroll [105], who realized that they are due to the fact that the adiabatic molecular basis states are calculated keeping the relative internuclear distance R fixed, whence the asymptotic translation of the electrons with the escaping nuclei is not contained in the basis. Bates and McCarroll showed that formal solution to the problem could be obtained by means of electron translation factors (ETF), by which the molecular states were multiplied.

$$\phi_n = \Phi_n exp\left[if_n\left(\vec{r},\vec{R}\right)\vec{v}\vec{r}\right], \tag{3.47}$$

where f_n is some arbitrary suitable function of $\vec{r}$ and $\vec{R}$. The form of f_n asymptotically must satisfy the following constraints:

$$\begin{aligned} &\lim_{R\to\infty} f_n = \gamma && \text{if } \phi_{\mathrm{n}} \text{ dissociates to a bound state of } (\mathrm{A}+\mathrm{e}),\\ &\lim_{R\to\infty} f_n = \gamma - 1 && \text{if } \phi_{\mathrm{n}} \text{ dissociates to a bound state of } (\mathrm{B}+\mathrm{e}), \end{aligned} \tag{3.48}$$

where γ is defined by: $\vec{OA} = \gamma\vec{R}$ and $\vec{OB} = (1-\gamma)\vec{R}$ (O is the origin of coordinates, A and B represent an atomic species, usually $A = X^{q+}$ is a multiply charged ion and $B = H^+$ or He^+).

Bates and McCarroll also proposed to use plane wave functions, which

are state-dependent translation factors and the function f_n depends on n. They are satisfactory only at large R where the electron is localized around one of the centers but some problems arise in the vicinity of avoided crossings, where the localization of the electron may change rapidly with R from one center to the other. In order to introduce more flexibility in the choice of f_n, Crothers and Todd [106] allowed f_n to vary with R, but not with r. Formally, f_n can be optimised variationally, but in practice this involves extensive and time-consuming calculations, due to the presence of the factors $exp\,(i\vec{v}\vec{r})$ in nonadiabatic matrix elements. In consequence, the use of the state-dependent electron translation factors is rather limited to few applications of very simple ion-atom systems [107, 108].

In most applications common translation factors are used, which are not specific to each molecular orbital. Inclusion of common translation factor was proposed by Schneidermann and Russek [109] and applied in many works [110, 111]. As mentioned previously, all molecular functions are multiplied by the same electron translation factor,

$$D\,(\vec{r},t) = exp\,[iU(\vec{r},t)]. \tag{3.49}$$

To introduce a correction in the coupling between molecular states, we have used common translation factor proposed by Errea et al. [112]

$$U\,(\vec{r},t) = f\left(\vec{r},\vec{R}\right)\vec{v}\vec{r} - \frac{1}{2}f^2\left(\vec{r},\vec{R}\right)v^2t, \tag{3.50}$$

with

$$f\left(\vec{r},\vec{R}\right) = \frac{R}{R^2+\beta^2}\frac{\vec{r}\vec{R}}{R+\alpha}. \tag{3.51}$$

In the particular case of $\alpha = \beta = 0$, the radial and rotational matrix elements are thus transformed respectively into

$$\langle\Phi_k|\,\frac{\partial}{\partial R} + \frac{z}{R}\frac{\partial}{\partial z}\,|\Phi_l\rangle = \langle\Phi_k|\,\frac{\partial}{\partial R}\,|\Phi_l\rangle + \frac{1}{2R}(\varepsilon_l-\varepsilon_k)\,\langle\Phi_k|\,z^2\,|\Phi_l\rangle\,, \tag{3.52}$$

and

$$\langle\Phi_k|\,iL_y + \left(x\frac{\partial}{\partial z} + z\frac{\partial}{\partial x}\right)|\Phi_l\rangle = \langle\Phi_k|\,iL_y\,|\Phi_l\rangle + (\varepsilon_l-\varepsilon_k)\,\langle\Phi_k|\,zx\,|\Phi_l\rangle\,, \tag{3.53}$$

where ε_k and ε_l are the electronic energies of states $|\Phi_k\rangle$ and $|\Phi_l\rangle$, z^2 and zx, the components of the quadrupole moment tensor.

In this manner cross sections become independent of the origin of coordinates and spurious coupling terms are eliminated at long range.

4 Chapter

Application of Techniques

A detailed analysis of the mechanisms at the molecular level is of fundamental importance for a better understanding of radiation damage. In particular, the study of collisions of ions with molecular targets would provide important information on indirect processes, as collision of carbon ions with water, or small molecules. We have been interested in particular in charge-transfer processes involving diatomic targets, as the OH radical in order to model the action of ions on OH radicals formed in the human organism. Such study has been extended in the present work in order to have a better understanding of the charge-transfer mechanism for different diatomics, taking account of the characteristics of the molecular target (electronic structure, electronegativity of its elements). We have considered the charge transfer of C^{2+} ions in collisions with hydrogen halide molecules (HF, HCl), influenced by the proposed experimental results. All along this work, a detailed analysis of the charge-transfer mechanism has been performed in relation with the nonadiabatic interactions between the different molecular states involved in the process.

This chapter is based on work done by myself jointly with the co-authors of the published papers. The calculations related to the results discussed below have been performed for the greatest part by myself. Each point presented in the Summary of this thesis also lists clearly my tasks during of this research.

4.1 Application to the $C^{2+} + HF$ Collision System

Two main points have been considered during the theoretical treatment of charge-transfer processes induced by collision of the C^{2+} projectile ions on the HF molecule: the anisotropy of the charge transfer with regard to the orientation of the projectile towards the target and the influence of the vibration of the diatomic molecule during the collision.

The molecular calculations have been carried out using the MOLPRO suite of *ab initio* programs [59]. The molecular orbitals have been optimized at the state-averaged Complete Active Space Self-Consistent Field (CASSCF) level with Multireference Configuration Interaction (MRCI) calculations using the correlation-consistent triple-ζ aug-cc-pVTZ basis set of Dunning [113]. The exponents and contraction coefficients for the basis functions are presented in Table 4.1. Pseudopotentials have not been used for this collision system. The active space includes the $n = 2$ and $n = 3(sp)$ orbitals for carbon and fluorine, and the $1s$ orbital for hydrogen. The $1s$ orbitals of carbon and fluorine have been frozen in the calculation.

The spin-orbit coupling is negligible in the collision energy range of interest, thus electron spin can be conserved during the collision process.

The geometry of $^1\Sigma^+$ ground state of HF has been optimized at the MRCI level of theory leading to an equilibrium distance $r_{HF} = 1.73836832$ a.u. The corresponding vertical ionization potential 16.12 eV is in excellent agreement with the 16.1 eV experimental value [114–116] and previous calculations [117, 118].

		Exponents	Contraction Coefficients				
Hydrogen	s	33.870	0.0060680	0.0	0.0	0.0	
		5.0950	0.0453080	0.0	0.0	0.0	
		1.1590	0.2028220	0.0	0.0	0.0	
		0.32580	0.0000000	1.0	0.0	0.0	
		0.10270	0.0000000	0.0	1.0	0.0	
		0.025260	0.0000000	0.0	0.0	1.0	
	p	1.4070	1.0	0.0	0.0		
		0.3880	0.0	1.0	0.0		
		0.1020	0.0	0.0	1.0		
	d	1.0570	1.0	0.0			
		0.2470	0.0	1.0			
Carbon	s	8236.0	0.0005310	-0.0001130	0.0	0.0	0.0
		1235.0	0.0041080	-0.0008780	0.0	0.0	0.0
		280.80	0.0210870	-0.0045400	0.0	0.0	0.0
		79.270	0.0818530	-0.0181330	0.0	0.0	0.0
		25.590	0.2348170	-0.0556600	0.0	0.0	0.0
		8.9970	0.4344010	-0.1269950	0.0	0.0	0.0
		3.3190	0.3461290	-0.1703520	0.0	0.0	0.0
		0.36430	-0.0089830	0.05986840	0.0	0.0	0.0
		0.90590	0.0000000	0.00000000	1.0	0.0	0.0
		0.12850	0.0000000	0.00000000	0.0	1.0	0.0
		0.04402	0.0000000	0.00000000	0.0	0.0	1.0
	p	18.710	0.0140310	0.0	0.0	0.0	
		4.1330	0.0868660	0.0	0.0	0.0	
		1.20	0.2902160	0.0	0.0	0.0	
		0.38270	0.0000000	1.0	0.0	0.0	
		0.12090	0.0000000	0.0	1.0	0.0	
		0.03569	0.0000000	0.0	0.0	1.0	
	d	1.0970	1.0	0.0	0.0		

		0.3180	0.0	1.0	0.0		
		0.10	0.0	0.0	1.0		
	f	0.7610	1.0	0.0			
		0.2680	0.0	1.0			
Fluorine	s	19500.0	0.0005070	-0.0001170	0.0	0.0	0.0
		2923.0	0.0039239	-0.0009120	0.0	0.0	0.0
		664.50	0.020200	-0.0047170	0.0	0.0	0.0
		187.50	0.079010	-0.0190860	0.0	0.0	0.0
		60.620	0.2348170	-0.0596550	0.0	0.0	0.0
		21.420	0.4344010	-0.140010	0.0	0.0	0.0
		7.950	0.3499640	-0.1767820	0.0	0.0	0.0
		0.8815	-0.007892	0.6050430	0.0	0.0	0.0
		2.2570	0.0000000	0.0000000	1.0	0.0	0.0
		0.3041	0.0000000	0.0000000	0.0	1.0	0.0
		0.09158	0.0000000	0.0000000	0.0	0.0	1.0
	p	43.880	0.0166650	0.0	0.0	0.0	
		9.9260	0.1044720	0.0	0.0	0.0	
		2.930	0.3172600	0.0	0.0	0.0	
		0.91320	0.0000000	1.0	0.0	0.0	
		0.26720	0.0000000	0.0	1.0	0.0	
		0.07361	0.0000000	0.0	0.0	1.0	
	d	3.1070	1.0	0.0	0.0		
		0.8550	0.0	1.0	0.0		
		0.2920	0.0	0.0	1.0		
	f	1.9170	1.0	0.0			
		0.7240	0.0	1.0			

4.1. Table: Exponents and contraction coefficients of the aug-cc-pVTZ basis set of Dunning [113] for H, C and F.

A number of states may be considered with regard to the respective ionization potentials and different excited states of HF^+ and C^+ ions [118,119]:

Configuration	Molecular states
$C^{2+}(1s^2 2s^2)^1S + HF(^1\Sigma^+)$	$^1\Sigma^+$,
$C^+(1s^2 2s 2p^2)^4P + HF^+(^2\Pi)$	$^3\Sigma^+$,$^3\Pi$,$^3\Delta$, $^5\Sigma^+$,$^5\Pi$,$^5\Delta$,
$C^+(1s^2 2s^2 2p)^2P^\circ + HF^+(^2\Sigma^+)$	$^1\Sigma^+$,$^1\Pi$, $^3\Sigma^+$,$^3\Pi$,
$C^+(1s^2 2s^2 2p)^2P^\circ + HF^+(^2\Pi)$	$^1\Sigma^+$,$^1\Pi$,$^1\Delta$, $^3\Sigma^+$,$^3\Pi$,$^3\Delta$.

Taking account of the $^1\Sigma^+$ symmetry of the $C^{2+}(1s^2 2s^2)^1S + HF(^1\Sigma^+)$ entry channel, only doublet C^+ excited states could be involved in the collision process. Besides, only $^1\Pi$ states could be correlated to the $^1\Sigma^+$ entry channel by means of rotational coupling interaction. Three $^1\Sigma^+$ states and two $^1\Pi$ states must be considered in this process with regard to the different excited states of HF^+ and spin considerations:

Configuration	Molecular states
$C^{2+}(1s^2 2s^2)^1S + HF(^1\Sigma^+)$	$^1\Sigma^+$,
$C^+(1s^2 2s^2 2p)^2P^\circ + HF^+(^2\Sigma^+)$	$^1\Sigma^+$,$^1\Pi$,
$C^+(1s^2 2s^2 2p)^2P^\circ + HF^+(^2\Pi)$	$^1\Sigma^+$,$^1\Pi$.

4.1.1 Linear Approach

a) Adiabatic Potential Energy Curves

The potential energy curves for the equilibrium distance and associated radial and rotational coupling matrix elements between $^1\Sigma^+$ and $^1\Pi$ states have been calculated in the $[2.0-14.0]$ a.u. internuclear distance range. The potential energy curves are presented in Fig. 4.1 for the collinear approach of the C^{2+} ion toward the HF target ($\theta = 0°$). In linear geometry the molecular calculations have been performed in the C_{2v} symmetry group.

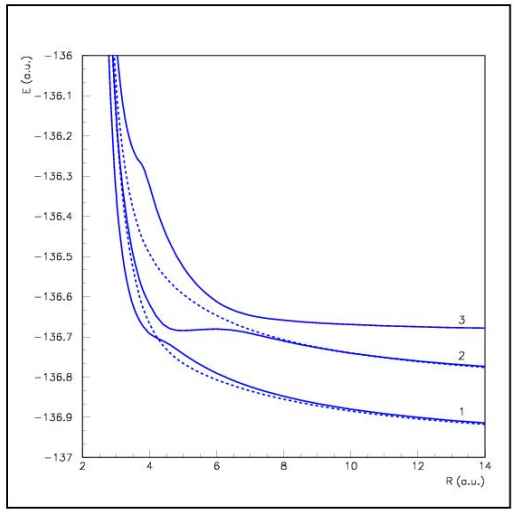

4.1. Figure: Potential energy curves for the $^1\Sigma^+$ (solid line) and $^1\Pi$ (dashed line) states of the $C^{2+} - HF$ molecular system at equilibrium, $\theta = 0°$: 1, $C^+(1s^22s^22p)^2P^\circ + HF^+(^2\Pi)$; 2, $C^+(1s^22s^22p)^2P^\circ + HF^+(^2\Sigma^+)$; 3, $C^{2+}(1s^22s^2)^1S + HF(^1\Sigma^+)$ entry channel.

The entry channel is almost horizontal at large internuclear distances, while the exit channels represent an $1/R$ character due to the repulsive Coulomb potential between the ions C^+ and HF^+. In order to obtain the asymptotic values for the energies of exit channels the Coulomb repulsion term $\frac{qq'}{R}$ has to be taken into account: $E_{\text{asympt}} = E_{MOLPRO,14au} - \frac{1}{14}$.

In a first approach, the potential energy of the entry channel reached at long internuclear distances remains the same asymptotically: $E_{\text{asympt}} = E_{MOLPRO,14au}$.

As shown in Table 4.2 the asymptotic energies compare satisfactorily with the calculation of separated species taking account of experimental values for carbon ions [119] and ionization potential of the HF molecule [114, 115] with MRCI calculations at optimized equilibrium geometry for the ground and excited states of the target molecule.

Configuration	This calculation	Separated species
$C^{2+}(^1S) + HF(^1\Sigma^+)$	8.368	8.279
$C^{+}(^2P^\circ) + HF^{+}(^2\Sigma^+)$	3.824	3.909
$C^{+}(^2P^\circ) + HF^{+}(^2\Pi)$	0	0

4.2. Table: Comparison of asymptotic energies from separated species calculation at the optimized $HF(^1\Sigma^+)$ distance (in eV).

The $^1\Sigma^+$ states show two avoided crossings, a smooth one at this geometry between the entry channel and the $2^1\Sigma^+\{C^+(1s^2 2s^2 2p)^2 P^\circ + HF^+(^2\Sigma^+)\}$ exit channel around 6.5 a.u. and a sharper one, at shorter range, around $R = 4.5$ a.u., between the $2^1\Sigma^+$ and $1^1\Sigma^+\{C^+(1s^2 2s^2 2p)^2 P^\circ + HF^+(^2\Pi)\}$ exit channels.

In contrast, $^1\Pi$ channels do not present significant avoided crossing in the distance range of interest; they interact only in the repulsive part of the potential energy curves.

b) Radial Couplings

The radial coupling matrix elements between all pair of states of the same symmetry have been calculated using the finite difference technique according to the formula determined previously in Section 3.9.1. We choose the parameter $\Delta = 0.0012$ a.u. The three-point numerical differentiation method is used to achieve the required numerical accuracy.

The radial coupling matrix elements between $^1\Sigma^+$ states exhibit two main peaks as displayed in Fig. 4.2. for $\theta = 0^\circ$.

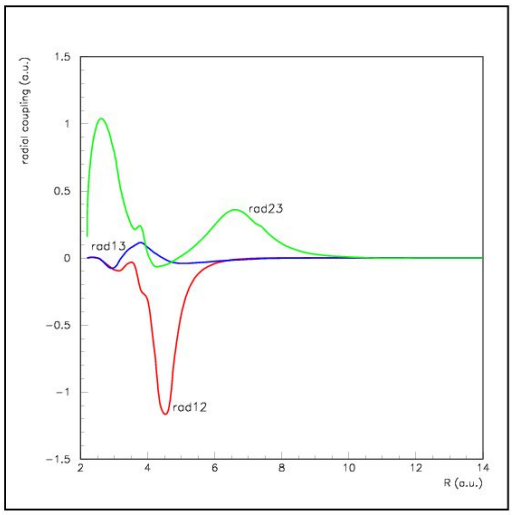

4.2. Figure: Radial coupling matrix elements between $^1\Sigma^+$ states of the $C^{2+} - HF$ molecular system at equilibrium, $\theta = 0°$. Same labels as in Fig. 4.1.

The radial nonadiabatic coupling matrix element between the $2^1\Sigma^+$ and $1^1\Sigma^+$ exit channels reaches up to 1.2 a.u. in absolute value at $R = 4.5$ a.u., in correspondence to the strong avoided crossing between the potential energy curves. The smooth peak, around $R = 6.5$ a.u. corresponds to the avoided crossing between the entry channel and the $2^1\Sigma^+$ charge-transfer level. A detailed calculation at short range exhibits besides a sharp radial coupling peak at $R = 2.55$ a.u. in the repulsive part of the potential energy curves between the entry channel and the $2^1\Sigma^+$ charge-transfer state. All the states are very close to one another in the repulsive part of the potential energy curves and this may cause avoided crossings. A smooth radial coupling between the entry channel and the $1^1\Sigma^+$ state is also exhibited around $R = 4.0$ a.u.

c) Rotational Couplings

The rotational matrix elements $\langle \Psi_K | \, iL_y \, | \Psi_L \rangle$ between states of angular momentum $\Delta\Lambda = \pm 1$ have been calculated directly from the quadrupole moment tensor. They are presented in Fig. 4.3 in the linear approach of the projectile toward the hydrogen atom of HF ($\theta = 0°$).

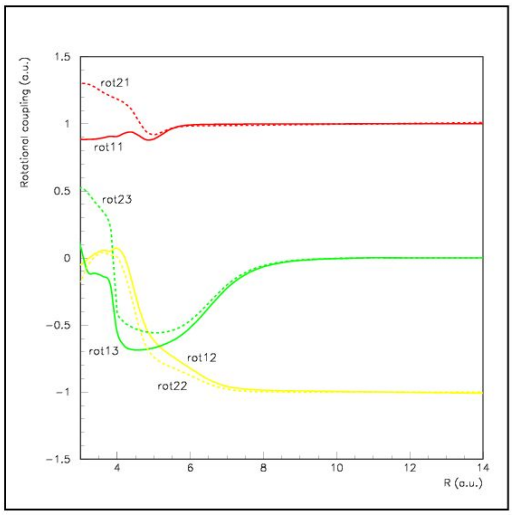

4.3. Figure: Rotational coupling matrix elements between $^1\Sigma^+$ and $^1\Pi$ states for the $C^{2+} - HF$ molecular system at equilibrium, $\theta = 0°$. Same labels as in Fig. 4.1.: rot11=$\langle 1^1\Pi|\, iLy\, |1^1\Sigma^+\rangle$, rot12=$\langle 1^1\Pi|\, iLy\, |2^1\Sigma^+\rangle$, rot13=$\langle 1^1\Pi|\, iLy\, |3^1\Sigma^+\rangle$, rot21=$\langle 2^1\Pi|\, iLy\, |1^1\Sigma^+\rangle$, rot22=$\langle 2^1\Pi|\, iLy\, |2^1\Sigma^+\rangle$, rot23=$\langle 2^1\Pi|\, iLy\, |3^1\Sigma^+\rangle$.

Rotational coupling matrix elements between $^1\Pi$ states and the entry channel, or between $^1\Pi$ states and the $2^1\Sigma^+\{C^+(1s^2 2s^2 2p)^2 P^\circ + HF^+(^2\Sigma^+)\}$ exit channel, vary abruptly in correspondence with the avoided crossing around 6.5 a.u. Effectively the corresponding change of character of the $^1\Sigma^+$ wave functions in this region induces strong variation on rotational coupling matrix elements. In contrast low interaction is observable between the lowest $1^1\Sigma^+\{C^+(1s^2 2s^2 2p)^2 P^\circ + HF^+(^2\Pi)\}$ state and entry channel and corresponding rotational couplings rot11 and rot21 remain rather unchanged.

d) Collision Dynamics

The collision dynamics has been performed by means of the EIKONX code [120] in the keV laboratory energy range. As straight-line trajectories are satisfying for energies higher than 10 eV/amu [121], semiclassical approaches may be used with good accuracy in this collision energy range. Because electronic transitions are much faster than vibrational and rota-

tional motion, the sudden approximation may be used and cross sections, corresponding to purely electronic transitions are determined by solving the impact-parameter equation, considering the internuclear distance of the molecular target fixed in a given geometry.

This treatment has been performed for different geometries of the $C^{2+} - HF$ collision system, taking account of all the transitions driven by radial and rotational coupling matrix elements. The partial and total cross sections have been calculated between the different quasimolecular states involved in the process.

The collision treatment has been carried out in the adiabatic representation and thus integrated the collision coupled equation using adiabatic data. This representation has the disadvantage to perform integration with couplings which are strongly varying around the avoided crossings. Integration is thus longer and could be difficult, but it was not the case in this work.

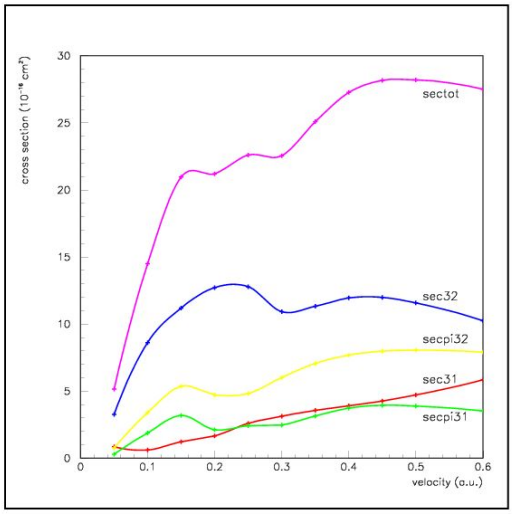

4.4. Figure: Total and partial charge-transfer cross sections for the $C^{2+} - HF$ molecular system at equilibrium, $\theta = 0°$: sectot, total cross section; sec32, partial cross section on ${}^1\Sigma^+\{C^+(1s^22s^22p)^2P^\circ + HF^+({}^2\Sigma^+)\}$; secpi32, partial cross section on ${}^1\Pi\{C^+(1s^22s^22p)^2P^\circ + HF^+({}^2\Sigma^+)\}$; sec31, partial cross section on ${}^1\Sigma^+\{C^+(1s^22s^22p)^2P^\circ + HF^+({}^2\Pi)\}$, secpi31, partial cross section on ${}^1\Pi\{C^+(1s^22s^22p)^2P^\circ + HF^+({}^2\Pi)\}$.

At first translation effects has not been included in the dynamical study, as the translation effects has been shown to be almost negligible for collision energies lower than 100 keV, even for long-range rotational couplings [122]. Such cross sections are presented in Fig. 4.4 for the linear C-H-F geometry ($\theta = 0°$).

The charge-transfer process is clearly driven mainly by means of the nonadiabatic interactions in the vicinity of avoided crossings. The most important interaction corresponds to the radial coupling between the entry channel and the highest $2^1\Sigma^+\{C^+(1s^22s^22p)^2P^\circ + HF^+(^2\Sigma^+)\}$ exit channel, and effectively the corresponding partial cross section presents the highest values. The rotational effect is quite significant for this system as this highest $\{C^+(1s^22s^22p)^2P^\circ + HF^+(^2\Sigma^+)\}$ exit channel may also be correlated with the entry channel by means of rotational coupling, and the partial cross section on the corresponding $2^1\Pi$ channel reaches values up to 7×10^{-16} cm^2 (see also papers **A2** and **A3**).

d) Inclusion of Translation Factors

The present analysis may be extended by inclusion of the translation factors. They may be evaluated in the approximation of the common translation factors [123, 124]. The results presented in this subsection have been published in the paper **A4**.

The corresponding cross sections for the linear C-H-F geometry ($\theta = 0°$) are displayed in Fig. 4.5. The introduction of translation factors induces a very small variation on the total cross sections, less than 3% at $E_{lab} = 100$ keV. The effect decreases at lower collision energies and is completely negligible below about 30 keV. Such effect depends of course of the collision system, but, in a first approach, it can be considered with a good approximation to be weak in the energy range we are dealing with.

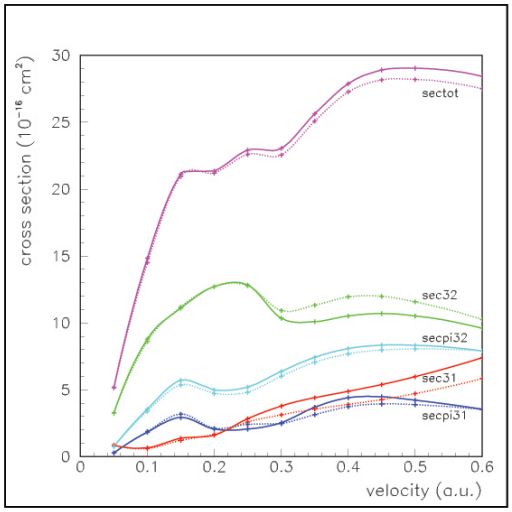

4.5. Figure: Total and partial charge-transfer cross sections for the $C^{2+} - HF$ collision system at equilibrium, $\theta = 0°$. Full line: with translation factors; broken line: without translation factors. sectot: total cross section; sec32: partial cross section on ${}^1\Sigma^+\{C^+(1s^2 2s^2 2p)^2 P^\circ + HF^+({}^2\Sigma^+)\}$; secpi32: partial cross section on ${}^1\Pi\{C^+(1s^2 2s^2 2p)^2 P^\circ + HF^+({}^2\Sigma^+)\}$; sec31: partial cross section on ${}^1\Sigma^+\{C^+(1s^2 2s^2 2p)^2 P^\circ + HF^+({}^2\Pi)\}$, secpi31: partial cross section on ${}^1\Pi\{C^+(1s^2 2s^2 2p)^2 P^\circ + HF^+({}^2\Pi)\}$.

4.1.2 Anisotropic Effect

a) Adiabatic Potential Energy Curves

In order to study the anisotropy of the process, a series of calculations have been performed for different orientations of the projectile corresponding to specific values of the angle θ, about every 20°, from the linear $C - H - F$ geometry ($\theta = 0°$) to the linear $C - F - H$ one ($\theta = 180°$). For nonlinear geometries, the calculations have been carried out using the C_s symmetry group and considering the plane of the molecular system as the plane of symmetry. Potentials for selected geometries are presented in Fig. 4.6 to 4.10.

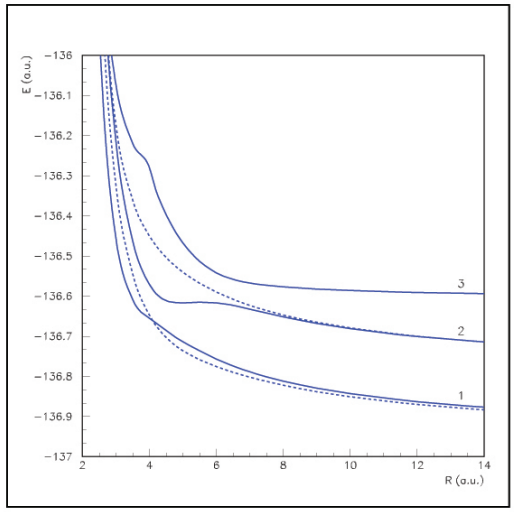

4.6. Figure: Potential energy curves for the $^1\Sigma^+$ (solid line) and $^1\Pi$ (dashed line) states of the $C^{2+} - HF$ molecular system at equilibrium, $\theta = 20°$. Same labels as in Fig. 4.1.

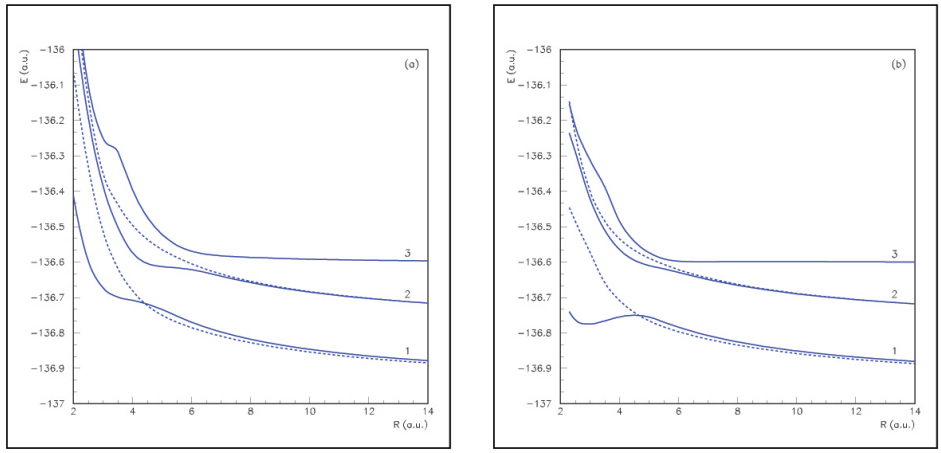

4.7. Figure: Potential energy curves for the $^1\Sigma^+$ (solid line) and $^1\Pi$ (dashed line) states of the $C^{2+} - HF$ molecular system at equilibrium, (a) $\theta = 45°$, (*b*) $\theta = 70°$. Same labels as in Fig. 4.1.

A strong evolution may be observed on the potential energy curves when the angle θ increases from the linear geometry $\theta = 0°$ to nonlinear geometries, up to $\theta = 90°$. The avoided crossing between the entry channel and the $2^1\Sigma^+$ level becomes sharper and moves toward shorter internuclear distances. On the other hand, the avoided crossing between $2^1\Sigma^+$ and $1^1\Sigma^+$ exit channels becomes smoother, as shown in the potential energy curves for values at $\theta = 20°, 45°, 70°, 90°$ presented in Fig. 4.6, Fig. 4.7 and Fig. 4.8.

The evolution is inverse between the $2^1\Sigma^+$ and $1^1\Sigma^+$ charge-transfer levels when the angle θ increases still up to 180° in the linear $C - F - H$ geometry shown in Fig. 4.9 and Fig. 4.10. Nevertheless, the nonadiabatic interaction between the entry channel and the $2^1\Sigma^+$ level remains sharper in this half-plane, where the C^{2+} ion collides with the fluorine atom.

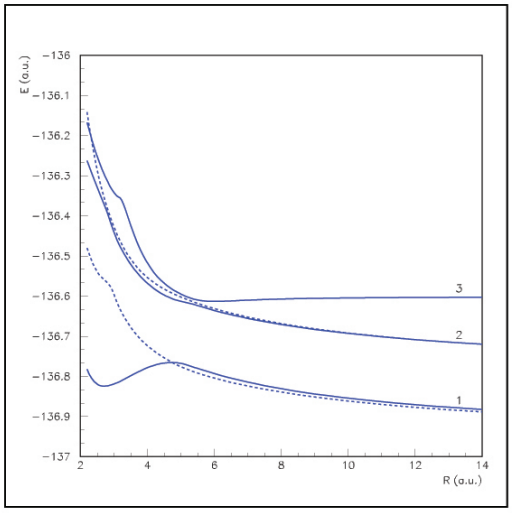

4.8. Figure: Potential energy curves for the $^1\Sigma^+$ (solid line) and $^1\Pi$ (dashed line) states of the $C^{2+} - HF$ molecular system at equilibrium, $\theta = 90°$. Same labels as in Fig. 4.1.

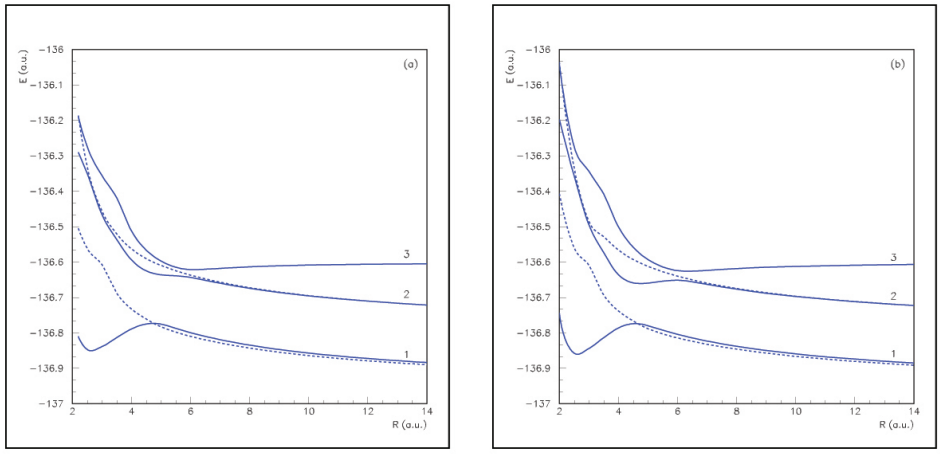

4.9. Figure: Potential energy curves for the $^1\Sigma^+$ (solid line) and $^1\Pi$ (dashed line) states of the $C^{2+} - HF$ molecular system at equilibrium, (a) $\theta = 110°$, (b) $\theta = 135°$. Same labels as in Fig. 4.1.

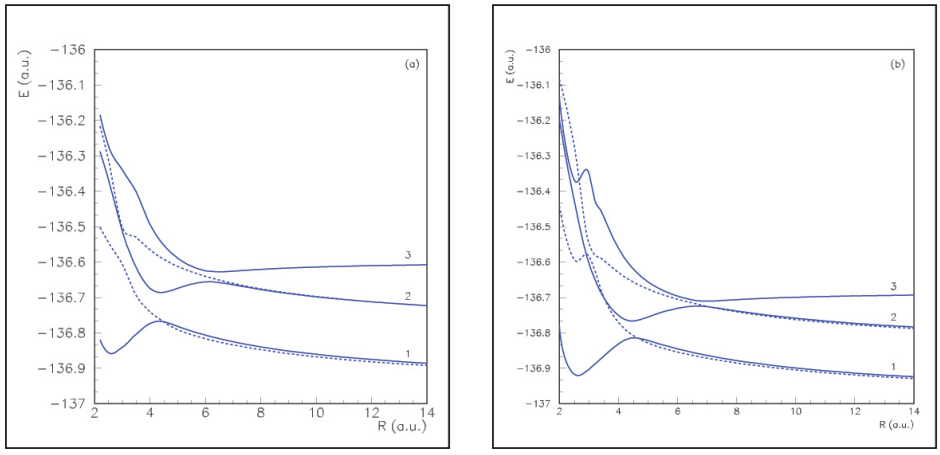

4.10. Figure: Potential energy curves for the $^1\Sigma^+$ (solid line) and $^1\Pi$ (dashed line) states of the $C^{2+} - HF$ molecular system at equilibrium, (a) $\theta = 160°$, (b) $\theta = 180°$. Same labels as in Fig. 4.1.

b) Radial Couplings

The dependence of the radial couplings on the orientation of the projectile towards the molecular target is presented for the chosen specific values of the angle $\theta = 45°$ and $160°$ in Fig. 4.11. As discussed previously, the radial coupling matrix elements between $^1\Sigma^+$ states show two main peaks. The radial coupling rad23 exhibits besides a sharp peak at short range corresponding to an interaction in the repulsive part of the potential energy curve.

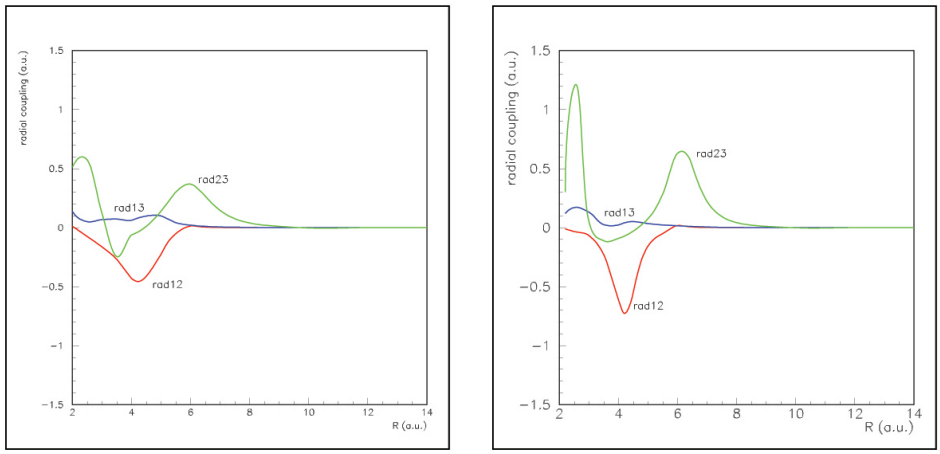

4.11. Figure: Radial coupling matrix elements between $^1\Sigma^+$ states of the $C^{2+} - HF$ molecular system at equilibrium, $\theta = 45°$, $160°$, respectively. Same labels as in Fig. 4.1.

As pointed out previously, a strong evolution is observed in the potential energy curves when the angle θ increases from the linear geometry $\theta = 0°$ to nonlinear geometries, up to $\theta = 90°$. This may be visualized particularly on the radial coupling matrix elements displayed in Fig. 4.12 and Fig. 4.13.

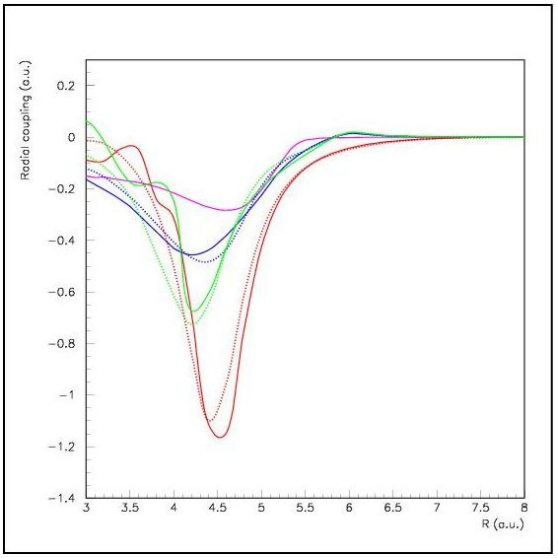

4.12. Figure: Variation of the rad12 radial coupling matrix element between $^1\Sigma^+$ levels for different orientation of the C^{2+} projectile toward the HF molecule at equilibrium. Same labels as in Fig. 4.1; — $\theta = 0°$ (red); — $\theta = 20°$ (green); — $\theta = 45°$(blue); — $\theta = 90°$(magenta); · · · $\theta = 135°$ (blue); · · · $\theta = 160°$ (green); · · · $\theta = 180°$(red).

We can observe a strong lowering of the radial coupling rad12 for $\theta = 90°$. The orientations $\theta = 45°$, $\theta = 20°$, $\theta = 0°$ for the approach toward the hydrogen atom of HF appear in correspondence to $\theta = 135°$, $\theta = 160°$, $\theta = 180°$, respectively. The radial coupling rad23 associated to the avoided crossing between the entry channel and the $2^1\Sigma^+$ level becomes larger and moves toward shorter internuclear distances when the angle θ increases from the linear geometry $\theta = 0°$ to nonlinear geometries, up to $\theta = 90°$, whereas it remains strong when the angle θ increases still up to $\theta = 180°$. Both rad12 and rad23 are maximum for the linear geometry toward fluorine ($\theta = 180°$) and decrease significantly for perpendicular orientation. The radial coupling rad23 remains anyway not negligible at $\theta = 90°$.

The radial coupling matrix elements between $^1\Pi$ states have not been presented as no significant avoided crossing may be observed in the distance range of interest.

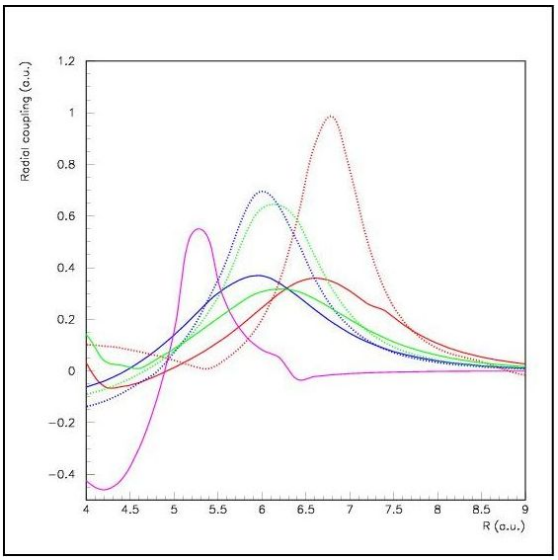

4.13. Figure: Variation of the rad23 radial coupling matrix element between $^1\Sigma^+$ levels for different orientation of the C^{2+} projectile toward the HF molecule at equilibrium. Same labels as in Fig. 4.1; — $\theta = 0°$ (red); — $\theta = 20°$ (green); — $\theta = 45°$(blue); — $\theta = 90°$(magenta); · · · $\theta = 135°$ (blue); · · · $\theta = 160°$ (green); · · · $\theta = 180°$(red).

c) Rotational Couplings

As an example, rotational couplings for the perpendicular geometry are presented in Fig. 4.14. Rotational coupling corresponding to the same configuration reaches the asymptotic value 1 a.u., as for instance the coupling between $2^1\Pi$ and $2^1\Sigma^+$ levels corresponding to the $\{C^+(1s^2 2s^2 2p)^2 P^\circ + HF^+(^2\Sigma^+)\}$ configuration. Rotational coupling between states corresponding to different configurations vanishes at asymptotic distances, as the coupling between the entry channel and the $1^1\Pi\{C^+(1s^2 2s^2 2p)^2 P^\circ + HF^+(^2\Pi)\}$ state. In C_{2v} symmetry group rotational couplings rot12 and rot21 are not zero at asymptotic distances, because the corresponding states are described by the same configurations. In C_s symmetry the rotational couplings between $^1\Sigma^+$ and $^1\Pi$ states correlated to different molecular states are becoming zero, as shown in Fig. 4.14 for the perpendicular geometry.

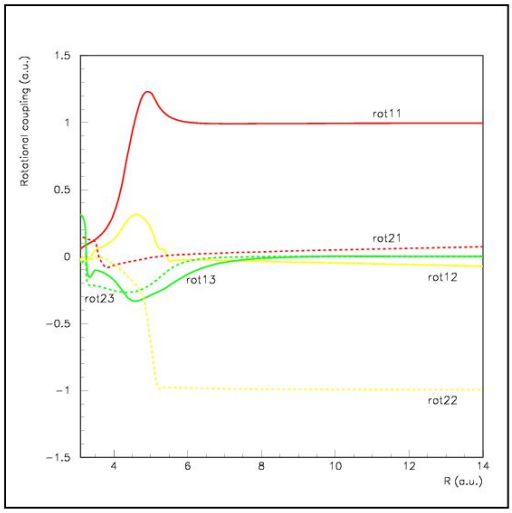

4.14. Figure: Rotational coupling matrix elements between $^1\Sigma^+$ and $^1\Pi$ states for the $C^{2+} - HF$ molecular system at equilibrium, $\theta = 90°$. Same labels as in Fig. 4.1.: rot11=$\langle 1^1\Pi | \, iLy \, | 1^1\Sigma^+ \rangle$, rot12=$\langle 1^1\Pi | \, iLy \, | 2^1\Sigma^+ \rangle$, rot13=$\langle 1^1\Pi | \, iLy \, | 3^1\Sigma^+ \rangle$, rot21=$\langle 2^1\Pi | \, iLy \, | 1^1\Sigma^+ \rangle$, rot22=$\langle 2^1\Pi | \, iLy \, | 2^1\Sigma^+ \rangle$, rot23=$\langle 2^1\Pi | \, iLy \, | 3^1\Sigma^+ \rangle$.

d) Collision Dynamics

The strong evolution observed in the potential energy curves when the angle θ increases from the linear $C - H - F$ geometry ($\theta = 0°$) to perpendicular ($\theta = 90°$) and then to the linear $C - F - H$ one ($\theta = 180°$) may be analyzed for chosen specific values $\theta = 0°, 45°, 90°, 135°$ and $180°$, in parallel with the total cross sections and radial coupling matrix elements displayed in Fig. 4.15.

From cross-section results, it appears quite clear that charge-transfer process is favoured in the linear geometry. The collision with the fluorine atom ($\theta = 180°$) is particularly efficient. In contrast, the charge-transfer process is markedly non-favoured in the perpendicular geometry corresponding to significantly lower charge-transfer cross sections (paper **A2**). Such a result absolutely corroborates to previous studies on the $C^{2+} + OH$ and $C^{2+} + CO$ collision systems [127]. In such collisions with heteronuclear molecular tar-

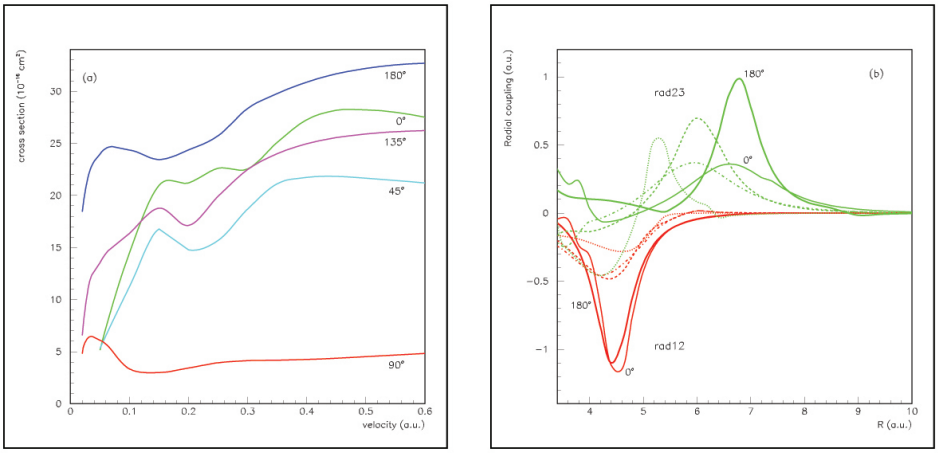

4.15. Figure: (a) Total charge-transfer cross sections for the $C^{2+} - HF$ system at equilibrium, for different orientations θ from 0° to 180°: — $\theta = 90°$; — $\theta = 45°$; — $\theta = 135°$; — $\theta = 0°$; — $\theta = 180°$. (b) Radial coupling matrix elements between $^1\Sigma^+$ states of the $C^{2+} - HF$ system at equilibrium for different orientations. Upper curves, rad23; lower curves, rad12. Dotted line, $\theta = 90°$; dot-dashed line, $\theta = 45°$, dashed line, $\theta = 135°$; thin solid line, $\theta = 0°$; thick solid line, $\theta = 180°$.

gets, the charge transfer is always favoured in a collinear approach toward the most electronegative atom, preferentially fluorine or oxygen rather than hydrogen for HF and OH, or carbon in the case of the CO molecular target. In the previous study on $C^{2+} + CO$ charge transfer, such a result was connected directly to the variation of the nonadiabatic interaction between the entry channel and the main exit channel characterized by the corresponding radial coupling matrix element. The discussion is a bit more complex in the present case, as the cross sections may be related to simultaneous variations of two avoided crossings, the avoided crossing between the entry channel and the $2^1\Sigma^+\{C^+(1s^2 2s^2 2p)^2 P^\circ + HF^+(^2\Sigma^+)\}$ level corresponding to the radial coupling rad23 on one hand, and the avoided crossing between the $2^1\Sigma^+$ and $1^1\Sigma^+\{C^+(1s^2 2s^2 2p)^2 P^\circ + HF^+(^2\Pi)\}$ exit channels characterized by the radial coupling rad12, on the other hand (see papers **A2** and **A6**). Effectively, both rad23 and rad12 present a maximum for the linear geometry toward fluorine ($\theta = 180°$). The radial coupling matrix element rad12

shows a simple behaviour that is almost symmetric for both sides of the collision and significantly sharper in both collinear orientations. In contrast, the radial coupling matrix element rad23 is relatively smooth for the geometries corresponding to a collision with the hydrogen atom, in particular from $\theta = 0^\circ$ to $\theta = 45^\circ$. These two nonadiabatic interactions may be assigned to the two bumps of the partial cross section sec32. The bump at lower energies assigned to the interaction between the entry channel and the $2^1\Sigma^+$ level clearly increases from the linear $\theta = 0^\circ$ geometry to $\theta = 45^\circ$ geometry as shown in Fig. 4.4 and Fig. 4.16. It is shifted toward lower energies in nonlinear orientations until perpendicular geometry is obtained.

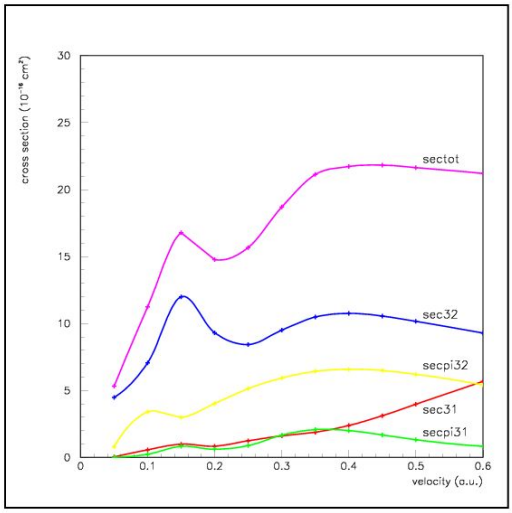

4.16. Figure: Total and partial charge-transfer cross sections for the $C^{2+} - HF$ molecular system at equilibrium, $\theta = 45^\circ$: sectot, total cross section; sec32, partial cross section on ${}^1\Sigma^+\{C^+(1s^22s^22p)^2P^\circ + HF^+({}^2\Sigma^+)\}$; secpi32, partial cross section on ${}^1\Pi\{C^+(1s^22s^22p)^2P^\circ + HF^+({}^2\Sigma^+)\}$; sec31, partial cross section on ${}^1\Sigma^+\{C^+(1s^22s^22p)^2P^\circ + HF^+({}^2\Pi)\}$, secpi31, partial cross section on ${}^1\Pi\{C^+(1s^22s^22p)^2P^\circ + HF^+({}^2\Pi)\}$.

The second bump, on the contrary, becomes smoother in connection with a lower nonadiabatic interaction between $1^1\Sigma^+$ and $2^1\Sigma^+$ exit channels. More generally, such nonadiabatic interactions driven by radial cou-

pling matrix elements lead to lower partial cross sections from the linear to perpendicular geometries. The values of the cross section on $^1\Pi$ levels, in particular the $2^1\Pi\{C^+(1s^22s^22p)^2P^\circ + HF^+(^2\Sigma^+)\}$ channel, on the contrary remain significant for every orientation of the projectile toward the target. This leads, globally, to a significant rotational effect, which follows from the values of the cross section averaged over the different orientations presented in Table 4.3. The averaged total cross sections increase from about 14×10^{-16} to 22×10^{-16} cm^2 in the $3 - 100$ keV collision energy range.

Velocity (a.u.)	E_{lab} (keV)	sec32 $3^1\Sigma^+ - 2^1\Sigma^+$	secpi32 $3^1\Sigma^+ - 2^1\Pi$	sec31 $3^1\Sigma^+ - 1^1\Sigma^+$	secpi31 $3^1\Sigma^+ - 1^1\Pi$	sectot
0.05	0.75	7.04	2.68	0.48	0.34	10.54
0.1	3.00	8.41	3.99	0.86	0.96	14.22
0.15	6.75	8.78	4.79	1.04	1.48	16.10
0.2	12.00	8.75	5.31	1.24	1.33	16.64
0.25	18.75	8.56	6.04	1.76	1.53	17.89
0.3	27.00	8.13	6.97	2.19	1.81	19.10
0.35	36.75	8.18	7.68	2.52	2.10	20.51
0.4	48.00	8.25	8.10	2.89	2.25	21.49
0.45	60.75	8.16	8.22	3.38	2.24	22.01
0.5	75.00	7.94	8.15	3.96	2.15	22.20
0.6	108.00	7.37	7.64	5.25	1.96	22.23

4.3. Table: Charge-transfer cross sections averaged over the different orientations for the $C^{2+} + HF$ collision systems (in $10^{-16}cm^2$).

4.1.3 Vibrational Effect

The collision of the C^{2+} projectile ion toward the HF molecular target may also depend on the geometry of the system corresponding to different values of the vibration coordinate r_{HF}. Two values of the vibration coordinate around the equilibrium distance have been considered in the linear approach of the projectile toward the hydrogen atom of HF ($\theta = 0^\circ$) in

order to test the vibration effect for this collision system. As shown in Fig. 4.17 for $r_{HF} = 1.5$ a.u. the avoided crossing between the entry channel and the $2^1\Sigma^+$ level appears sharper and moves toward longer internuclear R distances. On the other hand, the avoided crossing between the $2^1\Sigma^+$ and $1^1\Sigma^+$ exit channels becomes smoother and moves toward shorter R distances. In the other case (for $r_{HF} = 2.0$ a.u.), the position of the crossing between the entry channel and the $2^1\Sigma^+$ level moves toward shorter R distances and the avoided crossing exhibits smoother, while the crossing between the $2^1\Sigma^+$ and $1^1\Sigma^+$ exit channels appears at longer internuclear distances with sharper interaction.

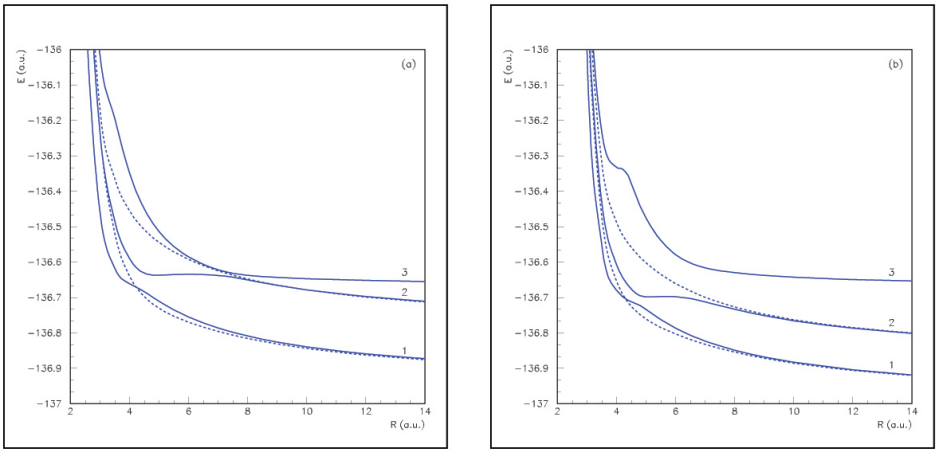

4.17. Figure: Potential energy curves for the $^1\Sigma^+$ (solid line) and $^1\Pi$ (dashed line) states of the $C^{2+} - HF$ molecular system at (a) $r_{HF} = 1.5$ a.u. and (b) $r_{HF} = 2.0$ a.u. Same labels as in Fig. 4.1.

The cross sections for velocities between 0.05 and 0.6 a.u. carried out for different values of the vibration coordinate r_{HF} are presented in Fig. 4.18. The total cross sections for different geometries of the HF molecule presented in Fig. 4.19(a) show a regular increase when the vibration coordinate r_{HF} is reduced from 2.0 a.u. to 1.5 a.u., in agreement with the increase of the radial coupling matrix element rad23 between the entry channel and the $2^1\Sigma^+$ level displayed in Fig. 4.19(b) (see papers **A2** and **A6**). Such coupling is moved toward longer internuclear distances when the r_{HF} vibration

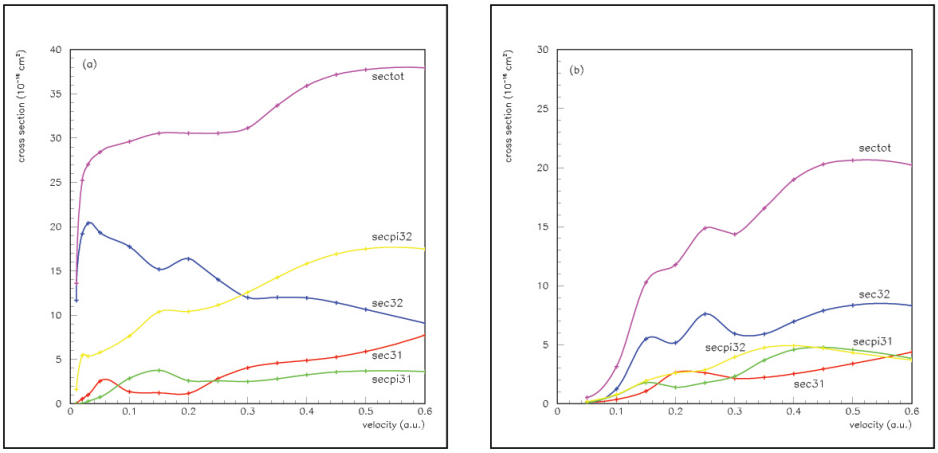

4.18. Figure: Total and partial charge-transfer cross sections for the $C^{2+} - HF$ system for the vibration coordinate (a) $r_{HF} = 1.5$ a.u. and (b) $r_{HF} = 2.0$ a.u., $\theta = 0°$: sectot, total cross section; sec32, partial cross section on $^1\Sigma^+\{C^+(1s^22s^22p)^2P^\circ + HF^+(^2\Sigma^+)\}$; secpi32, partial cross section on $^1\Pi\{C^+(1s^22s^22p)^2P^\circ + HF^+(^2\Sigma^+)\}$; sec31, partial cross section on $^1\Sigma^+\{C^+(1s^22s^22p)^2P^\circ + HF^+(^2\Pi)\}$, secpi31, partial cross section on $^1\Pi\{C^+(1s^22s^22p)^2P^\circ + HF^+(^2\Pi)\}$.

coordinate decreases. In contrast, the radial coupling rad12 between $1^1\Sigma^+$ and $2^1\Sigma^+$ exit channels decreases with the r_{HF} vibration coordinate. The corresponding interaction becomes smoother and moves toward shorter internuclear distances. Such observations may directly link the nonadiabatic interactions between $^1\Sigma^+$ channels to the shape of the partial cross section sec32. Two bumps may be observed for this partial cross section, one at lower collision energies, which may be attributed mainly to the avoided crossing between the entry channel and the $2^1\Sigma^+$ level. Such interaction increases for shorter r_{HF} values, as pointed out on the radial coupling matrix elements rad23 presented in Fig. 4.19(b), leading to an increase of the corresponding bump exhibited by the partial cross section sec32 shown in Fig. 4.4 and Fig. 4.18(a). On the other hand, the partial cross section sec32 exhibits a smoother bump at higher collision energies, which may be associated with the nonadiabatic interaction between $2^1\Sigma^+$ and $1^1\Sigma^+$ exit channels. Its shape becomes smoother for shorter values of the vibration

coordinate r_{HF} as presented in Fig. 4.4 and Fig. 4.18(a), in agreement with the variation of the radial coupling matrix element rad12 presented in Fig. 4.19(b). This analysis provides an interesting insight into the mechanism of the charge-transfer process with regard to the vibration of the molecular target. The collision of C^{2+} ions with the OH radical presented a specific behaviour at very constrained geometry of the OH target, which could lead to a first strong and very rapid relaxation of the molecule (Ref. [128] or see paper **A1**). In the present case no specific behaviour is exhibited at very constrained HF geometry and no first relaxation process may be expected for this system.

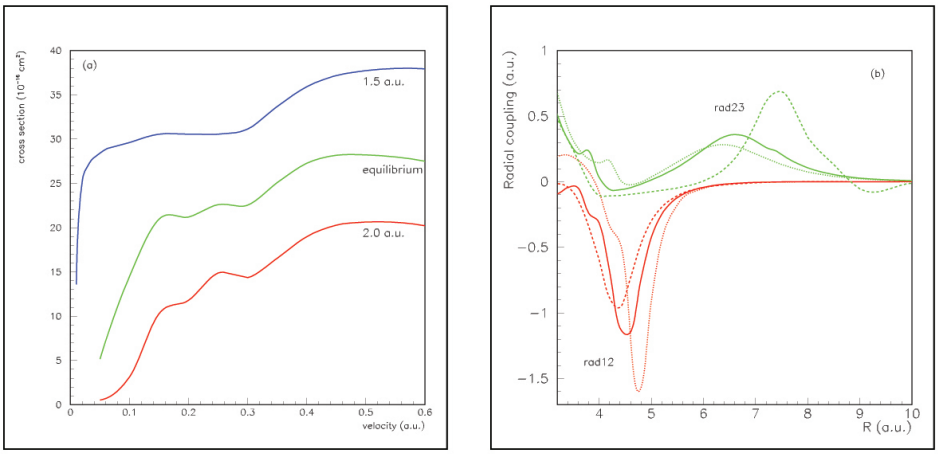

4.19. Figure: (a) Total charge-transfer cross sections for the $C^{2+} - HF$ system in the linear approach, $\theta = 0°$, for different values of the vibration coordinate r_{HF}. — $r_{HF} = 2.0$ a.u. (red); — $r_{HF} = 1.73836823$ a.u. (green); — $r_{HF} = 1.5$ a.u. (blue); (b) Radial coupling matrix elements between $^1\Sigma^+$ states of the $C^{2+} - HF$ system in the linear approach, $\theta = 0°$, for different values of the vibration coordinate r_{HF}. Upper curves, rad23; lower curves, rad12. Dotted line, $r_{HF} = 2.0$ a.u. ; solid line, $r_{HF} = 1.73836823$ a.u.; dashed line, $r_{HF} = 1.5$ a.u.

An estimate of the cross sections on the different vibrational levels ν in $C^{2+} + HF_{(\nu=0)} \rightarrow C^{+} + HF^{+}_{(\nu)}$ may be achieved by developing the wavefunction on the vibrational functions. An estimate of the vibration motion of the diatomics, neglecting the rotational modes, can be obtained by introduc-

ing Franck-Condon factors in the framework of the centroid approximation. This approximation has been widely discussed and, while not satisfactory at low energies, it has been shown to provide nevertheless a reasonable accuracy for impact energies greater than 500 eV/amu [129]. Furthermore, the regular variation of cross sections with regard to the vibration coordinate may give confidence in the use of such an approximation.

The vibration energy levels and Franck-Condon factors have been calculated in the anharmonic approximation using the program LEVEL 7.7 of R. J. Le Roy [130], taking for HF and HF^+ the potentials determined at the CASSCF-MRCI level of theory. The total charge-transfer cross sections in $C^{2+}(^1S)+HF_{(\nu=0)} \rightarrow C^+ + HF^+_{(\nu)}$ are given in Table 4.4 for a series of values of the collision velocities corresponding to impact energies between about 6 and 40 keV. The charge-transfer cross sections decrease very rapidly wit increasing vibration number. They present significant values for $\nu = 0$, $\nu = 1$, and up to $\nu = 2$. The electron capture resulting in higher vibration levels of HF^+ is very weak.

ν	$v = 0.15$	$v = 0.2$	$v = 0.25$	$v = 0.3$	$v = 0.35$
	E_{lab}=6.75 keV	E_{lab}=12 keV	E_{lab}=18.75 keV	E_{lab}=27 keV	E_{lab}=36.75 keV
0	14.260	14.424	15.379	15.339	17.071
1	5.007	5.064	5.400	5.385	5.994
2	1.279	1.293	1.379	1.375	1.531
3	0.305	0.308	0.329	0.328	0.365
4	0.073	0.075	0.080	0.079	0.088

4.4. Table: Total cross sections for the $C^{2+} + HF_{(\nu=0)} \rightarrow C^+ + HF^+_{(\nu)}$ charge-transfer process (in $10^{-16} cm^2$) for different velocities v (in a.u.).

4.1.4 Concluding Remarks

The study presents a theoretical treatment of charge-transfer processes induced by collision of the C^{2+} projectile on HF molecule. A two crossing mechanism is observed, mainly driven by the interaction at shorter range with the $\{C^+(1s^2 2s^2 2p)^2 P^\circ + HF^+(^2\Sigma^+)\}$ exit channel leading to important

values of the total cross section at higher collision energy by contribution of radial coupling with a significant rotational effect. The collision process is highly anisotropic: the charge transfer is favoured in the linear approach with the collision of the C^{2+} ion toward the fluorine atom, and, on the contrary, very significantly non-favoured in the perpendicular approach. The vibrational effect is regular. In the $C^{2+}(^1S) + HF_{(\nu=0)} \rightarrow C^+ + HF^+_{(\nu)}$ process, only low vibrational levels are expected to be populated.

Such remarks may be extended to provide a general understanding of charge-transfer processes in collision of ions with heteronuclear molecular targets.

4.2 Application to the $C^{2+} + HCl$ Collision System

The C^{2+} projectile ion has been chosen as in previous work in order to have a comparative analysis for a series of diatomics [127,128,131]. Hydrogen halide targets offer the advantage to lead to a relatively simple fragmentation pattern. Effectively, with regard to the relative atomic mass of hydrogen and halogen atoms, the fragments have very different kinetic energies and may be easily separated experimentally [132]. The work has been extended to the hydrogen chloride target corresponding to a similar electronic configuration, but a quite higher size and mass of the heteroatom. The reaction may be compared to the $C^{2+} + HF$ collision system, in particular to have a look at the efficiency of the charge-transfer process with regard to possible steric or electronic effects. This section is mainly based on the results of the papers **A4** and **A5**.

As previously, the molecular calculations have been carried out using the MOLPRO suite of *ab initio* programs [59]. A pseudopotential has been used to take account of the core electrons of the chlorine atom. Different tests have been performed for the choice of this pseudopotential and the basis set of atomic orbitals. The ECP10sdf 10 core-electron relativistic pseudopotential has been used for chlorine [133]. As in previous case, the correlation-consistent aug-cc-pVTZ basis set of Dunning [113] has been chosen for all atoms. The following Table 4.5 lists the exponents and contraction coefficients for the chlorine. Calculations have been performed using state-averaged CASSCF-MRCI (Complete Active Space Self-Consistent Field-Multireference Configuration Interaction) methods. The active space includes the $1s$ orbital of hydrogen, the $n = 2$ and $n = 3(sp)$ orbitals for carbon, and the $n = 3$ orbitals for chlorine, the core electrons being treated by a pseudopotential. The 1s orbital of carbon has been frozen in the calculation. The optimized geometry of the $^1\Sigma^+$ ground state of HCl at the CASSCF (Complete Active Space Self-Consistent Field) level of theory is r_{HCl}=2.40988808 a.u. in good agreement with the 2.4086 a.u. experimental value [115]. The corresponding vertical ionization potential calculated using MRCI (Multireference Configuration Interaction) methods is 12.6901 eV, in good agreement with the 12.748 eV experimental value obtained from photoelectron spectra measurements [115, 134].

		Exponents	Contraction Coefficients					
Chlorine	s	456100	0.492970D-04	-0.138304D-04	0.418546D-05	0.0	0.0	0.0
		68330	0.383029D-03	-0.107279D-03	0.324395D-04	0.0	0.0	0.0
		15550	0.200854D-02	-0.565083D-03	0.171105D-03	0.0	0.0	0.0
		1439	0.294703D-01	-0.845886D-02	0.256705D-02	0.0	0.0	0.0
		520.40	0.878325D-01	-0.259638D-01	0.788552D-02	0.0	0.0	0.0
		203.10	0.211473D+00	-0.686362D-01	0.210867D-01	0.0	0.0	0.0
		83.96	0.365364D+00	-0.141874D+00	0.442264D-01	0.0	0.0	0.0
		36.20	0.340884D+00	-0.199319D+00	0.651670D-01	0.0	0.0	0.0
		15.83	0.102133D+00	-0.195662D-01	0.603012D-02	0.0	0.0	0.0
		6.3340	0.311675D-02	0.499741D+00	-0.206495D+00	0.0	0.0	0.0
		2.6940	0.105751D-02	0.563736D+00	-0.405871D+00	0.0	0.0	0.0
		0.43131	0.156136D-03	-0.835091D-02	0.725661D+00	0.0	0.0	0.0
		0.9768	0.0	0.0	0.0	1.0	0.0	0.0
		0.1625	0.0	0.0	0.0	0.0	1.0	0.0
		0.0591	0.0	0.0	0.0	0.0	0.0	1.0
	p	663.30	0.240448D-02	-0.652145D-03	0.0	0.0	0.0	
		156.80	0.192148D-01	-0.519445D-02	0.0	0.0	0.0	
		49.98	0.885097D-01	-0.246938D-01	0.0	0.0	0.0	
		18.42	0.25602D+00	-0.728167D-01	0.0	0.0	0.0	
		7.24	0.436927D+00	-0.13403D+00	1.0	0.0	0.0	
		2.922	0.350334D+00	-0.947742D-01	0.0	1.0	0.0	
		0.3818	-0.458423D-02	0.564667D+00	0.0	0.0	0.0	
		1.0220	0.0	0.0	1.0	0.0	0.0	
		0.1301	0.0	0.0	0.0	1.0	0.0	
		0.0419	0.0	0.0	0.0	0.0	1.0	
	d	1.0460	1.0	0.0	0.0			
		0.3440	0.0	1.0	0.0			
		0.135	0.0	0.0	1.0			

	f	0.7060	1.0	0.0
		0.3120	0.0	1.0

4.5. Table: Exponents and contraction coefficients of the aug-cc-pVTZ basis set of Dunning [113] for the Cl atom.

The spin-orbit effects can be neglected in the collision energy range of interest thus electron spin may be conserved in the collision process. Taking account of the $^1\Sigma^+$ symmetry of the $C^{2+}(1s^2 2s^2)^1S + HCl(^1\Sigma^+)$ entry channel, only $C^+(^2P^o)$ or $C^+(^2D)$ states could be involved in the collision process. Effectively, $C^+(^4P)$ states could lead only to triplet and quintet states which cannot be correlated to the entry channel as spin-orbit coupling is negligible. With regard to the different excited states of HCl^+, there are thus four $^1\Sigma^+$ states which can be correlated by means of radial coupling, the entry channel and three charge-transfer levels. We have also to take into account the $^1\Pi$ states which can be correlated to the $^1\Sigma^+$ entry channel by rotational coupling interaction. Four $^1\Sigma^+$ states and three $^1\Pi$ states must thus be considered in this process with regard to the different excited states of HCl^+ and spin considerations:

Configuration	Molecular states
$C^{2+}(1s^2 2s^2)^1S + HCl(^1\Sigma^+)$	$^1\Sigma^+$,
$C^+(1s^2 2s^2 2p)^2D + HCl^+(^2\Pi)$	$^1\Sigma^+$,$^1\,\Pi$,
$C^+(1s^2 2s^2 2p)^2P^\circ + HCl^+(^2\Sigma^+)$	$^1\Sigma^+$,$^1\,\Pi$,
$C^+(1s^2 2s^2 2p)^2P^\circ + HCl^+(^2\Pi)$	$^1\Sigma^+$,$^1\,\Pi$.

The asymptotic energies of the $C^{2+} - HCl$ molecular system may be compared to separated species calculations taking account of experimental ionization potentials and carbon ion levels [115, 119, 134] combined with MRCI calculations at optimized equilibrium geometry for the HCl and HCl^+ ground and excited states. The calculated asymptotic energy difference between the entry channel and the highest $^1\Sigma^+\{C^+(1s^2 2s^2 2p)^2D + HCl^+(^2\Pi)\}$ exit channel is 2.35 eV, with a discrepancy of 0.06 eV with

experimental data assuming a good description of both entry and exit channels. The asymptotic energy difference of the two lowest charge-transfer levels $^1\Sigma^+\{C^+(1s^22s^22p)^2P^\circ + HCl^+(^2\Pi)\}$ and $^1\Sigma^+\{C^+(1s^22s^22p)^2P^\circ + HCl^+(^2\Sigma^+)\}$ is 4.15 eV, in agreement with the 4.00 eV separated species calculation.

4.2.1 Adiabatic Potential Energy Curves

The corresponding potential energy curves have been calculated in the [2.0-15.0] a.u. internuclear distance range. They are presented in Fig. 4.20 for the equilibrium distance in the linear $C-H-Cl$ geometry ($\theta = 0^\circ$). The

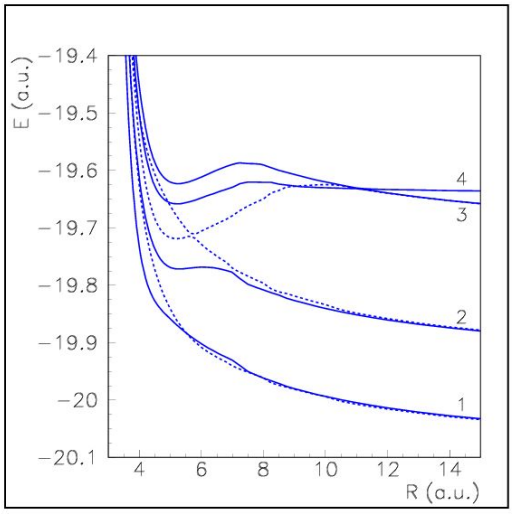

4.20. Figure: Potential energy curves for the $^1\Sigma^+$ (solid line) and $^1\Pi$ (dashed line) states of the $C^{2+} - HCl$ molecular system at equilibrium, ($\theta = 0^\circ$): 1, $C^+(1s^22s^22p)^2P^\circ + HCl^+(^2\Pi)$; 2, $C^+(1s^22s^22p)^2P^\circ + HCl^+(^2\Sigma^+)$; 3, $C^+(1s^22s^22p)^2D + HCl^+(^2\Pi)$; 4, $C^{2+}(1s^22s^2)^1S + HCl(^1\Sigma^+)$ entry channel.

main feature is a very strong avoided crossing between the $^1\Sigma^+$ entry channel and the $3^1\Sigma^+\{C^+(1s^22s^22p)^2D + HCl^+(^2\Pi)\}$ charge-transfer level around R=11 a.u. This avoided crossing appears to be the leading nonadiabatic

interaction in the present collision system. The other avoided crossings, between $1^1\Sigma^+\{C^+(1s^22s^22p)^2P^\circ + HCl^+(^2\Pi)\}$ and $2^1\Sigma^+\{C^+(1s^22s^22p)^2P^\circ + HCl^+(^2\Sigma^+)\}$ exit channels, or between the $2^1\Sigma^+\{C^+(1s^22s^22p)^2P^\circ + HCl^+(^2\Sigma^+)\}$ and $3^1\Sigma^+\{C^+(1s^22s^22p)^2D + HCl^+(^2\Pi)\}$ levels are significantly smoother and correspond to large energy gaps. They could certainly not be determinant in the process. Such a strong interaction between the entry channel and one charge-transfer level was not present in the $C^{2+} + HF$ collision system. Effectively, in that case the $3^1\Sigma^+\{C^+(1s^22s^22p)^2D + HF(^2\Pi)\}$ level was higher in energy than the entry channel with regard to the ionization potential of HF and could not be populated directly. Therefore, the only exit channel which could be accessible from the entry channel was the $^1\Sigma^+\{C^+(1s^22s^22p)^2P^\circ + HF^+(^2\Sigma^+)\}$ showing a relatively smooth interaction around $R = 6.5$ a.u., and of course the lowest $^1\Sigma^+\{C^+(1s^22s^22p)^2P^\circ + HF^+(^2\Pi)\}$ charge-transfer state, which is certainly too low in energy to be determinant in the process. Another important feature to point out in the $C^{2+} + HCl$ collision, always in tight connection with the existence of the $\{C^+(1s^22s^22p)^2D + HCl^+(^2\Pi)\}$ exit channel, is the strong nonadiabatic interaction observed between the $2^1\Pi\{C^+(1s^22s^22p)^2P^\circ + HCl^+(^2\Sigma^+)\}$ and $3^1\Pi\{C^+(1s^22s^22p)^2D + HCl^+(^2\Pi)\}$ charge-transfer levels. This interaction was, of course, not present in the $C^{2+} + HF$ collision system and could induce an increase of the rotational effect.

4.2.2 Radial and Rotational Couplings

As in previous case, the radial coupling matrix elements between all pairs of states of the same symmetry have been calculated by means of the finite difference technique with the same value of the parameter $\Delta = 0.0012$ a.u. The rotational coupling matrix elements have been determined from the quadrupole moment tensor from the expression $iL_y = x\dfrac{\partial}{\partial z} - z\dfrac{\partial}{\partial x}$. The radial and rotational coupling matrix elements are displayed in Fig. 4.21 and Fig. 4.22, respectively.

Both couplings rad12 and rad 23 between the $2^1\Sigma^+\{C^+(1s^22s^22p)^2P^\circ + HCl^+(^2\Sigma^+)\}$ and the $1^1\Sigma^+\{C^+(1s^22s^22p)^2P^\circ + HCl^+(^2\Pi)\}$ exit channels, and between the $3^1\Sigma^+\{C^+(1s^22s^2\ 2p)^2D + HCl^+(^2\Pi)\}$ and $2^1\Sigma^+\{C^+(1s^2\ 2s^22p)^2P^\circ + HCl^+\ (^2\Sigma^+)\}$ exit channels show a smooth variation with

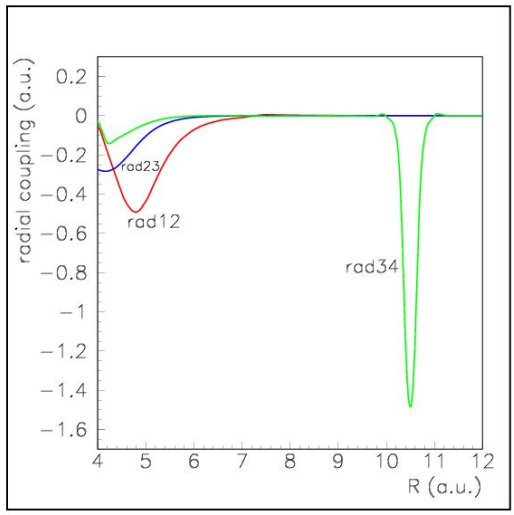

4.21. Figure: Radial coupling matrix elements between $^1\Sigma^+$ states of the $C^{2+} - HCl$ molecular system at equilibrium, $\theta = 0°$. Same labels as in Fig. 4.20.

a hump around $R = 4.4$ a.u. and $R = 4.1$, respectively. The radial nonadiabatic coupling matrix element between the entry channel and the $3^1\Sigma^+\{C^+(1s^22s^22p)^2D + HCl^+(^2\Pi)\}$ level exhibits a strong peak, 1.48 a.u. high, in correspondence to the very strong avoided crossing between the potential energy curves. Such coupling is more than three times higher than the other radial couplings. Besides, the strong interaction between the $2^1\Pi\{C^+(1s^22s^22p)^2P^\circ + HCl^+(^2\Sigma^+)\}$ and $3^1\Pi\{C^+(1s^22s^22p)^2D + HCl^+$ $(^2\Pi)\}$ exit channels pointed out on the potential energy curves leads to a sharp crossing between rot22 and rot32 correlated to the change of character of the Π wavefunctions in the neighborhood of the avoided crossing. On the contrary, the interaction between states 1 and 2 being very smooth for both $^1\Sigma^+$ and $^1\Pi$ symmetries, the rotational coupling rot11 remains almost equal to 1 for all distances.

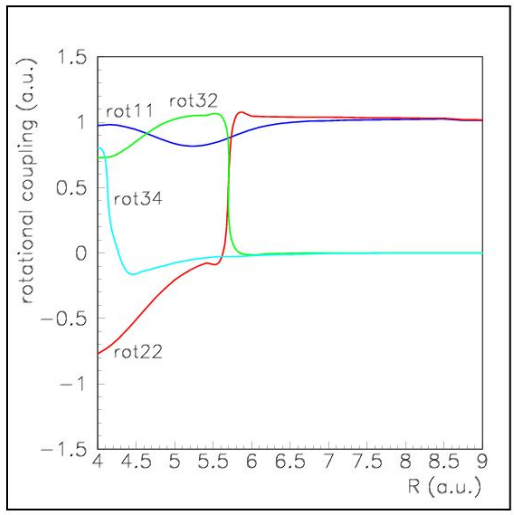

4.22. Figure: Rotational coupling matrix elements between $^1\Sigma^+$ and $^1\Pi$ states of the $C^{2+}-HCl$ molecular system at equilibrium, $\theta = 0°$. Same labels as in Fig. 4.20. (rot11=$< 1^1\Pi|iL_y|1^1\Sigma^+ >$; rot22=$< 2^1\Pi|iL_y|2^1\Sigma^+ >$; rot32=$< 3^1\Pi|iL_y|2^1\Sigma^+ >$; rot34=$< 3^1\Pi|iL_y|4^1\Sigma^+ >$).

4.2.3 Collision Dynamics

The collision dynamics has been performed by means of the EIKONX code [120] in the keV laboratory energy range.

It has been shown in the previous section the effect of translation factors can be considered with a good approximation weak in the energy range we are dealing with and has not been taken into account in the present $C^{2+} + HCl$ collision treatment.

The partial and total cross sections are presented in Fig. 4.23 and Table 4.6 for the linear $C - H - Cl$ geometry ($\theta = 0°$). The total cross section presents a peak around $v_{coll} = 0.1$ a.u. ($E_{lab} = 3\ keV$) and then decreases at higher collision energy. Such a peak is mainly due to the contribution of the corresponding peak of the partial cross section sec43. As pointed out from the potential energy curves, the charge-transfer process appears clearly dominated by one nonadiabatic interaction corresponding to the avoided crossing between the entry channel and the highest

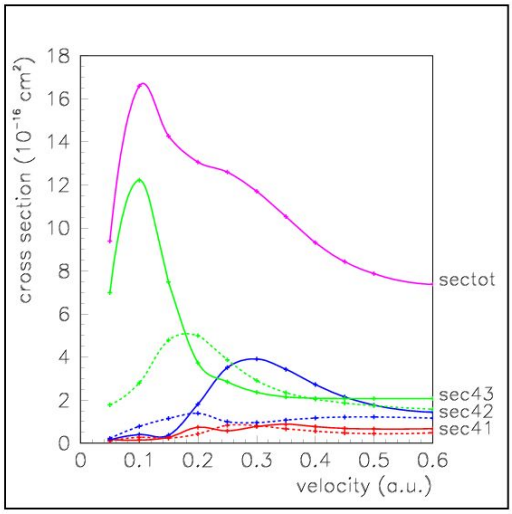

4.23. Figure: Total and partial charge-transfer cross sections for the $C^{2+} - HCl$ system at equilibrium, $\theta = 0°$. Full line, transition to $^1\Sigma^+$ states; broken line, transition to $^1\Pi$ states. (sectot, total cross section; sec 43, partial cross section on $\{C^+(1s^22s^22p)^2D + HCl^+(^2\Pi)\}$; sec42, partial cross section on $\{C^+(1s^22s^22p)^2P^\circ + HCl^+(^2\Sigma^+)\}$; sec41, partial cross section on $\{C^+(1s^22s^22p)^2P^\circ + HCl^+(^2\Pi)\}$).

$3^1\Sigma^+\{C^+(1s^22s^22p)^2D + HCl^+(^2\Pi)\}$ charge-transfer level, which gives rise to the strong peak of the partial cross section sec43. The shorter-range crossing between $3^1\Sigma^+\{C^+(1s^22s^22p)^2D + HCl^+(^2\Pi)\}$ and $2^1\Sigma^+\{C^+(1s^22s^22p)$ $^2P^\circ + HCl^+(^2\Sigma^+)\}$ channels is also involved in the C^{2+} + HCl charge-transfer process; it leads in particular to a hump in the sec42 partial cross section, but its contribution is largely lower than the strong interaction between the entry channel and the $3^1\Sigma^+\{C^+(1s^22s^22p)^2D + HCl^+(^2\Pi)\}$ charge-transfer channel. Such behaviour is completely different from the mechanism observed in the C^{2+} + HF collision system, where the $^1\Sigma^+$,$^1\Pi\{C^+(1s^22s^22p)$ $^2D + HF^+(^2\Pi)\}$ exit channel could not be accessible. The charge-transfer process was thus driven by shorter-range crossings, in particular between the entry channel and the $2^1\Sigma^+\{C^+(1s^22s^22p)^2P^\circ + HF^+(^2\Sigma^+)\}$ exit channel around $R = 6.5$ a.u. and a competition with the avoided crossing with

the lowest $1^1\Sigma^+\{C^+(1s^22s^22p)^2P^\circ + HF^+(^2\Pi)\}$ charge-transfer level was observed. These interactions were leading, at variance from the $C^{2+} + HCl$ collision, to an increase of the charge-transfer cross sections at higher energies around $E_{lab} = 100$ keV and the charge transfer appears more efficient in the collision of C^{2+} ions with HF than with the HCl target (Table 4.3 and Table 4.6).

As already pointed out for C^{2+}+HF, rotational effect may be observed also for this system as charge-transfer channels may be all correlated to the entry channel by means of rotational coupling. In particular, a hump is shown on the partial cross section on the $2^1\Pi\{C^+(1s^22s^22p)^2P^\circ + HCl^+(^2\Sigma^+)\}$ exit channel in connection with the nonadiabatic interaction between the $2^1\Pi\{C^+(1s^22s^22p)^2P^\circ + HCl^+(^2\Sigma^+)\}$ and $3^1\Pi\{C^+(1s^22s^22p)^2D + HCl^+(^2\Pi)\}$ charge-transfer levels pointed out in the molecular calculations. However, the contribution of $^1\Pi$ exit channels decreases at higher collision energies, and is almost of the same order of magnitude as the contribution of corresponding $^1\Sigma^+$ charge-transfer states coupled by radial coupling (Table 4.6). The mechanism of the $C^{2+} + HCl$ charge transfer is clearly dominated by the nonadiabatic radial coupling interaction rad34. On the contrary, rotational effects remain significant in $C^{2+} + HF$ at higher collision energies, in particular for the $2^1\Pi\{C^+(1s^22s^22p)^2P^\circ + HF^+(^2\Sigma^+)\}$ channel, and contribute significantly to the total cross section.

v (a.u.)	E_{lab} (keV)	sec43	secpi43	sec42	secpi42	sec41	secpi41	sectot
0.05	0.75	6.99	1.78	0.14	0.22	0.17	0.09	9.38
0.1	3.00	12.22	2.80	0.39	0.77	0.14	0.27	16.58
0.15	6.75	7.48	4.78	0.36	1.14	0.27	0.23	14.26
0.2	12.00	3.73	4.99	1.80	1.38	0.73	0.42	13.05
0.25	18.75	2.84	3.86	3.50	0.99	0.57	0.82	12.59
0.3	27.00	2.36	2.91	3.91	0.95	0.77	0.81	11.70
0.35	36.75	2.14	2.34	3.43	1.07	0.88	0.66	10.52
0.4	48.00	2.08	2.03	2.72	1.16	0.77	0.55	9.32
0.45	60.75	2.07	1.86	2.14	1.21	0.68	0.47	8.42
0.5	75.00	2.06	1.74	1.77	1.21	0.65	0.43	7.87
0.6	108.00	2.07	1.57	1.44	1.15	0.67	0.48	7.37

4.6. Table: Charge-transfer cross sections for the $C^{2+} + HCl$ collision system (in 10^{-16}cm^2). (sec43, $4^1\Sigma^+ - 3^1\Sigma^+$; secpi43, $4^1\Sigma^+ - 3^1\Pi$; sec42, $4^1\Sigma^+ - 2^1\Sigma^+$; secpi42, $4^1\Sigma^+ - 2^1\Pi$; sec41, $4^1\Sigma^+ - 1^1\Sigma^+$, secpi41, $4^1\Sigma^+ - 1^1\Pi$)

4.2.4 Concluding Remarks

The present study of charge-transfer processes induced by collision of the C^{2+} projectile on hydrogen chloride may be compared to the C^{2+} + HF collision system involving a quite similar molecular target. A simple mechanism driven by the nonadiabatic radial coupling interaction between the entry channel and the highest $3^1\Sigma^+\{C^+(1s^2 2s^2 2p)^2 D + HCl^+(^2\Pi)\}$ charge-transfer channel is exhibited for this collision system. The total cross section presents a maximum of 16.6×10^{-16} cm^2 around $E_{lab} = 3\ keV$ and decreases at higher energies. This mechanism is completely different for the $C^{2+} + HF$ collision system. The charge transfer is globally more efficient with the HF molecular target with total cross sections from 14.2×10^{-16} cm^2 at $E_{lab} = 3\ keV$ to about 22.0×10^{-16} cm^2 at $E_{lab} = 100\ keV$. These comparative results show clearly that the charge-transfer mechanism is fundamentally dependent of the specific nonadiabatic interactions involved in each collision system.

5 Chapter

Summary and Outlook

5.1 Summary

Collisions of slow multiply charged ions with molecular species have been widely investigated in the past few years. Important experimental and theoretical effort has been focused on reactions with simple targets, such as H_2 or D_2 [136–139]. Consideration of more complex molecular targets are now of increasing interest, in particular with regard to possible direct or indirect processes occurring in the irradiation of the biological medium.

In these reactions, generally at relatively low energies, different processes have to be considered: excitation and fragmentation of the molecule, ionization of the gaseous target, and also possible charge transfer from the multicharged ion toward the biomolecule. Charge transfer can be investigated theoretically in the framework of the molecular representation of the collisions. Such studies provide important information on the mechanism as well as on the electronic structure of the projectile and target during the reaction.

Until now, direct processes where the ions are interacting directly with biomolecules have been mainly considered. Indeed, important damage has been shown to be due not only to the primary radiation itself, but also to the secondary particles, low energy electrons, radicals, and also ions which are generated along the track after interaction of the ionizing radiation with the biological medium [18]. Increasing interest has thus been devoted to the possible reactions involving secondary particles, in particular recent experi-

mental and theoretical studies have been undertaken on reactions involving ions.

Previously, we have investigated the $C^{2+} + OH$ collision system with the idea of modelling the action of ions on OH radicals formed in a biological system such as the human organism. Carbon ions used in radiotherapy may react with the numerous OH radicals present in the human body. Thus, the investigation of charge-transfer process induced by collision of C^{2+} ions with the OH radical is of great importance.

We have extended our research taking account of the characteristics of the molecular target (electronic structure, electronegativity of its elements) to have a better understanding of the charge-transfer mechanism for different diatomics and extract general rules for such process. Furthermore, experimental investigations of charge transfer in collisions with hydrogen halide molecules (HF, HCl) have been proposed by the Institute of Nuclear Research of the Hungarian Academy of Sciences. The comparison between the theoretical and experimental results gives us an opportunity to the study of the application regarding the theoretical methods. Therefore it would be possible to improve the description of collisions with targets getting more and more complex.

In this manner we have undertaken the theoretical study of the two charge-transfer processes $C^{2+} + HF$ and $C^{2+} + HCl$. The mechanism has been investigated in detail in each reaction, in connection with nonadiabatic interactions around avoided crossings between states involved in the process. The molecular calculations have been carried out using *ab initio* quantum chemistry methods in order to determine potential energy surfaces of the different states involved in the process and corresponding radial and rotational couplings. The collision dynamics has been derived in the keV energy range by means of semiclassical approaches. We have studied first the $C^{2+} + HF$ collision system, and compared its mechanism to the $C^{2+} + HCl$ reaction.

I summarize the main results of my work related to this thesis in the following points:

I. One of the main goals of this study is the investigation of the anisotropy of the charge transfer with consideration of the evolution of the nonadiabatic interactions with regard to the geometry of the system in order to provide a detailed understanding of the reaction.

- *Ab initio* study has been carried out on the $C^{2+}+HF$ collision system by using state-averaged Complete Active Space Self-Consistent Field (CASSCF) Multireference Configuration Interaction (MRCI) method. Accurate potential energy surfaces and nonadiabatic coupling terms have been calculated for different orientations of the projectile corresponding to specific values of the angle θ about every 20°, from the linear $C-H-F$ geometry ($\theta = 0^{\circ}$) to the linear $C-F-H$ one ($\theta = 180^{\circ}$).

- Dynamical calculations have been performed in the [0.05-0.6] a.u. collision velocity range ([0.75-108] keV laboratory energy range) using the semiclassical computational codes, taking account of all the transitions driven by radial and rotational coupling matrix elements.

- A two-crossing process has been observed, which leads to the increase of the total cross section with collision energy.

- I have pointed out the collision process being highly anisotropic. The charge transfer is favoured in the linear approach with collision of the C^{2+} ion toward the most electronegative atom, and, on the contrary, very significantly non-favoured in the perpendicular approach.

- The rotational effect has been found quite significant for this system even at lower collision velocity values.

II. The position and intensity of the avoided crossings depend on the geometry of the system corresponding to different values of the vibration coordinate. I have investigated the influence of the vibration of the diatomic molecule during the collision.

- Different values of the HF distance r_{HF} have been considered in the linear approach of the projectile toward the hydrogen atom of HF molecule. The corresponding cross sections show a regular increase when the vibration coordinate r_{HF} is reduced from 2.0 to 1.5 a.u.

- No specific behaviour has been specified at very constrained HF geometry, as observed previously in the $C^{2+}+OH$ collision system, and no first relaxation process may be expected in this system.

III. I have examined the evaluation of the cross sections on the different vibration levels of HF^+ in the Franck-Condon approximation. The vibrational analysis of the charge-transfer process $C^{2+}(^1S) + HF_{(\nu=0)} \rightarrow C^+ + HF^+_{(\nu)}$ revealed that only low vibrational levels would be populated.

IV. I have tested the effect of translation factors in the collision energy range we are dealing with. The introduction of translation factors induces a very small variation on the total cross sections. The effect decreases at lower collision energies and is completely negligible below about 30 keV.

V. Another focus of this thesis is the study of the charge transfer involving the hydrogen chloride target (corresponding to a similar configuration, but a higher size and mass of the heteroatom than in the case of the hydrogen fluoride molecule), with the aim to compare these reactions.

- The collision treatment has been performed by using the same methods that in the case of the $C^{2+} + HF$ system. I have determined potential energy surfaces of the different states involved in the process and corresponding radial and rotational couplings in the collision of the C^{2+} ion towards the hydrogen atom in the linear approach.
- A simple mechanism driven principally by the nonadiabatic coupling interaction between the entry channel and the highest charge-transfer channel has been pointed out.
- The mechanism has been found to be completely different from the behaviour of the $C^{2+} + HF$ collision system. The mechanism is essentially dependent of the specific nonadiabatic interactions involved in each collision system.

5.2 Outlook

As a further step in the investigation of the charge-transfer processes in ion-molecule reactions, studies of collisions on the H_2O are of great interest. Collisions of different multiply charged ions (He^{2+}, C^{q+}) with H_2O play an important role due to the fundamental relevance of these systems in medical applications. Therefore, a detailed analysis would be essential for these collisional systems.

6 Chapter

Az értekezés összefoglalása

6.1 Összefoglalás

A többszörös töltésű lassú ionok molekulákkal történő ütközéseit széles körben tanulmányozzák a szakirodalomban. Az egyszerű targetes (H_2, D_2) reakciókon [136–139] túl a komplexebb molekulák ionokkal történő ütközéseit egyre kiterjedtebben vizsgálják a biológiai szövetekben végbemenő sugárkárosodási folyamatok kapcsán. Ezekben a reakciókban általában kis ütközési energiákon a következő folyamatokat tekintik: gerjesztődést, fragmentációt, ionizációt, illetve a többszörösen töltött ionokról a biomolekulák felé irányuló töltésátvitelt. Ez utóbbi folyamat elméleti módszerekkel, molekuláris szinten is jól vizsgálható. Így a folyamat mechanizmusáról, valamint a lövedékion és targetmolekula elektronszerkezetéről is értékes információkat nyerhetünk.

Korábban főleg a direkt folyamatokat vizsgálták, amelyek során az ionok közvetlenül összeütköznek a biomolekulákkal. A direkt sugárkárosodási folyamatokon kívül az inderekt folyamatok is lényegesek. Ismert, hogy lényeges károsodás lép fel, amikor a biológiai környezetet érő sugárzás hatására másodlagos részecskék (alacsony energiás elektronok, szabad gyökök vagy ionok) keletkeznek a környezetnek az ionizáló sugárzással történő kölcsönhatása következtében [18]. Annak érdekében, hogy tisztázzák az ionok molekulákkal történő ütközései során végbemenő folyamatokat, további vizsgálatok szükségesek.

Munkám során olyan ion–kétatomos molekula ütközéseket vizsgáltam

elméleti módszerekkel, amelyek hozzájárulhatnak a nagyobb molekulákban lezajló reakciók leírásához.

A korábbi $C^{2+} + OH$ ütközés vizsgálata a szén ion OH gyökre való hatását modellezte. Az élő szervezetben számos OH gyök keletkezik, mellyel a szén ionnyaláb találkozhat. Az OH gyökkel lezajló ütközések vizsgálata éppen ezért jelentős fontosságú.

Az ion-kétatomos molekula ütközések átfogóbb tanulmányozása érdekében kiterjesztettük vizsgálatainkat olyan rendszerek esetére, amelyek hasonló felépítésű targetmolekulákat tartalmaznak, és amelyekre vonatkozóan kísérleti eredmények várhatók. A hasonló felépítésű rendszerek ütközéseire nyert eredmények egyszerűen összevethetők. Így egyértelmű következtetéseket tudunk levonni az egyszeres töltéskicserélődési folyamat mechanizmusára vonatkozóan. A Magyar Tudományos Akadémia Atommagkutató Intézetével történő egyeztetések során felmerült a szén ionnyaláb hidrogén-halogenidekkel (HF, HCl) végbemenő ütközések kísérleti vizsgálatának a megvalósítása. A kísérleti eredményekkel történő összevetés lehetőséget ad az elméleti módszerek alkalmazhatóságának ellenőrzésére. A helyesnek bizonyult eljárások pedig továbbfejleszthetők egyre komplexebb targetekkel történő ütközések leírására.

A fentiek alapján a C^{2+} ionnyaláb és a hidrogén-halogenidek (HF, HCl) között lejátszódó ütközések elméleti leírását tűztük ki célul keV-es ütközési energia tartományban.

A kvantumkémiai számítások nagy körültekintést igényelnek kis és közepes energiájú ütközések *ab initio* vizsgálatakor. CASSCF (Complete Active Space Self-Consistent Field) és MRCI (Multireference Configuration Interaction) módszereket alkalmaztam a potenciális energia felületek és nemadiabatikus csatolások minél pontosabb kiszámítására. A dinamikai számítások kivitelezésére a fél-klasszikus impakt paraméter módszert alkalmaztam közepes ütközési energia tartományban. A vibrációs átmenetek leírására pedig a Franck−Condon közelítést használtam.

Kutatásaim eredményeit az alábbi pontokban foglalom össze:

I. A $C^{2+} + HF$ ütközés anizotrópiájának vizsgálata során az ütközési szöget közel 20 fokonként változtattam, így számos ion-molekula orientációra elvégeztem a számításokat.

- Meghatároztam a potenciális energia felületeket és a nemadiabatikus

csatolásokat különböző ion-molekula orientációra.

- Viszonylag széles ütközési energia tartományban ([0.75–108] keV) molekuladinamikai számításokat végeztem a fél-klasszikus impakt paraméter módszer alkalmazásával.

- A $C^{2+}+HF$ ütközési rendszer esetén a bemeneti csatorna és a $2^1\Sigma^+$ állapot, valamint a $2^1\Sigma^+$ és az $1^1\Sigma^+$ állapotok közötti elkerült kereszteződések változásával összhangban, a különböző orientációk szerint kiátlagolt hatáskeresztmetszetek növekedést mutatnak az ütközési energia függvényében.

- Az ion-molekula orientáció változtatásával az ütközés erősen anizotróp jelleget mutat. A töltéskicserélődés a nagyobb elektronegativitású atom felőli lineáris irányban a legkedvezőbb, a legkevésbé pedig a kétatomos molekulát összekötő tengelyre merőleges irányban.

- Rámutattam, hogy a rotációs csatolás szerepe kis sebességek esetén is lényeges.

II. Az elkerült kereszteződések helye és erőssége függ a targetmolekulát alkotó atomok egymástól való távolságától, az ún. vibrációs koordinátától. A töltéskicserélődési folyamatot különböző vibrációs paraméter értékekre tanulmányoztam.

- Különböző H-F távolságok figyelembevételével számításokat végeztem a H atom felőli lineáris ütközések leírásához. A teljes hatáskeresztmetszetek szabályos növekedése figyelhető meg a vibrációs koordináta csökkenésével, amely összhangban van a csatolási görbék viselkedésével.

- A $C^{2+}+OH$ rendszer O atom felőli lineáris ütközés esetében a molekula gyors relaxációjára utaló hatáskeresztmetszet görbéket figyeltünk meg. A $C^{2+}+HF$ ütközési rendszer esetén ehhez hasonló viselkedést nem tapasztaltam.

III. A $C^{2+}(^1S)+HF_{(\nu=0)} \rightarrow C^+ + HF^+_{(\nu)}$ reakció esetén meghatároztam a vibrációs szintekhez tartozó hatáskeresztmetszet értékeket. A töltésátvitel a molekulaion legalacsonyabb rezgési kvantumszámú állapotait érinti a leginkább.

IV. Megmutattam, hogy az elektron transzlációs faktor figyelembevétele kismértékben befolyásolja a $C^{2+} + HF$ rendszerre vonatkozó töltéskicserélődési hatáskeresztmetszeteket. 30 keV alatti ütközési energia esetén pedig teljesen elhanyagolhatóvá válik.

V. Számításokat végeztem a $C^{2+} + HCl$ ütközés leírására és a kapott eredményeket összevetettem a hasonló elektronszerkezettel rendelkező targetmolekulával lejátszódó ütközés eredményeivel.

- A molekulaszerkezeti számításokat és az ütközés dinamikai leírását a H atom felőli lineáris irányban valósítottam meg.
- A $C^{2+} + HCl$ ütközés esetén a töltésátviteli mechanizmus egyszerűnek bizonyul. A töltésátvitel leginkább a $3^1\Sigma^+$ állapotot és a bemeneti csatornát összekötő radiális csatolás által vezérelt.
- Összehasonlítva az említett két rendszerre kivitelezett számításokat, megállapíthatjuk, hogy a töltésátvitel mechanizmusa nagy mértékben függ az egyes rendszerekben kialakuló sajátos nemadiabatikus kölcsönhatásoktól.

6.2 Kitekintés

Az ion-kétatomos molekula ütközések során alkalmasnak bizonyult eljárások továbbfejleszthetők nagyobb rendszerek leírására. Így lehetőség nyílik arra, hogy egyre komplexebb targetmolekulák képezzék a vizsgálatok tárgyát. Az előző módszerek továbbfejlesztett változatát először többszörösen töltött ionok (He^{2+}, C^{q+}) és víz molekulák közötti ütközések tanulmányozására alkalmaznánk. A vízzel történő ütközések vizsgálatának jelentősége abban rejlik, hogy az emberi szervezet legnagyobb részben vízből áll.

Bibliography

[1] T. E. Cravens, *Astrophys J.* **532**, L153 (2000).

[2] C. F. Maggi, I. D. Horton, H. P. Summers, *Plasma Phys. Control Fusion* **42**, 669 (2000).

[3] G. H. Henderson, *Proc. Roy. Soc. A* **102**, 496 (1923).

[4] E. Rutherford, *Phil. Mag. 6th Ser.* **47**, 276 (1924).

[5] G. H. Henderson, *Proc. Roy. Soc. A* **109**, 157 (1925).

[6] J. C. Jacobsen, *Nature* **117**, 858 (1926).

[7] L. H. Thomas, *Proc. Roy. Soc. A* **114**, 561 (1927).

[8] J. R. Oppenheimer, *Phys. Rev.* **31**, 349 (1928).

[9] H. C. Brinkman, H. A. Kramers, *Proc. Acad. Scien. Amsterdam* **33**, 973 (1930).

[10] H. S. W. Massey, R. A. Smith, *Proc. Roy. Soc. A* **142**, 142 (1933).

[11] D. R. Bates, B. L. Moiseiwitch, *Proc. Roy. Soc. A* **67**, 540 (1954).

[12] D. R. Bates, H. S. W. Massey, A. L. Stewart, *Proc. Roy. Soc. A* **216**, 437 (1955).

[13] T. J. M. Boyd, B. L. Moiseiwitch, *Proc. Roy. Soc. A* **70**, 55 (1957).

[14] D. R. Bates, *Proc. Roy. Soc. A* **274**, 294 (1958).

[15] D. R. Bates, R. McCarroll, *Proc. Roy. Soc. A* **245**, 175 (1958).

[16] B. H. Bransden and M. R. C. McDowell, *Charge Exchange and the Theory of Ion-Atom Collisions*, Oxford University Press (1992), ISBN 0198520204, p. 10-11.

[17] G. Kraft, *The Physics of Multiply and Highly Charged Ions*, Fred. J. Currell Ed., Kluwer Academic Publ., Dordrecht, Boston, London, **1**, 149 (2003).

[18] B. D. Michael, P. O'Neill, *Science* **287**, 1603 (2000).

[19] C. P. Hoeppner, E. Rietzel, T. Zeuner, H. Wyczisk, *Dose Reporting in Ion Beam Therapy*, IAEA-TECDOC-1560, 53 (2006).

[20] D. Schardt, T. Elsässer, *Reviews of Modern Physics* **82**, 383 (2010).

[21] G. Kraft, *Tumor Therapy with Heavy Ions* (Verein zur Förderung der Tumortherapie mit schweren Ionen e.V., Darmstadt, 2007), ISBN 3-9811298-2-2; 978-3-9811298-2-3, p.8.

[22] W. Bragg, R. Kleemann, *Phil. Mag.* **10**, 318 (1905).

[23] R. R. Wilson *Radiology* **47**, 487 (1946).

[24] J. R. Castro, *Hadrontherapy in Oncology*, U. Amaldi and B. Larsson Eds., Elsevier, 208 (1994).

[25] U. Weber, G. Kraft, *The Cancer Journal* **15**, 325 (2009).

[26] W. Enghardt, W. D. Fromm, H. Geissel, H. Keller, G. Kraft, A. Magel, P. Manfraß, G. Münzenberg, F. Nickel, J. Pawelke, D. Schardt, C. Scheidenberger, M. Sobiella, *Phys. Med. Biol.* **37**, 2127 (1992).

[27] G. Kraft, E. Badura, W. Becher, D. Böhne, H. Brand, C. Brusasco, H. Eickhoff, H.G. Essel, B. Franzcak. O. Geiß, Th. Haberer. J. Hoffmann, P. Kainsberger, M. KrĂ¤mer, K. Krause, N. Kurz, B. Langenbeck. W. Ott, K. Poppensieker, M. Richter, W. von Rüden, D. Schardt, M. Scholz, P. Spiller, R. Steiner, H. Stelzer, B. Voss, U. Weber, *Proceedings of the Sixth European Particle Accelerator Conference* **1**, 212 (1998).

[28] G. Kraft, `http://nupecc.org/iai2001/report/B31.pdf`.

[29] W. T. Chu, B. A. Ludewigt, T. R. Renner, *Rev. Sci. Instrum.* **64**, 2055 (1993).

[30] M. Spotheim-Maurizot, M. Bergusova, M. Charlier, *Actual. Chim.* **1112**, 97 (2003).

[31] D. Marx and Jürg Hutter, *Ab Initio Molecular Dynamics: Basic Theory and Advanced Methods*, Cambridge University Press (2009), ISBN 978-0-521-89863-8, p. 11-14.

[32] M. Born, R. Oppenheimer, *Ann. Phys* **79**, 361 (1927).

[33] J. von Neumann, E. Wigner *Z. Physik* **30**, 467 (1929).

[34] B. H. Bransden and M. R. C. McDowell, *Charge Exchange and the Theory of Ion-Atom Collisions*, Oxford University Press (1992), ISBN 0198520204, p. 106.

[35] G. Herzberg, H. C. Longuet-Higgins, *Discuss. Faraday Soc.* **35**, 77 (1963).

[36] D. G. Truhlar, C. A. Mead, *Phys. Rev. A* **68**, 032501 (2003).

[37] S. L. Mielke, B. C. Garett, K. A. Peterson, *J. Chem. Phys.* **116**, 4142 (2002).

[38] S. Han, D. R. Yarkony, *J. Chem. Phys.* **119**, 5058 (2003).

[39] G. J. Halász, Á. Vibók, A. M. Mebel, M. Baer, *J. Phys. Chem. Phys.* **118**, 3052 (2003).

[40] D. R. Yarkony, *J. Phys. Chem. A* **101**, 4263 (1997).

[41] M. Baer *Chem. Phys. Lett* **35**, 112 (1975).

[42] M. Baer *Chem. Phys.* **259**, 113 (2000).

[43] T. Pacher, L. S. Cederbaum, H. Köppel, *Adv. Chem. Phys.* **84**, 293 (1993).

[44] C. A. Mead, D. G. Truhlar *J. Chem. Phys.* **77**, 6090 (1982).

[45] M. Baer, T. Vértesi, G. J. Halász, Á. Vibók, S. Suhai, *Faraday Disc.* **127**, 337 (2004).

[46] M. Baer, T. Vértesi, G. J. Halász, Á. Vibók, *J. Phys. Chem. A* **108**, 9134 (2004).

[47] A. Macías, A. Riera, *Physics Reports* **90**, 299 (1982).

[48] G. Moliére, *Z. Naturforsch* **2A**, 133 (1947).

[49] R. J. Glauber, *Lectures in Theoretical Physics*, ed. by W. E. Brittin and L. G. Dunham, Interscience Publishers, Inc., New York, Volume I, 315 (1959).

[50] P. G. Burke and Jürg Charles J. Joachain, *Theory of Electron-Atom Collisions, Part 1. Potential Scattering*, Plenum Publishing Corporation (1995), ISBN 0-306-44546-8, p. 36.

[51] J. Al-Khalili, F. Nunes, *J. Phys. G: Nucl. Part. Phys* **29**, 89 (2003).

[52] J. Al-Khalili, E. Roeckl, *The Euroschool Lectures on Physics with Exotic Beams, Vol. I*, *Lect. Notes Phys.* **651**, Springer, Berlin Heidelberg (2004), ISBN 3-540-22399-1, p. 91.

[53] L. F. Errea, J. D. Gorfinkiel, A. Macías, L. Méndez, A. Riera, *J. Phys. B: At Mol. Opt. Phys.* **30**, 3855 (1997).

[54] R. J. Allan, Technical Memorandum, Daresbury laboratory *Introduction to charge transfer theory and calculations and documentation for EIKONX program*, (1990).

[55] C. Gaussorgues, R. D. Piacentini, A. Salin, *Comp. Phys. Comm.* **10**, 223 (1975).

[56] R. D. Piacentini, A. Salin, *Comp. Phys. Comm.* **12**, 199 (1976).

[57] R. D. Piacentini, A. Salin, *Comp. Phys. Comm.* **13**, 57 (1977).

[58] L. F. Errea, J. D. Gorfinkiel, C. Harel, H. Jouin, A. Macías, L. Méndez, B. Pons, A. Riera, *Physica Scripta* **T62**, 33 (1996).

[59] H. J. Werner, P. Knowles, computer code MOLPRO (vesrions 2009.1) package of *ab initio* programs.

[60] D. R. Hartree, *Proc. Cambridge Philos. Soc.* **24**, 328 (1928).

[61] V. A. Fock, *Z. Phys.* **15**, 126 (1930).

[62] C. Møller, M. S. Plesset, *Phys. Rev.* **46**, 618 (1934).

[63] E. A. Hylleraas, *Z. Physik* **48**, 469 (1928).

[64] G. Yan, D. Xie, A. Tian, *J. Phys. Chem.* **98**, 8870 (1994).

[65] J. Cízek, *J. Chem. Phys.* **45**, 4526 (1966).

[66] J. Cízek, *J. Chem. Phys.* **14**, 35 (1969).

[67] J. Cízek, J. Paldus, *Int. J. Quantum Chem.* **5**, 359 (1971).

[68] H.-J. Werner, P. J. Knowles, *J. Chem. Phys.* **82**, 5053 (1985).

[69] P. J. Knowles, H.-J. Werner, *Chem. Phys. Lett.* **115**, 259 (1985).

[70] B. O. Ross, P. R. Taylor, P. E. M. Siegbahn, *Chem. Phys.* **48**, 157 (1980).

[71] P. E. M. Siegbahn, J. Almlöf, A. Heiberg, B. O. Ross, *J. Chem. Phys.* **74**, 157 (1981).

[72] K. Ruedenberg, M. Schmidt, M. M. Gilbert, S. T. Elbert, *Chem. Phys.* **71**, 41 (1982).

[73] B. O. Ross, *Adv. Chem. Phys.* **69**, 399 (1987).

[74] H.-J. Werner, *Adv. Chem. Phys.* **69**, 1 (1987).

[75] H.-J. Werner, P. J. Knowles, *J. Chem. Phys.* **89**, 5803 (1988).

[76] P. J. Knowles, H.-J. Werner, *Chem. Phys. Lett.* **145**, 514 (1988).

[77] P. Hohenberg, W. Kohn, *Phys. Rev.* **136**, B864 (1964).

[78] W. Kohn, L. J. Sham, *Phys. Rev.* **140**, B864 (1965).

[79] C. J. Barden, H. F. Schaefer III, *Pure Appl. Chem.* **72**, 1405 (2000).

[80] F. Jensen, *Introduction to Computational Chemsitry*, John Wiley Sons, Ltd (2007), ISBN 978-0-470-01187-4, p. 133-143.

[81] W. J. Hehre, R. F. Stewart, J. A. Pople, *J. Chem. Phys.* **51**, 2657 (1969).

[82] J. S. Binkley, J. A. Pople, W. J. Hehre, *J. Am. Chem. Soc.* **102**, 939 (1980).

[83] M. S. Gordon, J. S Binkley, J. A. Pople, W. J. Pietro, W. J. Hehre, *J. Am. Chem. Soc.* **104**, 2797 (1982).

[84] W. J. Pietro, M. M. Francl, W. J. Hehre, D. J. DeFrees, J. A. Pople, J. S. Binkley, *J. Am. Chem. Soc.* **104**, 5039 (1982).

[85] T. H. Dunning Jr, P. J. Hay, in *Modern Theoretical Chemistry*, ed. by H. F. Schaefer, III. Plenum Press, New York, Vol. 3, p. 1. (1976).

[86] G. W. Spitznagel, *T. Chem. Phys.* **90**, 1007 (1989).

[87] D. J. DeFrees, B. A. Levi, S. K. Pollack, W. J. Hehre, J. S. Binkley, J. A. Pople, *J. Am. Chem. Soc* **101**, 4085 (1979).

[88] G. W. Spitznagel, T. Clark, J. Chandrasekhar, P. v. R. Schleyer, *J. Comp. Chem.* **3**, 363 (1982).

[89] T. Clark, J. Chandrasekhar, G. W. Spitznagel, P. v. R. Schleyer, *J.Comp. Chem.* **4**, 294 (1983).

[90] A. Szabo and N. S. Ostlund, *Modern Quantum Chemistry*, McGraw-Hill Publishing Company (1989), ISBN 0-486-69186-1, p. 234.

[91] H. Hellmann, *J. Chem. Phys.* **3**, 61 (1935).

[92] P. Habitz, C. Votana, *J. Chem. Phys.* **72**, 5532 (1980).

[93] V. Sidis, *J. Chem. Phys.* **55**, 5838 (1971).

[94] S. E. Butler, *Phys. Rev. A* **23**, 1 (1981)

[95] R. P. Feynman, *Phys. Rev.* **56**, 340 (1939).

[96] A. Macias, A. Riera, *J. Phys. B* **10**, 861 (1977).

[97] A. Macias, A. Riera, *J. Phys. B* **11**, 1077 (1978).

[98] I. D. Petsalakis, G. Theoradokopoulos, R. J. Buenker, *Chem. Phys. Lett* **148**, 285 (1988).

[99] M. C. Bacchus-Montabonel, C. Courbin, R. McCarroll, *J. Phys. B* **24**, 4409 (1991).

[100] J. F. Castillo, L. F. Errea, A. Macias, L. MĂŠndez, A. Riera *J. Chem. Phys.* **103**, 2113 (1995).

[101] M. C. Bacchus-Montabonel, R. Cimiraglia, M. Persico, *J. Phys. B* **17**, 1931 (1984).

[102] A. Macias, A. Riera *Phys. Rep.* **81**, 299 (1982).

[103] M. C. Bacchus-Montabonel *Phys. Rev. A* **36**, 1994 (1987).

[104] J. Grosserl, T. Menzel, A. K. Belyaec *Phys. Rev. A* **59**, 1309 (1999).

[105] D. R. Bates, R. McCarroll, *Proc. Roy. Soc. A* **245**, 175 (1958).

[106] D. S. F. Crothers, N. R. Todd *J. Phys. B* **14**, 2233 (1981).

[107] L. F. Errea, J. M. Maidagan, L. Méndez, B. Pons, A. Riera, *J. Phys. B* **24**, L387 (1991).

[108] L. F. Errea, C. Harel, H. Jouin, J. M. Maidagan, L. Méndez, B. Pons, A. Riera, *Phys. Rev. A* **46**, 5617 (1992).

[109] S. B. Schneidermann, A. Russek, *Phys. Rev.* **181**, 311 (1969).

[110] L. F. Errea, C. Harel, H. Jouin, L. Méndez, B. Pons, A. Riera, *J. Phys. B* **27**, 3603 (1994).

[111] L. F. Errea, L. Méndez, B. Pons, A. Riera, C. Harel, H. Jouin, B. Pons, *Phys. Rev. A* **50**, 418 (1994).

[112] L. F. Errea, L. Méndez, A. Riera, *J. Phys. B* **15**, 101 (1982).

[113] D. E. Woon, T. H. Dunning Jr., *J. Chem. Phys.* **98**, 1358 (1993).

[114] M. S. Banna, B. E. Mills, D. W. Davis, D. A. Shirley *J. Chem. Phys.* **61**, 4780 (1974).

[115] K. P. Huber, G. Herzberg, in *Molecular Spectra and Molecular Structure IV. Constants of Diatomic Molecules* (Van Nostrand Reinhold, New York, 1979).

[116] R. W. Shaw Jr., T. D. Thomas *Phys. Rev. A* **11**, 1491 (1975).

[117] W. von Niessen, L. S. Cederbaum, W. Domcke, G. H. F. Diercksen *Chem. Phys.* **56**, 43 (1981).

[118] R. K. Chaudhuri, K. F. Freed, S. A. Abrash, D. M. Potts, *J. Mol. Struct. Theochem* **547**, 83 (2001).

[119] NIST Atomic Spectra Database Levels Data, available at `http://physics.nist.gov/cgi-bin/AtData/main_asd`.

[120] R. J. Allan, C. Courbin, P. Sales, P. Wahnon *J. Phys. B* **23**, L461 (1990).

[121] B. H. Bransden and M. R. C. McDowell, *Charge Exchange and the Theory of Ion-Atom Collisions*, Oxford University Press (1992), ISBN 0198520204, p. 63-64.

[122] P. Honvault, M. C. Bacchus-Montabonel, R. McCarroll, *J. Phys. B* **27**, 3115 (1994).

[123] L. F. Errea, L. Méndez, A. Riera, *J. Phys. B* **15**, 101 (1982).

[124] F. Fraija, A. R. Allouche, M. C. Bacchus-Montabonel, *Phys. Rev. A* **49**, 272 (1994).

[125] A. Chenel, E. Mangaud, Y. Justum, D. Talbi, M. C. Bacchus-Montabonel, M. Desouter-Lecomte, *J. Phys. B* **43**, 245701 (2010).

[126] P. Honvault, M. Gargaud, M. C. Bacchus-Montabonel, R. McCarroll, *Astron. Astrophys.* **302**, 931 (1995).

[127] E. Bene, P. Martínez, G. J. Halász, Á. Vibók, M. C. Bacchus-Montabonel, *Phys. Rev. A* **80**, 012711 (2009).

[128] E. Bene, Á. Vibók, G. J. Halász, M. C. Bacchus-Montabonel, *Chem. Phys. Lett.* **455**, 159 (2008).

[129] L. F. Errea, J. D. Gorfinkiel, A. Maciás, L. Mendéz, A. Riera *J. Phys. B* **30**, 3855 (1997).

[130] R. J. Le Roy, LEVEL 7.7 computer program `http://leroy.uwaterloo.ca`.

[131] M. C. Bacchus-Montabonel, Y. S. Tergiman, *Chem. Phys. Lett.* **497**, 18 (2010).

[132] F. Frémont, D. Martina, O. Kamalou, P. Sobocinski, J.-Y. Chesnel, I. R. McNab, F. R. Bennett, *Phys. Rev. A* **71**, 042706 (2005).

[133] A. Nicklass, M. Dolg, H. Stoll, H. Preuss, *J. Chem. Phys.* **102**, 8942 (1995).

[134] A.A. Wills, D. Čubrić, M. Ukai, F. Currell, B.J. Goodwin, T. Reddish, J. Comer, *J. Phys. B* **26**, 2601 (1993).

[135] P. C. Stancil, B. Zygelman, K. Kirby, in *Photonic, Electronic, and Atomic Collisions*, edited by F. Aumayr and H.P. Winter(World Scientific, Singapore, 1998), p. 537.

[136] M. C. Bacchus-Montabonel, *Phys. Rev. A* **59**, 3569 (1999).

[137] R. E. Olson and C. R. Feeler, *J. Phys. B* **34**, 1163 (2001).

[138] P. Sobocinski, J. Rangama, G. Laurent, L. Adoui, A. Cassimi, J.-Y. Chesnel, A. Dubois, D. Hennecart, X. Husson, and F. Frémont, *J. Phys. B: At. Mol. Opt. Phys.* **35**, 1353 (2002).

[139] G. Laurent *et al.*, *Phys. Rev. Lett.* **96**, 173201 (2006).

List of Publications

The thesis is based on the following papers:

A1. E. Bene, E. Rozsályi, Á. Vibók, G. J. Halász, M. C. Bacchus-Montabonel: *Theoretical treatment of direct and indirect processes in ion-biomolecule collisions,* AIP Conf. Proc. 1080, 59-70 (2008).

A2. E. Rozsályi, E. Bene, G. J. Halász, Á. Vibók, M. C. Bacchus-Montabonel: *Theoretical treatment of charge transfer in collisions of C^{2+} ions with HF: Anisotropic and vibrational effect*, Phys. Rev. A **81**, 062711 (2010).

A3. E. Rozsályi, E. Bene, G. J. Halász, Á. Vibók, M. C. Bacchus-Montabonel: *Ab initio molecular treatment of C^{2+} + HF collision system,* Acta Physica Debrecina, XLIV, 118 (2010).

A4. E. Rozsályi, E. Bene, G. J. Halász, Á. Vibók, M. C. Bacchus-Montabonel: *Ab initio study of charge-transfer dynamics in collisions of C^{2+} ions with hydrogen chloride,* Phys. Rev. A **83**, 052713 (2011).

A5. E. Rozsályi: *Charge transfer in collisions of C^{2+} ions with HCl molecule*, Acta Physica Debrecina, XLV, 166 (2011).

A6. E. Rozsályi, E. Bene, G. J. Halász, Á. Vibók, M. C. Bacchus-Montabonel: *Analysis of the charge transfer mechanism in ion-molecule collisions.* Advances in the Theory of Quantum Systems in Chemistry and Physics; *Progress in Theoretical Chemistry and Physics;* **22**, (355-368), 2012, ISBN 978-94-007-2075-6, Springer.

Posters

P1. E. Bene, E. Rozsályi, Á. Vibók, G. J. Halász, M. C. Bacchus-Montabonel: *Theoretical treatment of direct and indirect processes in ion-biomolecule collisions*, 5^{th} International Conference on Radiation Damage in Biomolecular Systems, 13^{th} - 15^{th} June 2008, Debrecen, Hungary

P2. E. Rozsályi, E. Bene, Á. Vibók, G. J. Halász, M. C. Bacchus-Montabonel: *Theoretical treatment of indirect processes in ion-(bio)molecule collisions*, 7^{th} International Conference on Radiation Damage in Biomolecular Systems, 30^{th} June - 4^{th} July 2010, Madrid, Spain

P3. E. Rozsályi, Á. Vibók, G. J. Halász, M. C. Bacchus-Montabonel: *Theoretical treatment of charge transfer in C^{2+} + HF collision. Anisotropic and vibrational effect,* 10^{th} European Conference on Atoms, Molecules and Photons, 4^{th} - 9^{th} July 2010, Salamanca, Spain

P4. M. C. Bacchus-Montabonel, E. Bene, E. Rozsályi, G. J. Halász, Á. Vibók: *Anisotropic and vibrational effects in charge transfer processes* 36^{th} Conference of Theoretical Chemists of Latin Expression, 19^{th} - 24^{th} September 2010, Anglet-Biarritz, France

P5. E. Rozsályi, E. Bene, G. J. Halász, Á. Vibók, M. C. Bacchus-Montabonel: *Ab initio molecular treatment of charge transfer processes in C^{2+} + HF collisions*, Journee Commune LPCML/LASIM/LPMCN, 31^{st} January 2011, Lyon, France

P6. M. C. Bacchus-Montabonel, E. Rozsályi, E. Bene, Á. Vibók, G. J. Halász: *Theoretical treatment of indirect processes in ion-(bio)molecule collisions*, ISSOL and Bioastronomy Joint International Conference, 3^{rd} - 8^{th} July 2011, Montpellier, France

Acknowledgements

The present thesis has been completed under a joint supervision between the University of Debrecen and the University Claude Bernard Lyon 1. There are many people who deserve my gratitude for their contribution during the preparation of this thesis, and it would be impossible to mention each one in a few paragraphs. Nevertheless, I wish to express my sincere thanks to the following persons in particular.

Firstly I would like to thank to Dr. Ágnes Vibók, *who sparked my interest in Atomic and Molecular Physics. As my mentor, she has been a great source of advice for all aspects of my graduate career. I was very fortunate to have had the opportunity to work in her group.*

I would like to express my deep and sincere gratitude to Dr. Marie-Christine Bacchus Montabonel, *whom I have had the great experience of working with and learning from. She has taught me how to sort out the important issues and how to handle complicated results. She has always given me all the time and guidance that I needed. I am thankful for her persistent support throughout this work and for her detailed and constructive comments. Her experience had a major contribution in the preparation and completion of this study.*

I am grateful to my co-supervisor Dr. Gábor Halász *for all the scientific and technical support and his prompt answers to my several questions.*

I would like to note my appreciation to Dr. Erika Bene *for helping me greatly with my first steps regarding quantum chemical calculations.*

I would like to express my thanks to Kunné Dr. Sohler Dorottya *for taking care of all administrative tasks.*

My thanks are also extended to the entire staff at the Department of Theoretical Physics *and to all members of the* LASIM *group.*

I owe my whole-hearted gratitude to my family and Gergely Rozsonits *for their personal support.*

The work described in this thesis would not have been possible without the generous financial support of the COST CM0702 *action, the special grant* Bourse Accueil Doc de la Région Rhône Alpes *and the* TÁMOP-4.2.2/B-10/1-2010-0024 *project.*

The project is co-financed by the European Union and the European Social Fund.